Non-equilibrium two-phase flow simulation of an open feed water heater in the HPLWR power plant

A Smith

20727372

Dissertation submitted in partial fulfilment of the requirements for the degree Master of Engineering in Nuclear Engineering the Potchefstroom Campus of the North-West University

Supervisor: Prof M van Eldik

May 2017

Abstract

In 1996 the U.S Nuclear Regulatory Commission issued a notice that addressed the operation of pressurised water reactors (PWR's) above the licensed power limit due to a decrease in the feed water temperature which may also affect the measuring accuracy of nuclear instrumentation. The designed feed water operating temperature range may be inaccurate due to various assumptions made, including that of an equilibrium steady state approach which represents the conditions of the open feed water heater (OFWH).

The aim of the study is to simulate the open feed water heater for application in a high-performance light water reactor (HPLWR), using a non-equilibrium two-phase flow approach. The main reason is to evaluate the potential improvement in accuracy when predicting operating conditions compared to an equilibrium steady state approach.

The simulation developed consists of three integrated sub-models used to evaluate the heat and mass transfer of the open feed water heater of the HPLWR power plant. The first sub-model is a feed water preparation model in which various streams entering the OFWH are premixed, the properties of the prepared feed water serve as the initial boundary conditions for the second sub-model. The second sub-model is a detailed two-phase flow model for the bubble formation and ascension. The model includes the formation of a bubble at an orifice due to superheated steam being injected into premixed saturated water. The ascension of the bubble is then simulated by tracking the heat and mass being transferred from the bubble to the water body as it condenses and depletes. In the third sub-model, the heat and mass are transferred from a multiple bubble column to the premixed feed water. The non-equilibrium simulation model can furthermore be used to analyse transient effects by incorporating events such as mass flow and temperature variations.

The results gained from the non-equilibrium integrated transient simulation model of the OFWH were then compared to a steady state model that was based on the OFWH as designed by Lemasson for the HPLWR power plant. The non-equilibrium integrated transient approach delivered similar results to that of the equilibrium steady state analysis. The energy transferred from the steam to the bulk liquid was predicted within 90% accuracy and the outlet temperature with an error 0.21%.

Table of Contents

List of Tables

List of Figures

List of Symbols

$\#_{orifice}$	Total number of orifice openings [-]
A	Area [m^2]
C_p	Specific heat [J/kgK]
C_d	Coefficient of drag experienced by the bubble [-]
d	Diameter [m]
E	Entire part of a number [-]
f	Formation frequency [1/s]
Fo	Fourier's number [-]
g	Gravitational acceleration [m/s^2]
h	Enthalpy [kJ/kg]
$\bar{h}$	Convection coefficient [$J/s/m^2K$]
Ja	Jacobs's number
k_v	Velocity factor [-]
$\dot{m}$	Mass flow [kg/s]
n	Bubble number density [$1/m^3$]
Nu	Nusselt number [-]
Pe	Peclet number [-]
Pr	Prandl number [-]
$Q_{steam\ to\ fluid}$	Energy absorbed by the liquid during bubble condensation per unit mixture volume and time [$kJ/s/m^3$]
R	Radius [m]
r	Bubble radius at the moment it detachment [m]
Re	Reynolds number [-]
S	Vertical distance from the centre of the bubble above the point where gas is injected [m]

T	Temperature [K]
t	Time[s]
U	Bubble rise velocity [m/s]
V	Volume [m^3]
$\dot{V}$	Gas flow [m^3/s]
y_m	Mass fraction

Greek

α	Volumetric fraction [m^3/m^3]
$\beta_{Moalem\ and\ Sideman}$	Dimensionless radius correlation by Moalem and Sideman [-]
γ	Thermal liquid diffusivity [m^2/s]
μ	Viscosity [kg/m-s]
k	Conductivity [J/s/mK]
v	Velocity [m/s]
ρ	Density [kg/m^3]
$\Delta\rho$	Absolute difference in density between the gas and the liquid [kg/m^3]
τ	Dimensionless time step [-]

Subscripts

0	Initial parameter
1	Fluid stream one: Feed water from Preheater 5
2	Fluid stream two: Feed water from Preheater 4
3	Fluid stream three: Steam bled from Intermediate Pressure Turbine 3
Bubble	Parameter associated with the steam bubble
Bubble, new	Parameter associated with the next iteration of the steam bubble
C	Critical state
C1	Chamber 1
C2	Chamber 2
C3	Chamber 3

Feed water outlet	Fluid stream out of the Open Feed Water Heater
Liquid	Parameter associated with the surrounding liquid of the bubble
Liquid, new	Parameter associated with the next iteration of surrounding liquid of the bubble
Orifice	Parameter associated with the orifice
Steam	Parameter associated with steam extracted from Intermediate pressure turbine

List of Abbreviations

BWR	Boiling Water Reactors
CFWH	Closed Feed Water Heater
EES	Engineering Equation Solver
FWT/H	Feed Water Tank/Heater
GIF	Generation 4 International Forum
GW_e	Giga Watt electric
HPLWR	High-Performance Light Water Reactor
HPT	High-Pressure Turbine
IPT	Intermediate Pressure Turbine
ISSCWR	International Symposium on Supercritical Water-Cooled Reactors
LPT	Low-Pressure Turbine
LWR	Light Water Reactors
MS	Moisture Separator
MW	Mega Watt
NPP	Nuclear Power Plant
OFWH	Open Feed Water Heater
PH	Preheater
RPV	Reactor Pressure Vessel
SCWR	Supercritical Light Water Reactor
WNA	World Nuclear Association

1 Introduction

1.1 Background

The global need for electricity is ever increasing, even more so for clean energy alternatives. By 2008 nuclear energy accounted for 12.8% of the world's electricity production (OECD/IEA, 2008). In 2012 it was recorded by the World Nuclear Association (WNA) that there are approximately 436 reactors globally, which collectively produce 399.3 GWe of electrical power.

There are five main types of reactors that form part of power generation systems. The most common of these are Light Water Reactors (LWRs) which can be categorised into two groups namely Pressurised Water Reactors (PWRs), and Boiling Water Reactors (BWRs). The key property of a LWR is that it is cooled, moderated and reflected by light water. The main difference between PWRs and BWRs is that BWRs have boiling light water within the reactor thus no steam generators are required. The steam goes directly to the turbines as a generation fluid (Lamarsh, 2001).

When looking at the future of nuclear energy and reactors, clean, safe and cost effective technologies are key factors along with meeting increased energy demands. In 2002 the Generation 4 International Forum (GIF, 2002) announced six reactor technologies which are believed to represent the future in nuclear power generation (WNA, 2013). According to Professor Oka of Tokyo University, the most logical next evolutionary step of the LWR technology is the high-temperature Supercritical Light Water Reactor (SCWR) (Tsikluari, 2004). This type of reactor system is a high-pressure, high-temperature water-cooled reactor that operates above the thermodynamic critical point of water (WNA, 2013) (GIF, 2002). The estimated net plant efficiency of the SCWR is about 44% which is higher than the conventional LWR power plant with a net efficiency of approximately 33% (GIF, 2002).

One of the most recent concepts of the SCWR technology is the High-Performance Light Water Reactor (HPLWR) (GIF, 2002). This concept was first introduced by Bitterman in 2004, with improvements on the cycle done in 2008 (Schlagenhaufer, 2008). The main focus of the HPLWR technology is to decrease capital cost and increase efficiency, as the capital cost to construct a nuclear power plant (NPP) is greater than those of coal-fired power plants (WNA, 2013).

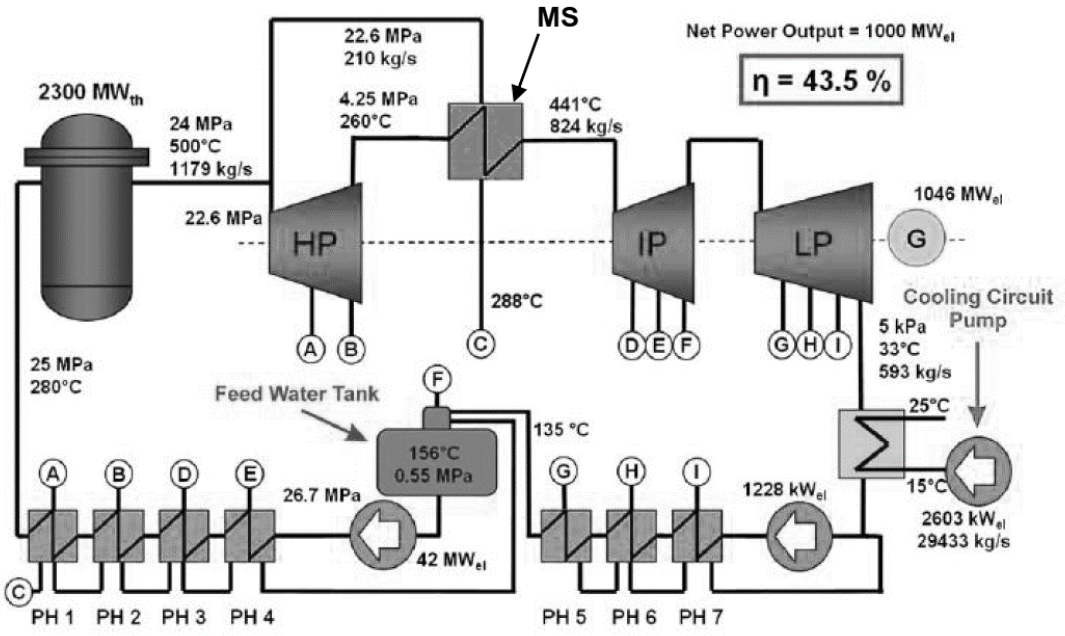

Figure 1: HPLWR steam cycle heat flow diagram (Brandauer, 2009).

Figure 1 shows the improved cycle as proposed by Schlagenhaufer et al. (Brandauer, 2009). In brief, the water is heated by the HPLWR, thereafter the steam is expanded in a high-pressure turbine (HPT) and dried by a moisture separator (MS) before entering consecutively an intermediate pressure turbine (IPT) and a low-pressure turbine (LPT). The two-phase mixture is then condensed into a liquid so that it can be pumped through three preheaters (PH 7 to PH5). In the different preheaters, water is heated by steam which is extracted from the LPT. The feed water from the PH's is then further heated in a feed water tank (FWT) by the direct mixing of the feed water with steam extracted from the IPT. The feed water is pumped through another set of four preheaters (PH4 to PH1) before it enters the reactor (Brandauer, 2009) (Schulenberg, 2011).

To heat the feed water in various stages is known as regenerative heating with the main purpose of increasing the thermal efficiency of a Rankine cycle (Hochreiter, 2004). Regenerative heating is also known as feed water heating which requires the use of heat exchangers. These heat exchangers can have a direct contact configuration, known as an open feed water heater (OFWH), or an indirect contact configuration known as a closed feed water heater (CFWH) (El-Wakil, 1984) .

In the HPLWR cycle, the preheaters are closed type feed water heaters and the feed water tank is an open feed water heater (Brandauer, 2009). Within the FWHs steam is used to increase the feed water temperature. Although the purpose of the FWHs is similar their configurations do differ. Within the CFWH water is indirectly heated, this means that the steam and water are kept separate and the heat is transferred through a separating wall. On the other hand, the OFWH allows for direct heat transfer and this is done by injecting steam into the feed water (El-Wakil, 1984).

When modelling the HPLWR system and the individual components, it is more commonly assumed that the fluids are in a state of thermodynamic equilibrium to simplify the simulation (Rastogi, 2008). Another approach would be to incorporate a more detailed non-equilibrium model. The advantage of using a non-equilibrium approach is that it more accurately describes the behaviour of the flow conditions in an actual system (Green & Perry, 2008).

1.2 Need for research

The main purpose of a FWH in a power plant (coal or nuclear) is that of regeneration. Regeneration increases the efficiency of a Rankine cycle and thus it is very important to understand how a FWH and more specifically the OFWH operates.

There are various approaches to model the OFWH, with the most basic approach to assume that it is in a state of equilibrium. This assumption makes calculations regarding the properties of the fluid less complex but does not necessarily give an accurate representation of the actual conditions in the OFWH. Another approach will be to model the steam-water mixing process in the OFWH using a non-equilibrium two-phase flow approach. This will result in a more complex model but should give more accurate answers when compared to the actual conditions within an OFWH. A need exists to compare these two approaches and determine what the advantages will be using the more complex non-equilibrium modelling.

1.3 Focus of this study

The focus of this study is to investigate the accuracy when predicting the operating conditions of an OFWH when applying a non-equilibrium modelling approach compared to an equilibrium approach.

1.4 Research objectives

The main research objectives for this study include:

- Develop an OFWH simulation model using an equilibrium approach.
- Develop a two-phase non-equilibrium transient simulation model of the OFWH, including:

- A bubble formation model when steam is injected into the feed water. This model includes the bubble formation diameter, bubble velocity and the mass of the steam bubble.
- A bubble ascension model for when a steam bubble ascends through the feed water. As the bubble ascends energy and mass are transferred from the steam to the feed water.

- Evaluate the accuracy when predicting the operating conditions of an OFWH when applying a non-equilibrium modelling approach compared to an equilibrium approach.

1.5 Method

The following method will be employed in this study:

- Research the HPLWR power generation cycle and the purpose of the regenerative heating process. Understand the function of the open feed water and the influence it has in the regenerative heating process.
- Research and evaluate methods to simulate the open feed water heater using an equilibrium approach and a non-equilibrium approach.
- Create a simulation model of the OFWH using an equilibrium approach in the fluid dynamics software Flownex (Anon., 2012). The purpose of the simulation is to illustrate the basic theory of the OFWH and to illustrate different theoretical operational conditions of the open feed water tank. The simulation model will be verified with the information published by Schlagenhaufer et al (2008).
- Flownex will be used to simulate the OFWH when it is subjected to a non-equilibrium state in which mass flow and temperature changes are incorporated so that the operational incidents on the OFWH can be determined.Flownex in conjunction with Engineering Equation Solver (EES) (Anon., 2014) will form the final integrated non-equilibrium transient simulation model. Flownex simulates a control volume according to equilibrium steady state heat and mass transfer equations. However, Flownex can simulate the OFWH for a non-equilibrium two-phase mixture when an EES subscript is included into the Flownex model. The EES subscript incorporates bubble formation and ascension models. Within dedicated time steps, the heat and mass transfer will be determined, along with parameters which are key factors during the formation and ascension. The integrated simulation model will then be used to predict transient state property changes of the open feed water heater when subjected to a state of non-equilibrium and compared to the results obtained from the equilibrium approach.

2 Literature study

The literature study will first review the research and design work that has been done on the HPLWR with the focus on the primary and secondary systems of its power generation plant. Within this chapter regenerative heating, in particular, open feed water heating and current non-equilibrium two-phase flow mixing processes in modern feed water heaters will also be reviewed. The effect of inaccurate design on operating conditions in feed water heating will be explored. The main focus of the literature study will then be on the thermal fluid modelling of open feed water heaters along with available mathematical bubble behaviour models developed for the formation and ascension of a superheated steam bubble in a sub-cooled liquid.

2.1 HPLWR concept and feed water heating

The High-performance Light Water Reactor (HPLWR) is a rather new concept in terms of research but its predecessor the Super Critical Water Reactor (SCWR) dates back to the 1950's. The design concept of the SCWR is discussed in more details in Appendix A.1. The HPLWR concept has been modified to suit various design and application needs over the last few decades. According to Squarer et al. (2003), the HPLWR is a feasible and promising concept.

The HPLWR power plant layout design is based on two concepts. The primary circuit, described in more details in Appendix A.2, is based on the conventional design used for PWRs and BWRs. The secondary system, which is known as the steam cycle, is based on fossil-fired power plants that operate at supercritical steam conditions (Schulenberg & Starflinger, 2012).

The main advantages of the HPLWR power plant are that the system is more compact and less complex than that of the SCWR. The concept eliminated the re-circulation of steam-water separation, the steam generator, the pressurizer and all primary piping which forms part of the PWR cycle. The use of a supercritical water coolant in the once-through cycle has the advantage of a higher enthalpy rise in the core along with a lower flow rate of the coolant and a higher thermal efficiency. Designs used for supercritical fossil fuelled power plants can be used for the balance of the plant. These designs include the water chemistry, the filtration system, the turbines, the feed water pumps and the heaters.

System optimisation, improvements and analysis were continuously done by a team of researchers and the work was presented at the 6th International Symposium on Supercritical Water-Cooled Reactors (ISSCWR) held during March 2013 in China.

2.1.1 Secondary system: Steam cycle

The secondary system represents the steam cycle of the HPLWR power plant. The fossil fuelled power plant that served as a foundation for the HPLWR power plant design was Unit K of the Niederaussem power plant in Germany and has been in operations since 2003 (Schulenberg & Starflinger, 2012). Niederaussem is one of the largest coal-fired plants in the world; the power generation plant consists of ten preheaters of which the number seven preheater is a feed water tank (Schulenberg & Starflinger, 2012). The layout of the Niederaussem power plant in Germany is illustrated in more details in Appendix A.3.

In 2004 Bitterman et al. re-evaluated the steam cycle that they helped to design in 2001, and adopted the cycle designed by Dobashi et al. in 1998.

The concept cycle of Bitterman et al. was improved on in 2008 by Schlagenhaufer et al. (Brandauer, 2009). The improvements made by Schlagenhaufer et al. were those of more realistic pressure drops and the elimination of a

pre-heater. A simulation of full load conditions was also done which solved the mass- and heat balance equations. The cycle designed by Schlagenhaufer is illustrated in Figure 2 (Brandauer, 2009).

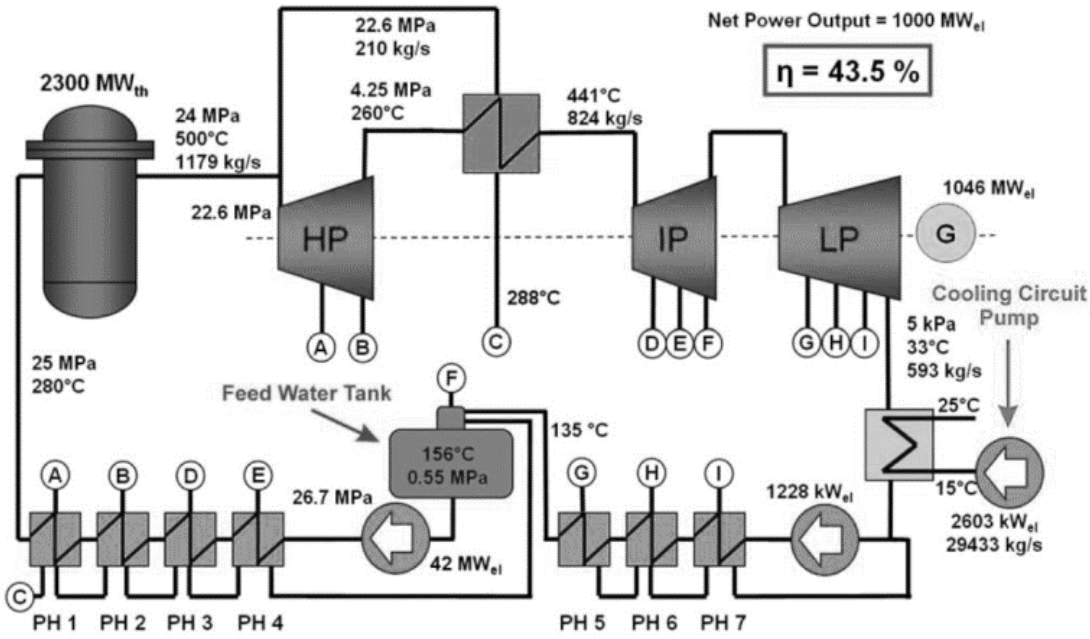

Figure 2: Diagram layout of the HPLWR power generation cycle after optimisation (Brandauer, 2009).

Additional optimisation was done in 2009 by Brandauer et al., with the main focus to generate a more realistic efficiency while maintaining a low capital cost (Brandauer, 2009). The initial core design parameters and characteristics were slightly altered, with the minor changes that were made being those of applying more realistic component efficiencies (such as isentropic, mechanical and electrical efficiencies) and taking various pressure drops into consideration.

The major changes involved a reduction in the number of re-heaters, preheaters and condensation pumps as well as the addition of a cooling water pump (to supply the condenser).The inlet water temperature to the condenser was changed from 10°C to 15°C, due to an averaged water temperature coming from the cooling towers. The temperature of the water flowing out of the condenser may only increase with 10°C, resulting in a temperature of 25°C. A feed water tank was also added and serves as a large buffer which reduces irregularities of the mass flow rate of the feed water. The feed water tank eases the control of the steam cycle and aid in the removal of non-condensable gases. (Brandauer, 2009)

Regenerative feed water heating is critical for an improved cycle performance in Rankine-cycle type power plants (El-Wakil, 1984), where feed water is heated by vapour which is bled from various turbine stages. The heating is divided into finite heating stages and occurs within a feed water heater. According to El-Wakil steam power plants usually consist of five to eight feed water heating stages (El-Wakil, 1984). Within the feed water system, there are two main types of FWH's, namely open feed water heaters and closed-type feed water heaters, and it is important to determine which is used within the steam cycle and what role it has.

A higher heat transfer rate is achieved by an open feed water heater. The different process streams consist of a superheated gas which is dispensed in bubble form into the second medium (Ribeiro & Lage, 2004). The purpose of steam injection is to raise the temperature of the water so that it can enter the boiler at the required temperature. Due to technology improvements, the concept of the open feed water has also improved in design and material selection. Some of the more modern concepts are discussed in Appendix A.4.

Open feed water heating allows for deaerating of the main condensate feed (Tordeas & Kazimi, 1990).Deaerating is also one of the main functions of a feed water tank and is required due to the formation of oxygen which is produced by the dissociation of water within the core as a result of radiation. Oxygen and non-condensable gases are then eliminated through the exhaust pipe, as this is only possible because oxygen's solubility is zero in saturated water conditions. No steam should exit the feed water tank and therefore the steam is cooled with the water from PH5 as illustrated in Figure 2. (Lemasson, 2009).

In the proposed thermodynamic cycle designed by Schulenberg et al., a range of seven closed feed water heaters are suggested to serve as feed water preheaters, with an open feed water heater to serve as a feed water tank (Schulenberg & Starflinger, 2012).

2.1.2 HPLWR: Open feed water heater

Lemasson (Lemasson, 2009) designed the feed water tank for the HPLWR steam cycle, as illustrated in Figure 3. The feed water tank consists of two chambers which are divided by a separation wall. In the separation wall, there are two holes. The first hole is located in the steam area, and the second in the water area at the bottom of the tank (Lemasson, 2009).

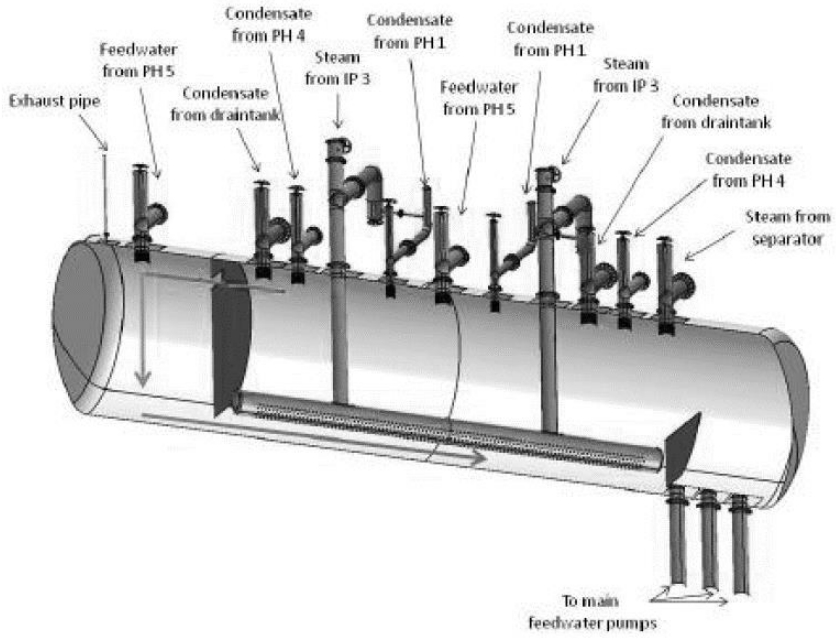

Figure 3: Illustration of the feed water tank as designed by Lemasson (Lemasson, 2009).

Figure 4 illustrates the designed in- and outlet conditions of the OFWH at full load. At full load water from pre-heater 5 (PH5), condensate from pre-heater 4 (PH4) and vapour from intermediate pressure turbine 3 (IPT 3) are collected and fed directly to the feed water pumps. The water fed to the pumps is at saturation conditions with a temperature of 155.6°C and a pressure of 0.5513 MPa. The feed water has a dual purpose during full load operating conditions; the initial purpose is to serve as a preheater and secondly to serve as a water reservoir (Lemasson, 2009).

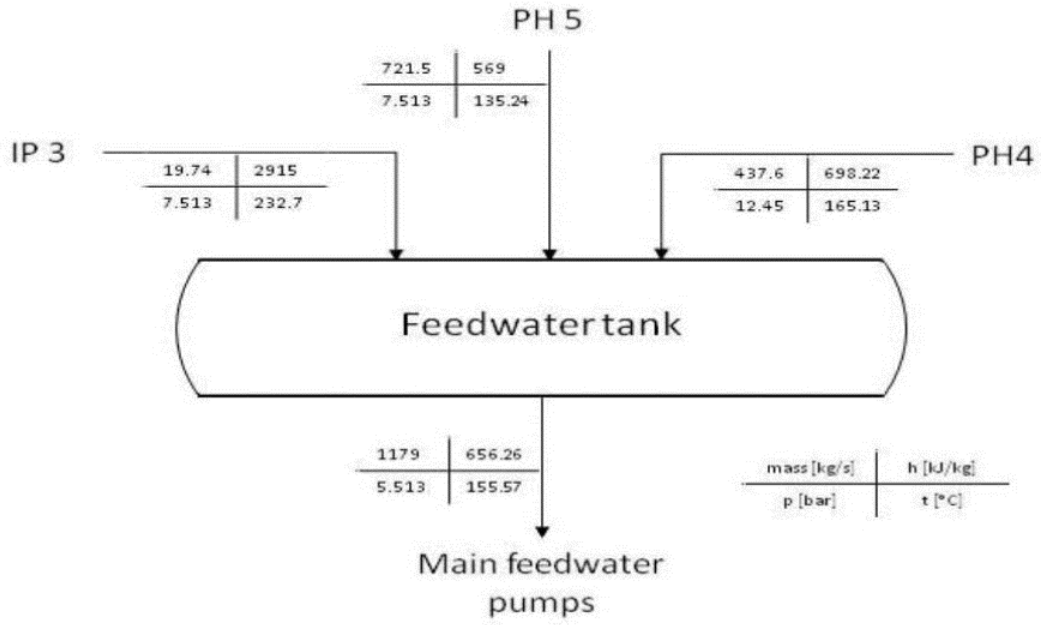

Figure 4: Diagram of inlet and outlet streams of the feed water tank during full load conditions (Lemasson, 2009).

During half to full load operation, 50% of the water from PH5 is sprayed into the first chamber and is heated by steam that cascades back from PH4. The steam is cooled down by the water and is partially condensed (Lemasson, 2009). The other 50% of the water from PH5 is sprayed into the second chamber to condense the remaining steam. The water level in the second smaller chamber increases due to condensation of steam. The condensate from the second chamber flows to the third chamber, within the third chamber steam from IPT3 is injected into the water and heat the water to 155.6°C. Saturation conditions are achieved by the circulation of water between the chambers (Lemasson, 2009).

Furthermore, Lemasson (2009) dimensioned the FWT based on the following conditions. If the HPLWR were to produce 2300MW_{th}, the tank had to have a theoretical volume of 350m^3. However, the real inner volume was 370m^3 due to a diameter of 4800 mm and a length of 21156 mm. This was determined by the extrapolation of data available for a range of smaller manufactured FWT's. From these basic dimensions Lemasson (2009) went on and determined the working pressure at full load conditions which is 0.5513 MPa. However, in a worst case scenario the pressure increases to 0.593 MPa due to hydraulic thrust. On top of that an additional 20% safety margin has been chosen to include a possibility of heterogeneity of the pressure in the FWT (Lemasson, 2009).

2.1.3 Effect of inaccurate design and operating conditions in feed water heating

The focus of this study is to investigate the accuracy when predicting the operating conditions of an OFWH when applying a non-equilibrium modelling approach compared to an equilibrium approach. In this section the influence and effect that inaccurate design and operation conditions on a nuclear power generation plant will be reviewed.

The U.S Nuclear Regulatory Commission issued a notice in 1996 that addressed the operation of PWR's above their licensed power limit due to inaccurate design and operating conditions. The increase in licensed thermal power was caused by the lowering in feed water temperatures. The notice also addressed that a reduction in feed water temperature may affect the accuracy of nuclear measuring instrumentation (Grimes, 1996).

According to the notice, The Comanche Peak Steam Electric Station (unit 2) operated at 95% of the rated thermal power. A reduction in feed water temperature occurred due to the loss of the feed water heaters. The reduction in temperature caused a decrease in the reactor coolant system cold leg temperature. A colder reactor coolant temperature caused the reactor power to increase to 102%. The turbine runback was initiated to counter the increase in reactor power and the plant stabilised at an indicated 97%.

Ninety minutes later a second turbine runback occurred while the plant tried to restore the balance of equipment, the reactor power was yet again stabilised at 100%. For 30 minutes the reactor operated at 100% power; however, the reactor coolant temperature was lower than normal. It was noted that the detection system indicated that the reactor was running at 106% power, however, the computer-based plant calorimetric meter system indicated 102% power operation.

From the occurrence, it was noted that with the loss of secondary plant efficiency the average temperature approach used can no longer predict the core thermal power reliably. It was also noted that for cold feed water the calorimetric meter system may not be accurate, and lastly, the transient was not accurately analysed in the final safety report.

After the second runback, the nuclear instrumentation indicated a reactor power of 100%, it was known that cold feed water could cause an increase in neutron attenuation. The amount of neutrons reaching the detectors was affected due to the cold-leg temperature decrease. The analysis indicated that for every 0.6°C cold-leg temperature difference, the nuclear instrumentation was affected and there was a 0.6-0.8% error in the measurement of reactor power (Grimes, 1996).

2.2 Thermal fluid modelling of open feed water heaters

This section will summarise the research done on two-phase flow including the heat and mass transfer of steam bubbles in feed water heaters. The direct contact evaporator is in principle a non-isothermal bubble column through which superheated gas is bubbled. A sparger, which is a perforated plate or tube, is located at the bottom of the column and is responsible for the bubble formation (Ribeiro & Lage, 2004). The steam bubbles account for the largest amount of the energy transferred to the feed water, with the remaining energy transferred via latent energy through the material of the sparger and the gas chamber walls (Ribeiro & Lage, 2004).

During operation when steam is at supercritical temperatures, a natural energy flux forms in the steam bubble. The temperature at the centre of the bubble is higher than at the surface. Heat transfer occurs at the interface of the bubble surface with the surrounding fluid (Ribeiro, 2004). Heat and the mass transfer happens simultaneously which heats up and vaporise the liquid phase. Gas holdup does occur within a direct contact heater however it can be neglected due to the minimal influence of the gas holdup on the energy transfer process.

Thus the two-phase process can be modelled by using a simultaneous heat and mass transfer approach for a single superheated bubble. The bubble is formed from a submerged orifice which is located on the surface of a sparge tube, after which it detaches and ascends through a continuous liquid phase (Campos, 2000 a).

To understand the heat transfer between steam bubbles and the surrounding liquid, the mathematical bubble models developed by three different studies will be discussed, namely Campos and Lage (2001), Kolev (2011), and Kalman and Mori (2002).

2.2.1 The Campos and Lage model

Campos and Lage (2011) developed two models namely a formation and ascension model, and then also a homogeneous direct evaporator model. These models will be discussed below.

2.2.1.1 The formation and ascension model

The formation volume of the bubble is determined by a model developed by Davidson and Shüler (1960). Davidson and Shüler assumed that internal pressure gradient of the bubble are minimal and therefore maintain a constant pressure due to short column height, resulting in the exclusion of the momentum conservation equation. It is also assumed that the bubble is spherical, that there is no circulation inside the bubble and the gas phase is an ideal binary mixture of air and water vapour. The study also assumed that a state of equilibrium exists at the bubble's surface and that there are no additional energy sources present in the system, and finally that viscous dissipation can be neglected.

The model developed also includes the complete heat and mass transfer phenomena which can be associated with the ascension of a superheated bubble. It incorporates the simultaneous solution of the continuity, energy, momentum and chemical species conservation equations, along with the following assumptions.

The change in the bubble radius is solved by coupling the conservation equations and the bubble dynamics model. The superheated bubble model consists of a gas-phase heat and mass transfer sub-model, a liquid phase and interface sub-model, a bubble dynamics sub-model along with a physical property evaluation sub-model. The models are all coupled and the results gained were verified with experimental data (Campos, 2000 a).

The gas-phase heat and mass transfer sub-model assume that the bubble is spherical and that the spherical residual bubble is formed at an orifice and then grows during the formation stage (Campos, 2000 a). The liquid phase model assumes that there is only pure water and thus no mass transfer. The bubble to liquid heat transfer coefficient was estimated by an analogy that incorporates the Calanderbank and Moo-Young correlation of the mass transfer of small bubbles (Campos, 2000 a).

The bubble formation diameter, frequency, bubble ascension velocity and bubble-liquid heat transfer coefficient are variables that should be determined and used within the Campos and Lage model. All of these parameters can be determined by supporting literature which was written by Davidson and Schuler in 1960, Karamanev in 1994, Calanderbank and Moo-Young in 1960 and many others (Campos & Lage, 2000).

2.2.1.2 The homogeneous direct evaporator model

Campos and Lage (2001) developed a dynamic model of a direct contact evaporator, which consists of a liquid-phase and a gas feed model, coupled to a superheated bubble model. The superheated bubble model takes into account the heat and mass transfer during the formation and ascension stages and predicts the gas holdup in non-isothermal systems. Verification showed that a good agreement had been found between the transient behaviour of the liquid-phase temperature and vaporisation rate when the model was subjected to quasi-steady state. The transient behaviour of the column height could not be verified to the same extent (Campos & Lage, 2001).

The entire model operates in two different time frames. The first takes several hours to achieve steady state and the second is that of the bubble residence time which occurs within seconds. Due to this, the model scale decomposition should be used so that dynamic models can be created for the two time frames (Campos & Lage, 2001).

The liquid-phase model includes the heat and mass balances in the evaporator and requires parameters like the transient values for gas-holdup, vaporisation rate, and rate of heat transfer from the bubbles to the liquid. These parameters are determined in the superheated bubble model making use of the continuity, energy and species conservation equations which are coupled to a bubble dynamics model designed by Campos and Lage in 2001 (Campos & Lage, 2001).

2.2.1.3 The Kolev model

In 2011, Kolev published a monograph that contained theoretical and practical experience in terms of research done on complex transient multiphase processes (Kolev, 2011). The purpose of the monograph was to enable scientists and engineers to understand industrial and natural processes containing the evolution of complex multiphase flows (Kolev, 2011). One of the main topics that Kolev focused on was the condensation of a pure steam bubble in the sub-cooled liquid. In the study, Kolev described various methods to determine the bubble collapse due to vapour condensation in sub-cooled liquids. The collapse of a stagnant bubble and a bubble in motion were determined. Heat transfer increases as the bubble motion increases through the bulk liquid and therefore the condensation of the bubble also increases (Kolev, 2011).

Kolev documented various correlations for the average heat-transfer coefficient. The correlations were based on the turbulence of the bulk liquid along with an average heat transfer coefficient correlation based on whether a swarm of bubbles were injected as well as whether bubbles had internal circulation or not. The main difference between the correlations that Kolev documented was that of a one component system and a two-component system. A one component system was described by Hunt in 1970 and the two-component system was researched by Isenberg and Sideman (Kolev, 2011). The correlations developed by Hunt and Isenberg were all theoretical. A correlation that was based on experimental data was published by Moalem and Sideman in 1973 and was also included in Kolev's monograph (Kolev, 2011). The correlation of Moalem and Sideman will be discussed in more details in the following section.

2.2.1.4 Moalem and Sideman

The effect of motion on a bubble collapsing was described by Moalem and Sideman, 1973. The article described a correlation that can be used to determine the effect of bubble velocity on the mass transfer rate of a single bubble. The correlation allowed for a single or a two component system as well as a pure system or the inclusion of non-condensable particles. A steam and water system is described by Moalem and Sideman as a single component system, with a two-component system typically similar to pentane in water. The experiment consisted of a steam bubble injected into a sub-cooled liquid by means of a nozzle and the bubble is assumed to rise freely in the bulk liquid. The experiment also allowed for small ($R<0.1cm$) and large bubbles ($0.2cm<R<0.4cm$), with the large bubbles exhibiting a constant rise velocity (Moalem & Sideman, 1973).

2.2.1.5 The Kalman and Mori model

In 2002 Kalman and Mori published an article on the experimental analysis of a vapour bubble condensing in sub-cooled liquid. In the study, they focussed on the dynamics of a bubble condensing in both a miscible and an immiscible liquid including the heat transfer thereof. They investigated the effect of the shape of the bubble along with its rigidity, and the inclusion of incondensables on the velocity and heat transfer. Kalman and Mori developed empirical correlations for the drag coefficient and Nusselt number for a range of experimental parameters (Kalman & Mori, 2002).

According to Kalman and Mori vapour bubble, condensation is an important phenomenon that occurs in liquid-vapour two-phase flow when the liquid temperature is lower than the saturation temperature of the vapour species. The bubble collapse is controlled either by inertia or heat transfer. If the bubble collapse is controlled by inertia then high liquid sub-cooling is present. If the sub-cooling is low then the bubble collapse is caused by heat transfer at

the vapour species interface. The collapse process due to heat transfer is very complex to model because the collapse rate is controlled by internal and external resistances as well as the temperature driving force. Other parameters that also influence the bubble collapse include the bubble shape, the rising velocity and whether the surrounding bulk liquid is miscible or immiscible (Kalman & Mori, 2002).

The rise velocity can be assumed as constant, which contributes to the simplification of the heat transfer bubble collapse model. The assumption of constant rise velocity has been proposed by many researchers and yields a reasonable approximation. If the rise velocity is not taken as constant then the delivery system of the bubble should be analysed as this determines the velocity of the bubble as it detaches and whether deceleration will occur after collapsing has occurred. Deceleration may alter the shape of the bubble as it may cause the envelopment of the bubble into its own wake (Kalman & Mori, 2002).

Kalman and Mori also investigated the heat transfer data published by Isenberg and Sideman, 1970. They stated that the theoretical models were accurate but required complicated analysis and numerical solutions (Kalman & Mori, 2002).

2.3 Conclusion

Table 1 lists the advantages and disadvantages of the mathematical models evaluated. Based on this, the work done by Campos and Lage as well as Kolev was selected for implementation in this study. Chapter 3 will discuss in more details all the relevant correlations to be implemented in the simulation model developed as part of this study.

Table 1: Comparison between mathematical models

Model	Advantages	Disadvantages
The Campos and Lage model (2011)	1) Multiple articles were published by the authors showing the progress of their model development. 2) The simulation model uses a simplified approach thus eliminating complex numerical analysis. 3) The formation model is verified (Davidson and Shüler). Thus proven to be accurate.	1) The model developed to describe a heat and mass transfer for a single bubble column is complex and requires intensive numerical mathematic modelling.
The Kolev model (2011)	1) Research is based on other published articles that can aid in the verification of the model. 2) The heat transfer model of Kolev is a simplified approach and can easily be incorporated into a simulation model. 3) The mass transfer model of Moalem and Sideman used can easily be incorporated into any simulation model. The model is verified and thus proven to be accurate. The mass and heat transfer of a bubble is dependent on one another and thus if the mass transfer of the bubble is verified then the heat transfer of the bubble will also be correct.	1) Experimental results to verify Kolev's heat transfer model were not published in the monograph.

Model	Advantages	Disadvantages
The Kalman and Mori model (2002)	1) Kalman and Mori's and Kolev's mathematical models are similar. 2) The theory and basic principles of the mathematical models developed are widely used.	1) Experimental results to verify the model is mainly focused on two-phase systems such as pethane-water.

3 Theoretical background

As mentioned in Chapter 1, the aim of this study is to determine whether it is more beneficial to model the open feed water heater using a non-equilibrium approach compared to the conventional equilibrium approach. This chapter will discuss the details of the correlations that were implemented in the models developed as part of this study.

This chapter will focus on the non-equilibrium approach to model an OFWH based on the Lemasson design. The non-equilibrium approach will include the modelling of a single and a multiple bubble column within a two-phase fluid, with the main focus on bubble heat and mass transfer during the formation and ascension stages until the bubble depletes. The equilibrium approach will first be briefly mentioned with the details given in Appendix B.1.

3.1 Equilibrium approach

There are two methods of pre-mixing for steady state approach, with the first consisting of single stage mixing and the second will consist of multi-stage mixing, which is described in more detail in Appendix B.1. For this approach, it is assumed that equilibrium conditions exist throughout thus there is no tendency to spontaneously change with time (Koretsky, 2004).

3.2 Non-equilibrium approach

As illustrated in Figure 5 and Figure 6, a state of non-equilibrium will only be applied to the third chamber of the feed water heater where two fluid streams of different phases are directly mixed. Superheated steam vapour is used to heat the saturated feed water, with the steam passing through a sparge tube. Bubbles are formed which transfers energy to the surrounding water mass as they move upward inside the chamber, resulting in an increase in the temperature of the surrounding water mass.

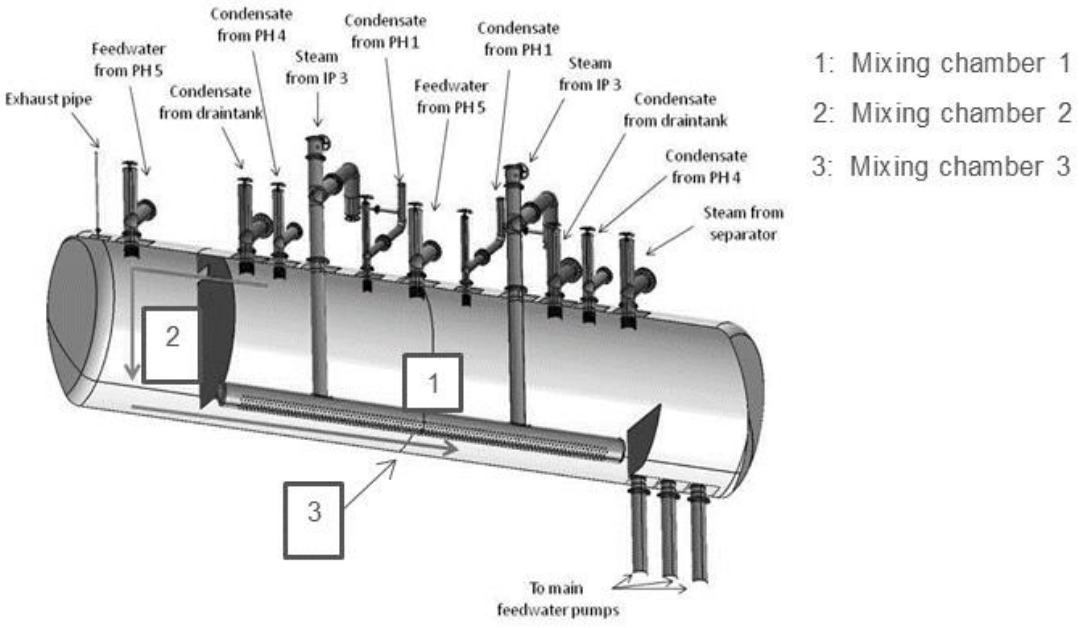

Figure 5: Open feed water tank with indicated mixing chambers (Lemasson, 2009).

The sparge tube through which the steam is injected contains multiple orifices facing in various directions meaning that the bubbles can be forced in a downward direction or in an upward direction relative to the tank. Some of the bubbles will be injected downwards however due to buoyancy the bubbles will at some point in time stop moving

downward and will start to accelerate upward. On the other hand, bubbles injected from the top face of the sparge pipe will only accelerate upward. To simplify the model it will be assumed that all bubbles will accelerate in an upward direction from the surface of the sparge tube.

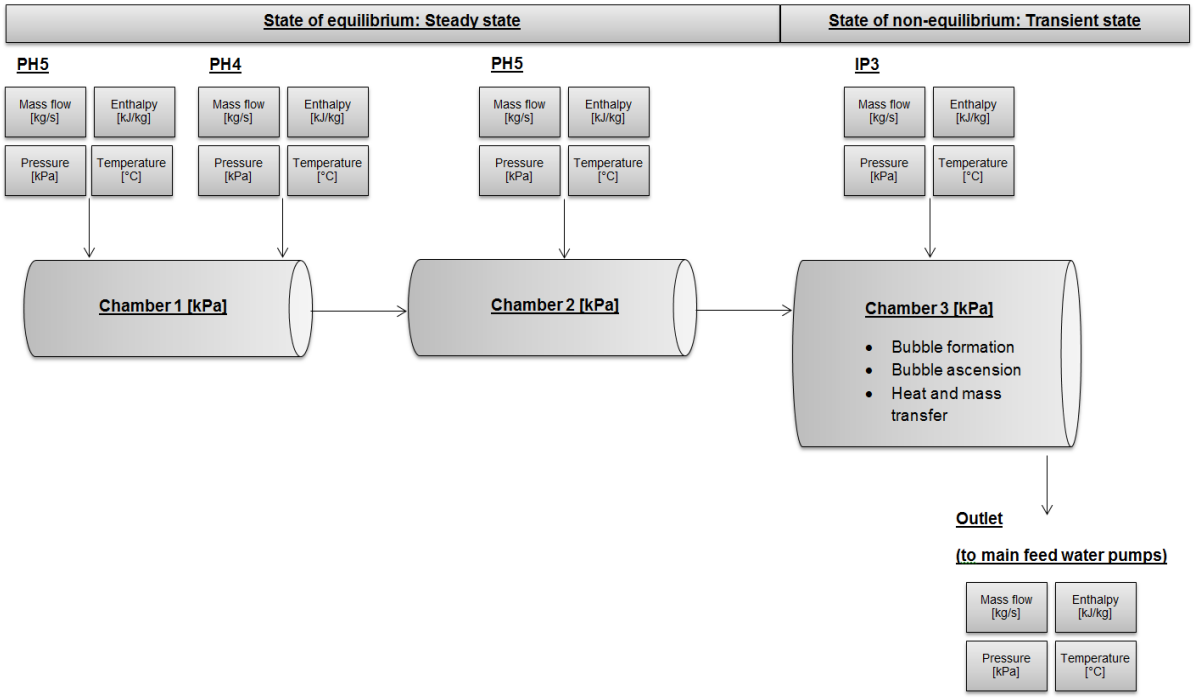

Figure 6: Diagram of integrated model equilibrium and non-equilibrium processes.

3.2.1 Single bubble column

As part of the development of the non-equilibrium model, a single bubble column will first be modelled. The bubble column is divided into two stages consisting of the formation of the bubble at an orifice, followed by the ascension of the bubble until it condenses.

3.2.1.1 Bubble formation

As steam is injected through the sparge tube, multiple bubbles start to form at the orifice holes and grow as steam is injected, as illustrated in Figure 7. Once the bubble becomes a certain size, which is dependent on the orifice size and the velocity of the steam injected, it detaches from the orifice, thus terminating the formation phase. The time required for the bubble to grow until detachment is known as the formation time. When the formation is terminated the bubble has a certain volume that is dependent on the formation diameter. The formation time and volume are very important parameters as it will serve as the initial conditions for the bubble ascension phase (Campos & Lage, 2000).

It is also important to note that during the formation phase energy is transferred from the steam bubble to the liquid, but this it is rather difficult to model. To simplify the model in the formation phase, the formation energy will be neglected from the study and the formation variables will only serve as initial conditions (Davidson & Shüler, 1960).

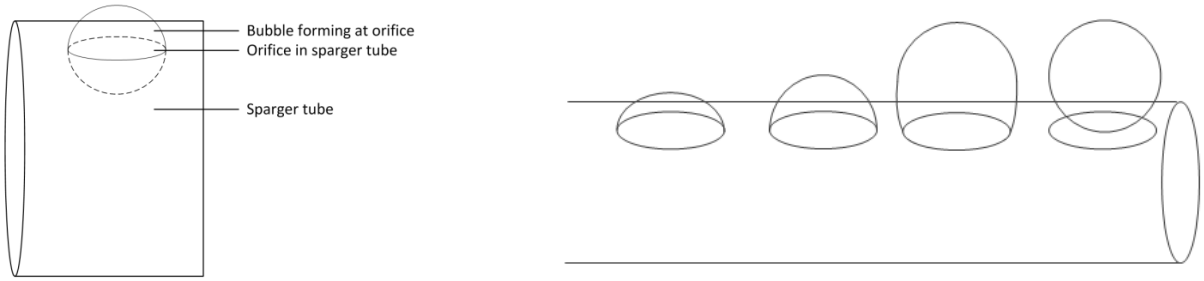

a) **b)**

Figure 7: a) Formation of a bubble through the sparging tube and b) bubble formation stages up until detachment.

Bubble formation: volume and time

After the steam has been extracted from the turbines it is injected into the feed water through multiple orifice holes. It will be assumed that the steam flow is divided equally between all of the orifice holes (Lemasson, 2009). The number of holes required is determined based on the known mass flow rate along with the desired speed of the steam. The total number of holes can be determined as follows (Lemasson, 2009):

$$\#_{orifice} = \left(\frac{4\dot{m}_{steam}}{\rho_{steam} v_{steam} \pi {d_{orifice}}^2}\right) + 1 \quad (3.1)$$

$\#_{orifice}[-]$ is the total number of orifice openings, $\dot{m}_{steam}\left[\frac{kg}{s}\right]$ is the mass flow rate of the steam, $\rho_{steam}\left[\frac{kg}{m^3}\right]$ is the density of the steam; $v_{steam}\left[\frac{m}{s}\right]$ is the velocity of the steam; and $d_{orifice}[m]$ is the diameter of the orifice opening. Once the total number of holes is determined the formation diameter and formation time of a single bubble can be calculated.

Campos and Lage (2000) incorporated the mathematical model of Davidson and Shüler (1960) who did an experimental and theoretical investigation into the formation of gas bubbles in an orifice for an inviscid liquid. The aim of the investigation was to describe the theory of bubble formation to estimate the bubble size and frequency. If a constant average gas flow rate is assumed, the method to determine the bubble size and velocity is summarised as follow.

The bubble is assumed to always be spherical during formation. Furthermore, the forces acting on a bubble, the buoyancy, and the upward mass acceleration of the fluid surrounding the bubble are always balanced. The upward motion is described by:

$$V_{bubble} * g = \frac{d}{dt}\left(\frac{11}{16} V_{bubble} \frac{ds}{dt}\right) \quad (3.2)$$

V_{bubble} is the volume of the bubble after time t, whereas s is the vertical distance from the centre of the bubble above the point where gas is injected. Davidson and Shüler (1960) assumed the flow of the surrounding bubble is non-rotational and not separated. The effective inertia, I, of the surrounding fluid is calculated as follows:

$$I = \frac{11\rho V}{16^3} \quad (3.3)$$

The drag coefficient is zero due to the sphere accelerating from a stagnant position in the fluid. The sphere's initial motion is non-rotational, and the wake is not yet fully established until it has moved an appreciable distance.

With a constant average gas flow rate through an orifice , $\dot{V}_{steam}$

$$\dot{V}_{steam}\left[\frac{m^3}{s}\right] = v_{steam}\left[\frac{m}{s}\right] * A_{orifice}[m^2] \;\; ; \;\; A_{orifice} = \pi {r_{orifice}}^2 \quad (3.4)$$

and the initial bubble volume taken as zero, the volume of the bubble is described by:

$$V_{bubble}[m^3] = \dot{V}_{steam}\left[\frac{m^3}{s}\right] * (t) \quad (3.5)$$

Equation 3.5 is substituted into Equation 3.2 and then integrated with the boundary conditions: $t = 0$ and $\frac{ds}{dt} = 0$.

It is assumed that the bubble has detached when the vertical distance moved, s, is equal to the radius, r, of the bubble at the moment it detaches as illustrated in Figure 8. The bubble volume can then be described by:

$$V_{bubble}[m^3] = 1.378 * \frac{\dot{V}_{steam}{}^{\frac{6}{5}}}{g^{\frac{3}{5}}} \quad (3.6)$$

As soon as a bubble detaches from an orifice a volume of gas is left behind, which is the nucleus of the next bubble to be formed, defined by $V_{bubble,initial}$. For smaller orifice diameters this volume can be neglected, however for larger diameters it needs to be taken into account. Therefore the detachment volume consists of the initial bubble volume that remained in the orifice as well as the volume of the bubble due to steam injection.

$$V_{bubble,detachment}[m^3] = V_{bubble}[m^3] + V_{bubble,initial}[m^3] \quad (3.7)$$

with

$$V_{bubble,detachment}[m^3] = \frac{4}{3}\pi r_{detachment}{}^3. \quad (3.8)$$

and

$$V_{bubble,initial}[m^3] = \frac{4}{3}\pi r_{orifice}{}^3. \quad (3.9)$$

For larger orifice diameters the equation for upward motion is integrated and the initial conditions used are $s = 0$ and $\frac{ds}{dt} = 0$, resulting in the vertical distance moved by a bubble described by:

$$s = \frac{16g}{11}\left[\frac{t^2}{4} + \frac{V_{bubble,initial}\,t}{2\dot{V}_{steam}} - \frac{V_{bubble,initial}{}^2}{2\dot{V}_{steam}{}^2}\ln\left(\frac{\dot{V}_{steam}t + V_{bubble,initial}}{V_{bubble,initial}}\right)\right] \quad (3.10)$$

As illustrated in Figure 8, the bubble will detach when $s = r + r_0$ (Davidson & Shüler, 1960).

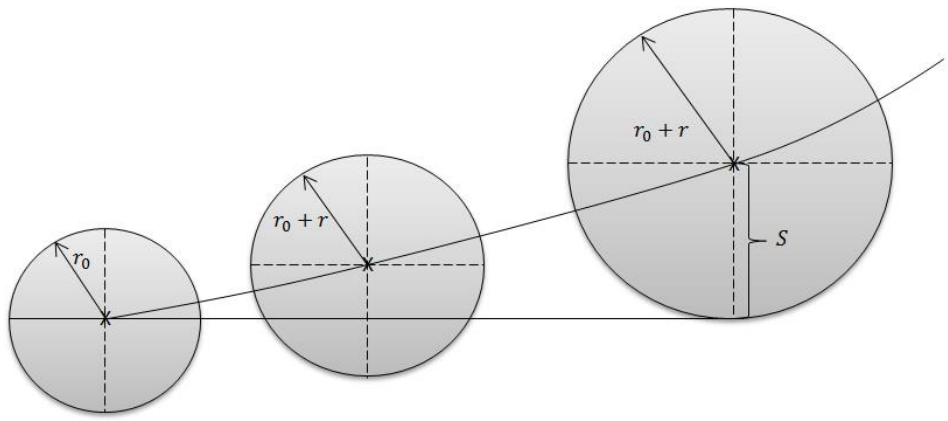

Figure 8: Bubble formation detachment parameters (Davidson & Shüler, 1960).

3.2.1.2 Bubble ascension

As soon as the bubble formation is complete and the bubble detaches from the orifice it enters the ascension stage. In the ascension stage, three processes occur simultaneously, namely the upward motion of the bubble and the mass and energy transfer (Campos & Lage, 2000).

While the bubble ascends through the water, the bubble surface cools down due to energy transfer from the bubble to the surrounding fluid. Mass is transferred to the surrounding bulk liquid due to the cooling and condensation of the steam bubble. The temperature at the centre of the bubble is greater than the temperature of the bubble surface, and once the centre reaches the temperature of the bulk liquid, the bubble depletes entirely. The three processes are simultaneously modelled to determine the bubble size, bubble temperature and position as illustrated in Figure 9.

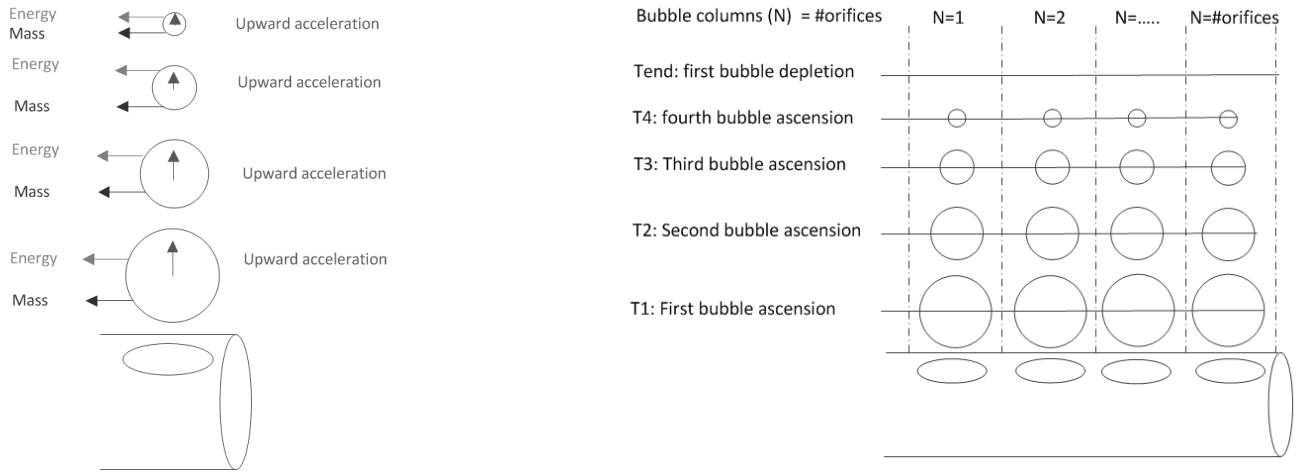

a) **b)**

Figure 9: Ascension of steam bubbles through a sub-cooled liquid whereas a) upward motion of a bubble as heat and mass are transferred and b) bubble column and ascension time intervals.

In Figure 9 it is assumed that the bubble will immediately start to transfer energy and mass to the surrounding medium as it moves upward. In Figure 9 (a) only a single bubble column is shown, with the total number of bubble columns equal to the total amount of orifice holes as shown in Figure 9 (b). One bubble column will be modelled with the remaining bubble columns a duplicate of the first. Thus for multiple bubble columns, it will be assumed that no bubbles coalesce to form larger bubbles.

Bubble ascension: velocity

During the initial stages of ascension, the bubble has an initial velocity. A method to determine the rise velocity of a single gas bubble has been developed by Karamanev (1994), for any size or shape through a quiescent liquid. The approach is based on the assumption that the recirculation within the bubble has no effect on its velocity, resulting in the drag coefficient of a bubble rising through the quiescent liquid being the same as that of a rising light solid particle. A second assumption that the approach is based on is that the drag coefficient of the bubble can be determined on the basis of the geometrical characteristics.

As the bubble rises through the medium the balancing force (Karamanev, 1994) is described as follows:

$$0.5 C_d A_{bubble} \rho_{liquid} U^2 = \Delta \rho g Vol_{bubble} \quad (3.11)$$

C_d is the coefficient of drag experienced by the bubble and is based on A_{bubble} which is the cross-sectional area of the bubble. ρ_{liquid} is the density of the surrounding liquid and $\Delta\rho$ is the absolute difference in density between the gas and the liquid, and g is the acceleration due to gravity. The volume, $Vol_{bubble,}$ of the bubble is also incorporated.

The area of the bubble should be calculated from the diameter projected from the horizontal plane.

$$A_{bubble} = \frac{\pi {d_h}^2}{4} \tag{3.12}$$

The volume should be calculated by using the equivalent diameter:

$$Vol_{bubble} = \frac{\pi {d_e}^3}{6} \tag{3.13}$$

Once volume and area are included into the velocity balancing equation then the rise velocity is calculated as follow:

$$U^2 = \frac{2\Delta\rho g Vol_{bubble}}{C_d \rho_{liquid} A_{bubble}} \tag{3.14}$$

The drag coefficient in the model is based on the drag curve for light particles.

$$C_d = \frac{24(1+0.173Re^{0.657})}{Re} + \frac{0.413}{1+16300\,Re^{-1.09}} \tag{3.15}$$

Where Re is the Reynolds number and is calculated as follows:

$$Re = \frac{\rho_{liquid} v_{steam} d_h}{\mu_{liquid}} \tag{3.16}$$

From the above equations, the rise velocity of the bubbles can be calculated and implemented in the model.

Bubble ascension: mass and heat transfer

Mass transfer and heat transfer occur as soon as the bubble starts to form at the orifice. Even though the heat and mass transfer during formation is significant it is rather complex to determine. To simplify the model it will be assumed that heat and mass transfer is not present during the formation of the bubble.

The transfer of heat and mass do occur during the ascension stage, resulting in a depleted steam bubble. In this section, it will be shown how to determine the heat and mass transfer during the ascension stage.

As mentioned in Chapter 2, Kolev (2011) published a monograph that contained theory and practical experience of research done on complex transient multiphase processes. The condensation of a pure steam bubble in a sub-cooled liquid is one of the topics that Kolev focussed on. Kolev adjusted the correlation of Moalem and Sideman (1973), distinguishing between pure vapour bubbles and impure bubbles, as well as small and large bubbles. The control volume described in his study includes pure large bubbles.

The Moalem and Sideman correlation for calculating the mass transfer, $\beta_{Moalem\ and\ Sideman}$, of a bubble within a time step is as follows (Moalem & Sideman, 1973):

$$\beta_{Moalem\ and\ Sideman} = \left[1 - \frac{3}{2}\left(\frac{k_v}{\pi}\right)^{\frac{1}{2}}\tau\right]^{\frac{2}{3}} \quad (3.17)$$

The correlation gives the ratio between the initial bubble radius and the new bubble radius,

$$\beta_{Moalem\ and\ Sideman} = \frac{R_{bubble,new}}{R_{bubble}} \quad (3.18)$$

in a dimensionless time step, τ. The dimensionless time step is calculated from the Jacob-, Peclet- and Fourier parameters of the two-phase system.

$$\tau \equiv JaPe_{liquid}{}^{\frac{1}{2}}\,Fo\ . \quad (3.19)$$

The correlation includes the velocity factor, k_v:

$$k_v = 0.25Pr^{-\frac{1}{3}} \quad (3.20)$$

The equation for the velocity factor is only applicable for a two component system, for a single component system $k_v = 1$. The simplified correlation can now be described as follows:

$$\beta_{Moalem\ and\ Sideman} = \left[1 - \frac{3}{2}\left(\frac{0.25Pr^{-\frac{1}{3}}}{\pi}\right)^{\frac{1}{2}} JaPe_{liquid}{}^{\frac{1}{2}}\,Fo\right]^{\frac{2}{3}} = \left[1 - 0.423\ Pr^{-\frac{1}{6}}JaPe_{liquid}{}^{\frac{1}{2}}\,Fo\right]^{\frac{2}{3}} \quad (3.21)$$

The correlation of the ratio published in Kolev is given by:

$$\beta_{Moalem\ and\ Sideman\ (Kolev)} = (1 - 0.846Re_{1o}{}^{\frac{1}{2}}Pr_{liquid}{}^{\frac{1}{2}}JaFo)^{\frac{2}{3}}. \quad (3.22)$$

Within the model equation, 3.22 will be used as it was specified by Kolev for a steam bubble in a sub-cooled liquid.

In order to calculate the ratio between the initial bubble radius and the new bubble radius, a few parameters which are based on the fluid properties need to be determined. The first variable is the thermal liquid diffusivity of the surrounding fluid, $\gamma_{liquid}\left[\frac{m^2}{s}\right]$, which incorporates the conductivity of the liquid, $k_{liquid}\left[\frac{W}{mK}\right]$, along with the density and the specific heat of the liquid represented by $\rho_{liquid}\ \left[\frac{kg}{m^3}\right]$ and $C_{p_{liquid}}\left[\frac{J}{kgK}\right]$ respectively. The thermal liquid diffusivity is calculated as follow:

$$\gamma_{liquid} = \frac{k_{liquid}}{\rho_{liquid}C_{p_{liquid}}}. \quad (3.23)$$

Another parameter that is used for the mass transfer is the Fourier number, Fo, which is a dimensionless time unit and describes the ratio of the heat conduction rate to the thermal energy storage rate within the solid. The Fourier number makes use of the thermal liquid diffusivity and the radius of the bubble at a specific moment in time.

$$Fo = \frac{\gamma_{liquid} * t}{R_{bubble}{}^2}. \quad (3.24)$$

The ratio of sensible and latent energy absorbed during the liquid-vapour phase change is represented by the Jacobs number, Ja, and can be calculated by making use of the liquid properties at a specific temperature and

pressure. The parameters that are part of the Jacobs number is the density of the surrounding liquid, the specific heat of the liquid, the temperature of the surrounding fluid, the saturated liquid temperature of the fluid at the specified pressure, the saturated vapour density of the liquid as well as the difference between the saturated vapour and liquid specific enthalpy (Kolev, 2011). The Jacobs number for condensation is calculated as follows:

$$Ja = \frac{\rho_{liquid}}{\rho_{saturated\ vapour}} \frac{C_{p_{liquid}}(T_{saturated\ liquid} - T_{liquid})}{h_{saturated\ vapour} - h_{saturated\ liquid}}. \quad (3.25)$$

The ratio of the momentum and thermal diffusivity, known as the Prandtl number is also used when determining the mass transfer of the bubble. The Prandtl number incorporates the dynamic viscosity of the liquid, μ_{liquid}, as well as the density of the liquid and the thermal liquid diffusivity, the Prandtl number is calculated as follows (Kolev, 2011):

$$Pr_{liquid} = \frac{\mu_{liquid}}{\rho_{liquid}\gamma_{liquid}}. \quad (3.26)$$

The Reynolds number,Re_{1o} , is calculated from the diameter of the bubble, the density of the liquid, the rise velocity of the bubble and the dynamic viscosity of the liquid.

$$Re_{1o} = \frac{D_{bubble}\rho_{liquid}U}{\mu_{liquid}}. \quad (3.27)$$

Based on the new bubble radius, the total steam mass that was transferred can be determined. The Peclet number, the Nusselt number, the condensing mass per unit time and the unit flow volume should be determined in order to calculate the energy transferred from the bubble to the surrounding fluid. Once the energy transfer is calculated, the new bubble temperature can be determined.

According to Brauer et al. (1976) (Kolev, 2011) for bubbles without internal circulation, the Peclet number, which is the ratio of advection to conduction heat transfer, can be determined by making use of the bubble diameter, rise velocity and thermal diffusivity

$$Pe_{liquid} = \frac{d_{bubble}U}{\gamma_{liquid}}. \quad (3.28)$$

The ratio of convection to pure conduction heat transfer is expressed by the Nusselt number, for bubbles without internal circulation according to Brauer et al (1976), is calculated as follows (Kolev, 2011):

$$Nu = 2 + \frac{0.65{Pe_{liquid}}^{1.7}}{\left(1+\left(0.84{Pe_{liquid}}^{1.6}\right)^3\right)^{\frac{1}{3}}\left(1+{Pe_{liquid}}^{1.2}\right)}. \quad (3.29)$$

The rate of change in bubble diameter is calculated so that it can be incorporated into the condensing mass per unit time and unit flow volume equations.

$$\frac{dR_{bubble}}{dt} = -\frac{\gamma_{liquid}\, Nu\, Ja}{2R_{bubble}} \quad (3.30)$$

The ratio, α_{system}, between the steam (V_{bubble}) and water volume (V_{liquid}) is then calculated. This ratio includes only the volume of one bubble.

$$\alpha_{system} = \frac{V_{bubble}}{V_{liquid}}. \quad (3.31)$$

The condensing mass per unit time and unit flow volume is then calculated by using the predetermined variables:

$$\mu_{transfer} = 4.84\,\rho_{\,saturated\ vapour}\left(n_{system}\right)^{\frac{1}{3}}\alpha_{system}{}^{\frac{2}{3}}\,\frac{dR_{bubble}}{dt}. \tag{3.32}$$

$$n_{system}[m^{-3}] = 1/V_{bubble} \tag{3.33}$$

The energy absorbed by the liquid during bubble condensation per unit mixture volume and time is then determined as follows:

$$Q_{heat\ absorbed\ by\ bulk\ liquid}\left[\frac{W}{m^3}\right] = \mu_{transfer}\left(h_{saturated\ vapour} - h_{saturated\ liquid}\right). \tag{3.34}$$

The new bubble temperature can also be calculated with the lumped capacitance method. This can be done due to the assumption that the steam bubble is a solid sphere and experiences a sudden change in its thermal environment. The influencing variable is the convection coefficient, $\bar{h}$, the area of the bubble, A_{bubble}, the density of the steam, volume of the steam bubble and the specific heat of the steam (Incropera, et al., 2007).

$$\bar{h} = Nu * \left(\frac{k_{liquid}}{D_{bubble}}\right) \tag{3.35}$$

The resulting temperature of the liquid is then calculated by using the energy transferred to the surrounding liquid, and the critical state convection coefficient.

$$\frac{T_{bubble,new} - T_{liquid}}{T_{bubble} - T_{liquid}} = e^{\left[-\frac{\bar{h}A_{bubble}}{\rho_{bubble}V_{bubble}Cp_{liquid}}t\right]}. \tag{3.36}$$

The energy transferred to the surrounding liquid is then used to determine the new temperature of the bulk liquid surrounding the steam bubble.

$$Q_{heat\ absorbed\ by\ bulk\ liquid} * V_{liquid} = \dot{m}_{liquid}C_{p_{liquid}}\left(T_{liquid,new} - T_{liquid}\right) \tag{3.37}$$

It is important to remember that the discussion was in terms of a single bubble and needs to be duplicated for multiple bubble columns.

For multiple bubble columns, the frequency of bubble formation and depletion time is utilised to determine the collective heat and mass transfer from the steam to the surrounding liquid. The theoretical background is in Appendix B.2.

3.3 Summary

The focus of this chapter was to discuss the relevant theory by Campos and Lage (2001), and Kolev (2011), to model the open feed water heater using a non-equilibrium approach. The simulation model of the open feed water that was developed as part of this study will be discussed in Chapter 4.

4 Simulation models and verification

This chapter focuses on the development of a simulation model which represents an OFWH. Initially, the simulation model will be subjected to equilibrium steady state conditions, as described by Lemasson (2009); thereafter the simulation model will be subjected to a non-equilibrium transient state. The simulation model, when subjected to a non-equilibrium transient state, consists of three sub-models. Each of the sub-models will be discussed and verified.

4.1 Equilibrium steady state model

The simulation model is based on the assumption that all of the inlet streams into the OFWH are instantaneously mixed. The inlet streams that supply the OFWH include the steam extracted from IPT3, the feed water stream from PH5, and the backwards cascading feed water stream from PH4. The results obtained from the single stage simulation is verified with the outlet fluid conditions as predetermined by Lemasson (2009) and illustrated in Figure 10.

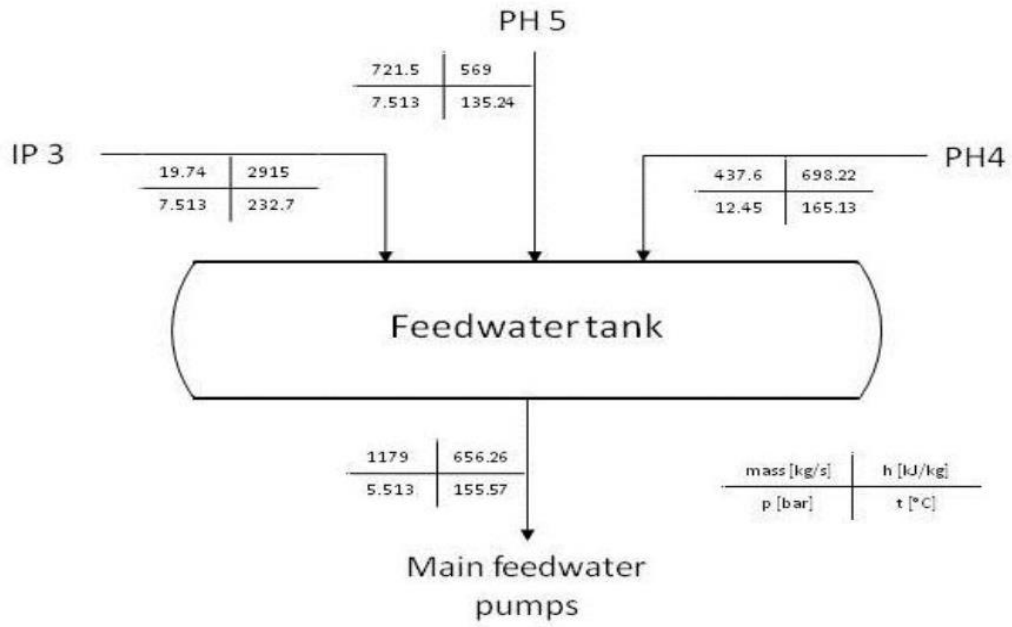

Figure 10: Diagram of the equilibrium steady state OFWH as designed by Lemasson (Lemasson, 2009).

The results of the Flownex model are compared to the Lemasson (2009) design in Appendix C.1. It is concluded that the Flownex simulation model deliver similar results (<0.1% error) to that of the conditions predetermined by Lemasson.

4.2 Non-equilibrium integrated transient simulation

In this section, the simulation model developed to represent an OFWH when it is subjected to a non-equilibrium transient state will be discussed. As illustrated in Figure 11 the model consists of multiple sub-models interacting with one another. Sub-model A is the feed water preparation model which is constructed in Flownex, the model represents the mixing of feed water from PH4 and PH5 as illustrated in Figure 12. The feed water preparation model is then combined with sub-model B which focuses on the heat and mass transfer of a multiple bubble column. Sub-model B is modelled in EES. The total heat and mass transfer calculated for a predefined time interval are then used in sub-model C, constructed in Flownex, to calculate the outlet conditions of the feed water that exit the OFWH. In the following section, the sub-models will be discussed and verified.

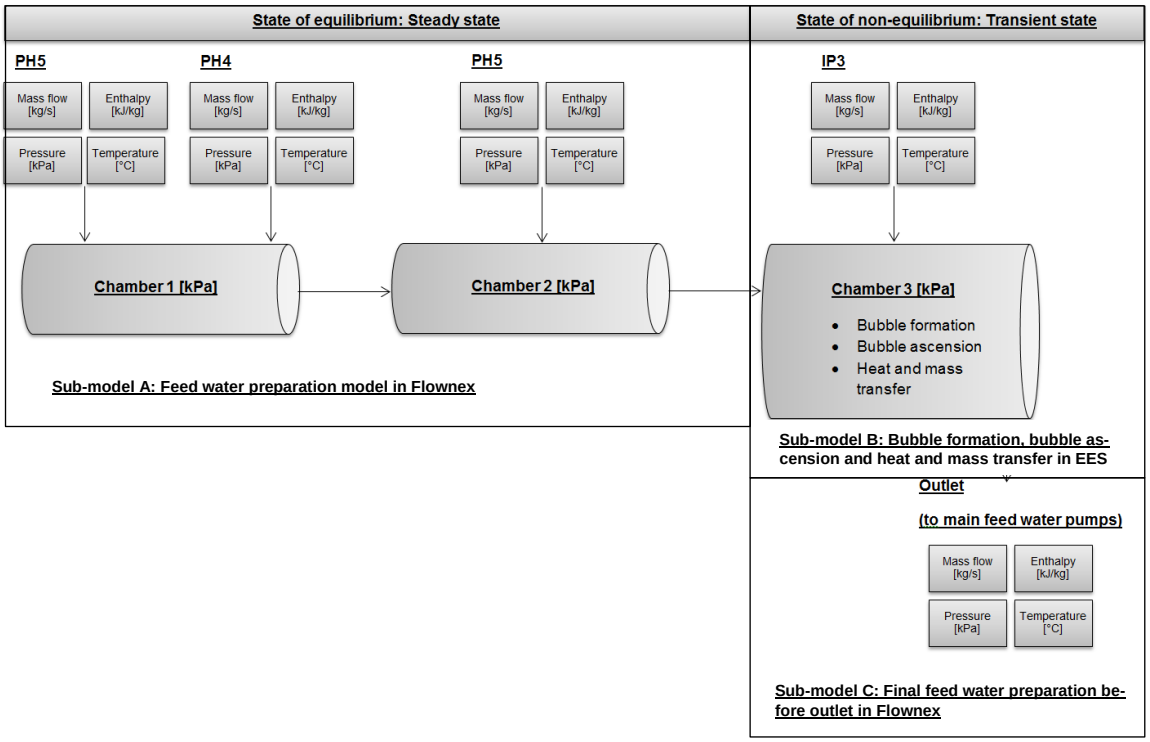

Figure 11: Diagram of the integrated simulation model of the OFWH.

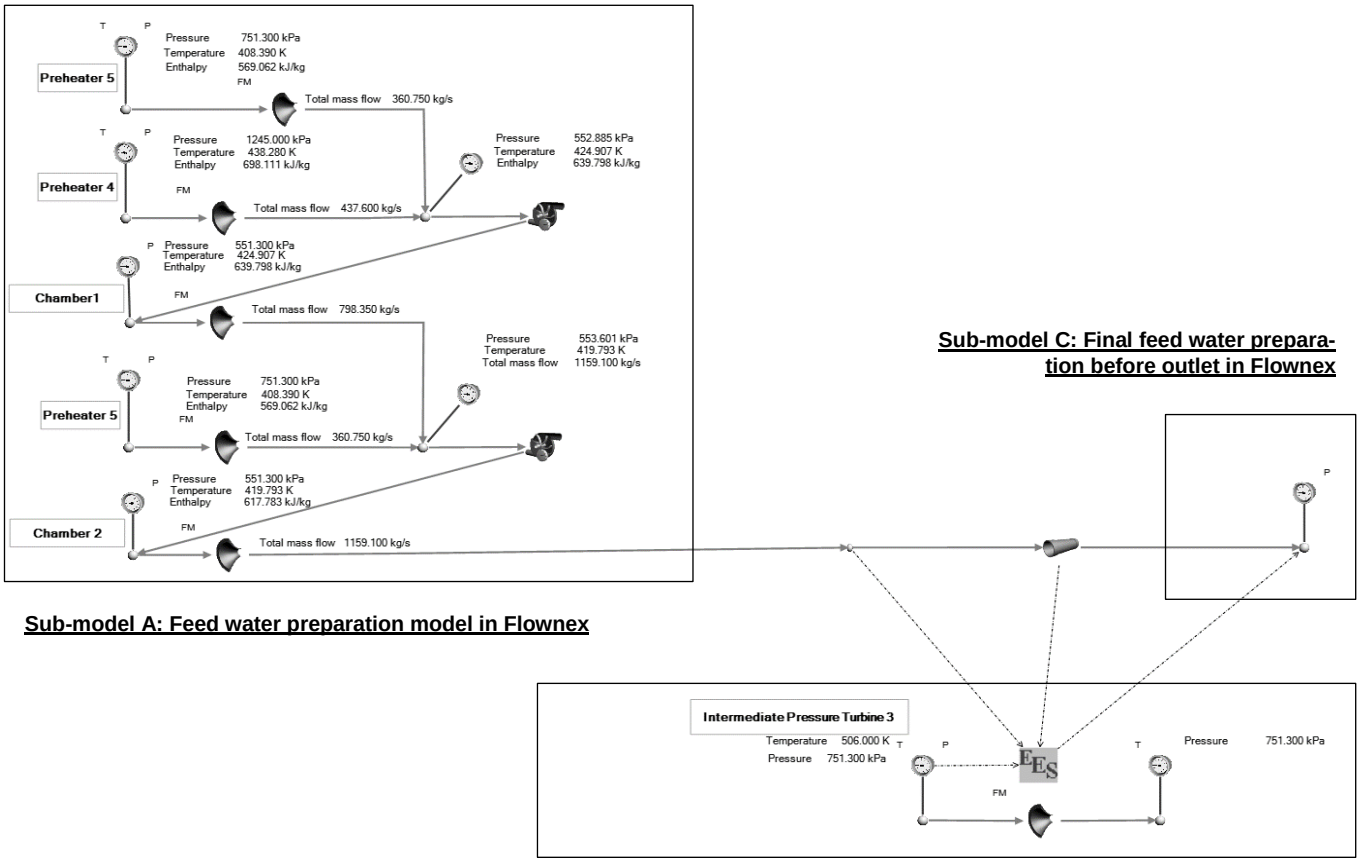

Figure 12: Diagram of an integrated simulation model of the OFWH with Flownex and EES sub-models.

4.2.1 Sub-model A: Feed water preparation

The feed water preparation model premixes the inlet streams of PH4 and PH5 (50% of the total mass flow rate) in Chamber 1. The combined stream then mixes with the remainder of the stream from PH5 in Chamber 2.

Sub-model A is based on the theory of multi-stage mixing as described in Appendix B.1.The simulation results of Sub-model A is included in Appendix C.2 and is verified against the predetermined conditions from Lemasson (2009). From the results, it can be concluded that the outlet conditions determined by the feed water preparation model are similar (<0.1% error) to that of Lemasson (2009).

4.2.2 Sub-model B: Bubble formation, bubble ascension and heat and mass transfer

A non-equilibrium approach is implemented when steam from IPT3 is injected into the feed water within the second chamber. Initially, the formation size and formation time of the steam bubble at an orifice will be determined. From there the ascension of the bubble is simulated. The ascension will include the rise velocity of the bubble as well as the mass and heat transfer from the steam bubble to the feed water up to the point that the bubble depletes.

4.2.2.1 Bubble formation simulation model

The bubble formation model, which is constructed in EES, is based on the experimental paper of Davidson and Shüler (Davidson & Shüler, 1960). The paper dealt with studies of bubble formation at an orifice in an inviscid liquid when the bubble formation is due to a constant flow of air being fed into a liquid by means of a capillary or sinter. The EES model for the bubble formation volume and time, as shown in Appendix C.3 is based on the mathematical model as described in Section 3.2 and illustrated in Figure 7.

In order to verify the bubble formation simulation model which estimates the bubble formation time and volume, the experimental results published by Davidson and Shüler (1960) is utilised. The experimental setup, illustrated in Figure 13, was constructed by Davidson and Shüler for constant and high flow rates consisted of two plates that formed the orifice. The upper plate is in contact with the liquid and a small hole, 0.3 - 0.5 cm, is drilled into the plate.

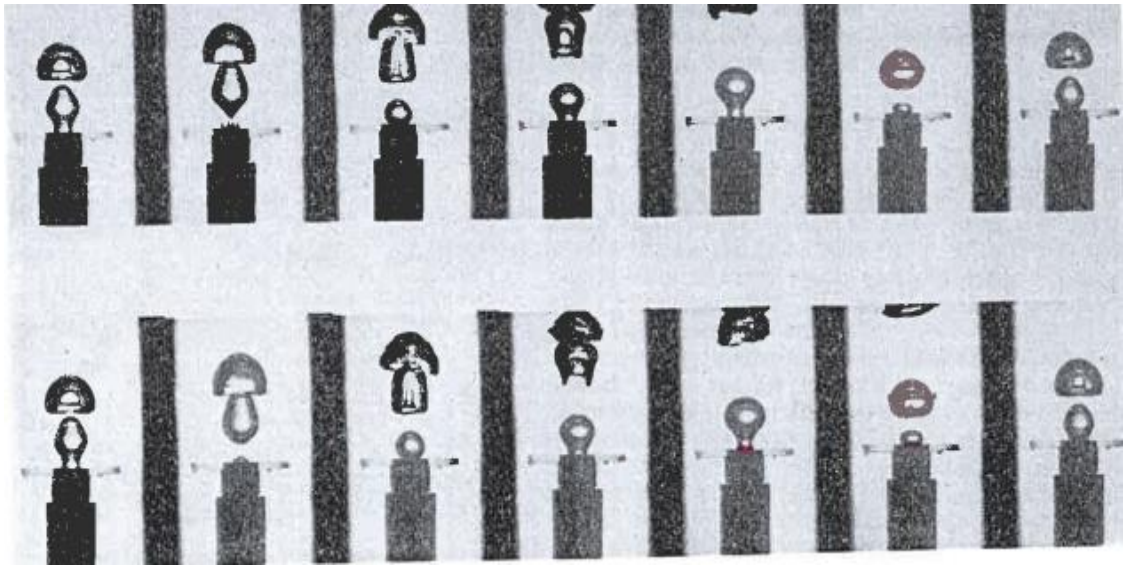

Figure 13: Experimental results with bubble formation in groups of two with a constant flow rate of 13.7 ml/s and an orifice radius of 0.2 cm (Davidson & Shüler, 1960).

Davidson and Shüler used a stroboscope to measure the bubble frequency, with higher flow rates double- and quadruple bubble formations were observed. Due to the impracticality of the stroboscopic method, pictures of the forming bubbles were taken to calculate the volume of each bubble illustrated in Figure 13.

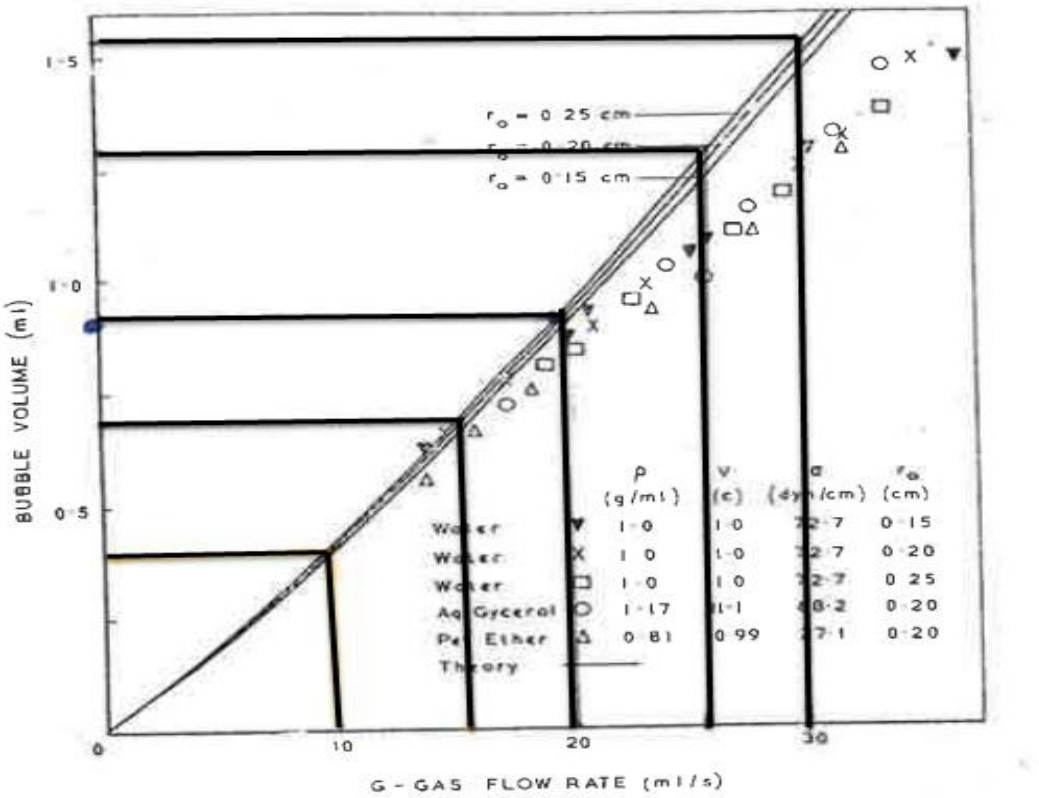

Figure 14: Theoretical and experimental bubble volumes for large constant flow rates (Davidson & Shüler, 1960).

Multiple sets of experimental results for the formation bubble volumes were published by Davidson and Shüler, as shown in Figure 14. Only three sets of data, steam injection into water, are relevant to the study. The varying factor in each test was the size of the orifice through which steam is injected. The experiment was conducted for steam injection through an orifice with a radius of 0.15cm, 0.2 cm and 0.25cm.

In an experimental test conducted by Davidson and Shüler, an assumption was made that the bubbles formed instantaneously, thus $t \rightarrow 0$, however the volume measured did not happen at exactly t=0.

To verify the theory of Davidson and Shüler, the bubble formation time was assumed to be equal and/or below 0.02 s, which is similar to the instantaneous bubble formation assumption of Davidson and Shüler.

In Figure 15, the experimental results for bubble formation volume when steam is injection through an orifice (radius 0.2 cm) is compared to the simulated bubble formation volume. In Appendix C.3 all three sets of experimental results are compared to the simulation results.

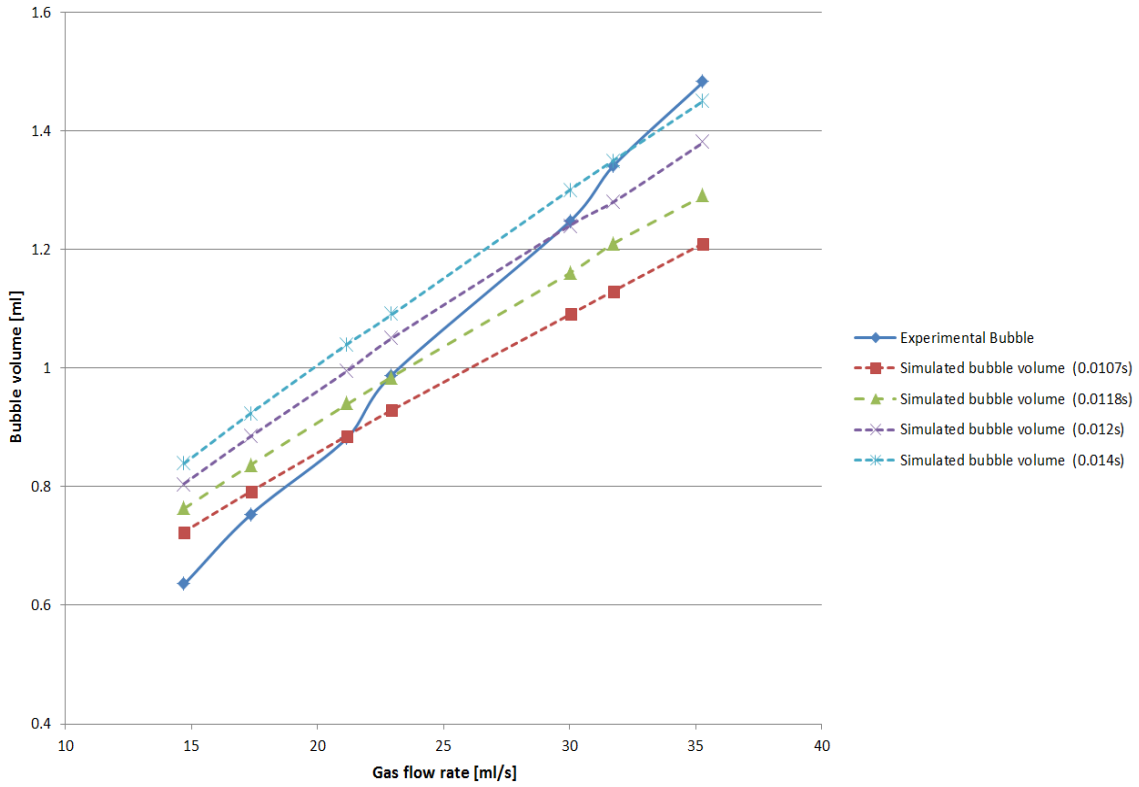

Figure 15: Graphical representation of the comparison between the experimental bubble formation volume, as determined by Davidson and Shüler, and the simulation bubble formation volume for a constant gas flow through an orifice of 0.2 cm.

The bubble formation volume represented in Figure 15 is for steam that is injected through an orifice of 0.2 cm at various constant gas flow rates ranging from 14.7 ml/s to 36 ml/s.

From the results (documented in Appendix C.3), it is noted that the average error between the experimental bubble formation volume and simulated bubble formation volume for an orifice size of 0.2 cm ranges between 9.71% and 12.88%. The most favourable result (average error of 9.71%) was for the simulated bubble formation time of 0.012s. The least favourable result (average error of 12.88%) was for the simulated bubble formation time of 0.014s.

It is of high importance to accurately predict the bubble formation volume, radius and detachment time as these parameters are the initial boundary conditions to the ascension models. Even though the marginal error for bubble formation volume ranges based on the bubble formation time, the simulation model results for bubble formation volume does converge. Due to the convergence of the bubble formation volume, an error of 13% is acceptable.

4.2.2.2 Bubble ascension simulation model

The bubble ascension simulation is based on three empirical correlations that represent the bubble rise velocity and heat and mass transfer of multiple bubble columns.

Bubble rise velocity

The bubble rise velocity is based on the mathematical model constructed by Karamev (1994). The simulation model estimates the rise velocity of the bubble as it ascends through the surrounding liquid after detachment. The EES model for the bubble ascension velocity is based on the mathematical model as described in Section 3.2 and illustrated in Figure 9.

Heat and mass transfer

As the steam bubble ascends through the surrounding liquid, it transfers both its energy and mass to the surrounding fluid. The mass and heat transfer mathematical models are based on experimental tests done by Moalem and Sideman (1973) for pure vapour systems when the bubbles have a constant velocity. (1976). The EES model for the heat and mass transfer of a steam bubble, as shown in Appendix C.3, is based on the mathematical model as described in Section 3.2 and illustrated in Figure 9. According to Moalem and Sideman, a constant bubble velocity can be assumed for large bubbles; therefore the rise velocity is independent of the radius of the bubble (Moalem & Sideman, 1973).

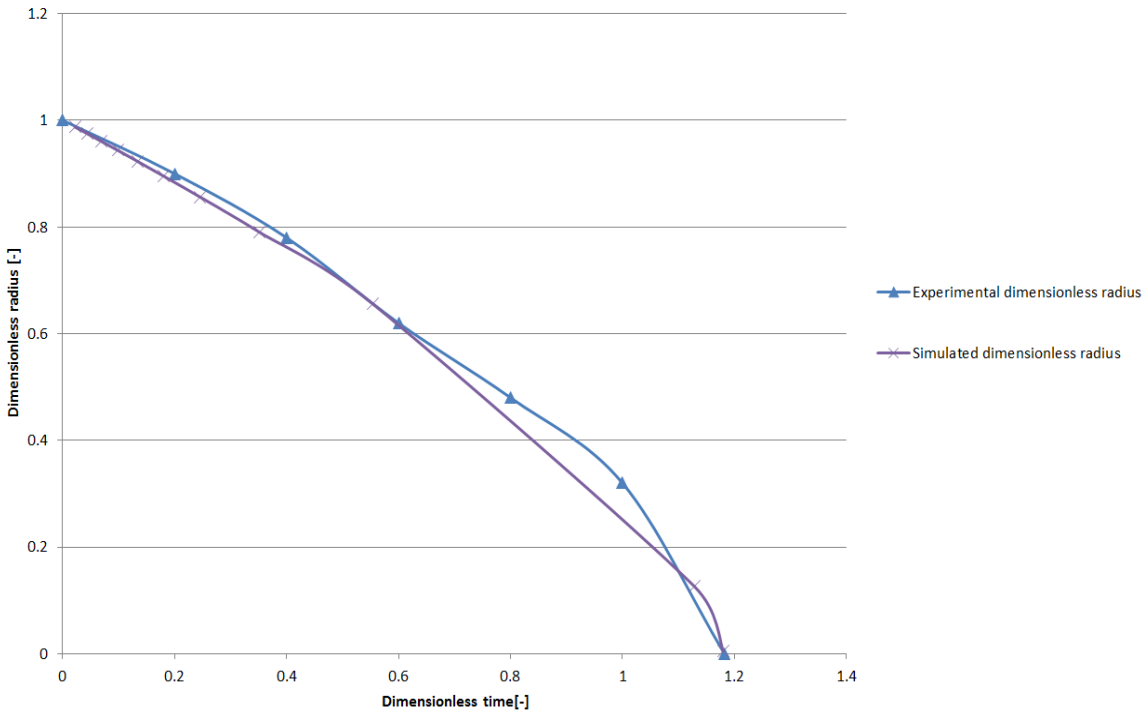

Figure 16: Comparison between the constant and radius dependent rise velocity (Moalem & Sideman, 1973).

In Figure 16, the experimental dimensionless radius which is a function of dimensionless time is compared to that of the simulation results. The comparison, which is documented in Appendix C.3 shows an average error of 1.988%.

4.2.3 Sub-model C: Final feed water preparation before the outlet

The heat and mass transferred to the feed water from the multiple bubble columns are illustrated in Figure 11 and Figure 12. The mathematical model behind Sub-model C is described in Appendix B.2.

4.3 Summary

This chapter discussed the development and verification of the equilibrium steady state and non-equilibrium transient state simulation models for the OFWH. In the next chapter, the results of the non-equilibrium transient state simulation that represent an OFWH will be assessed.

5 Results

Various sub-models were developed to form the non-equilibrium transient state simulation model. In this chapter, the results for an open feed water heater when simulated with a non-equilibrium transient approach will be compared to the equilibrium steady state approach. The chapter also illustrates the change bubble behaviour when operational incidents are applied to the non-equilibrium transient state simulation.

5.1 Non-equilibrium integrated simulation results

The integrated simulation model is illustrated in Figure 17. The model is also included in Appendix D.1.

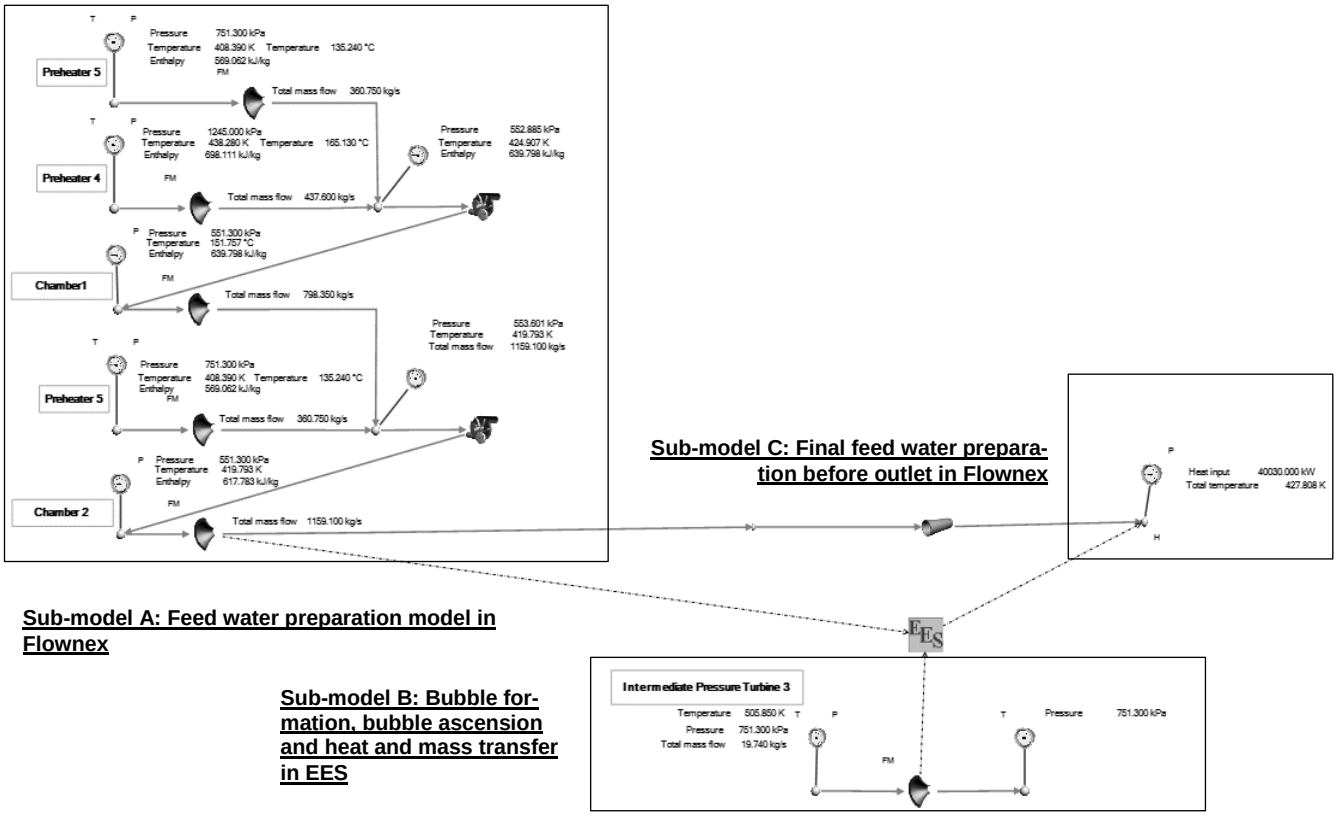

Figure 17: Diagram of the integrated simulation model of the OFWH with Flownex and EES sub-models.

5.1.1 Results obtained from Sub-model A

The purpose of the feed water preparation model is to simulate the mixing of fluid streams from PH4 and PH5 in Chamber 1 and Chamber 2. As seen in Figure 11, 50% of the feed water from PH5 is mixed with the feed water from PH4 in Chamber 1. The feed water from Chamber 1 flows over into Chamber 2 and mixes with the remaining feed water from PH5.

The results gained for the feed water preparation model is compared to the conditions predicted by Lemasson (2009) in Table 2.

Table 2: Comparison between equilibrium and non-equilibrium transient state simulation results for Sub-model A.

		Lemasson	Integrated simulation results	Integrated simulation results	
		Equilibrium steady state	**Equilibrium steady state**	**Non-equilibrium transient state**	
		Value	**Value**	**Value**	**Error**
Sub-model A	**Input : PH5**				
	Temperature [K]	408.39			
	Pressure [kPa]	751.3			
	Mass flow [kg/s]	721.5			
	Input: PH4				
	Temperature [K]	438.28			
	Pressure [kPa]	1245			
	Mass flow [kg/s]	437.6			
	Input: Chamber 3				
	Pressure [kPa]	551.3			
	Mass flow [kg/s]	1159.1			
	Output: Chamber 3				
	Temperature [K]	-	419.79	419.79	-

It is noted that the conditions of the prepared feed water within the third chamber does not differ for the non-equilibrium and equilibrium approaches.

5.1.2 Results obtained from Sub-model B

Steam from IPT3 is injected into the bulk liquid of Chamber 3 within the OFWH. The following subsections will discuss the results gained from the bubble formation, bubble ascension and mass and heat transfer simulations.

5.1.2.1 Bubble formation simulation results

A steam bubble will start to form at an orifice in the OFWH, Figure 18 . The initial radius of the steam bubble is 20mm. The steam bubble grows in radius until the bubble becomes too large and detaches from the orifice.

In this study a steam bubble will increase in size up until a bubble radius of 59 mm is achieved. The time to reach bubble detachment is 0.1 seconds, after the detachment, the following bubble will form.

The results gained from the formation simulation are tabulated in Table 3, the bubble formation time and radius was only determined by the non-equilibrium transient state approach and not for the equilibrium approach.

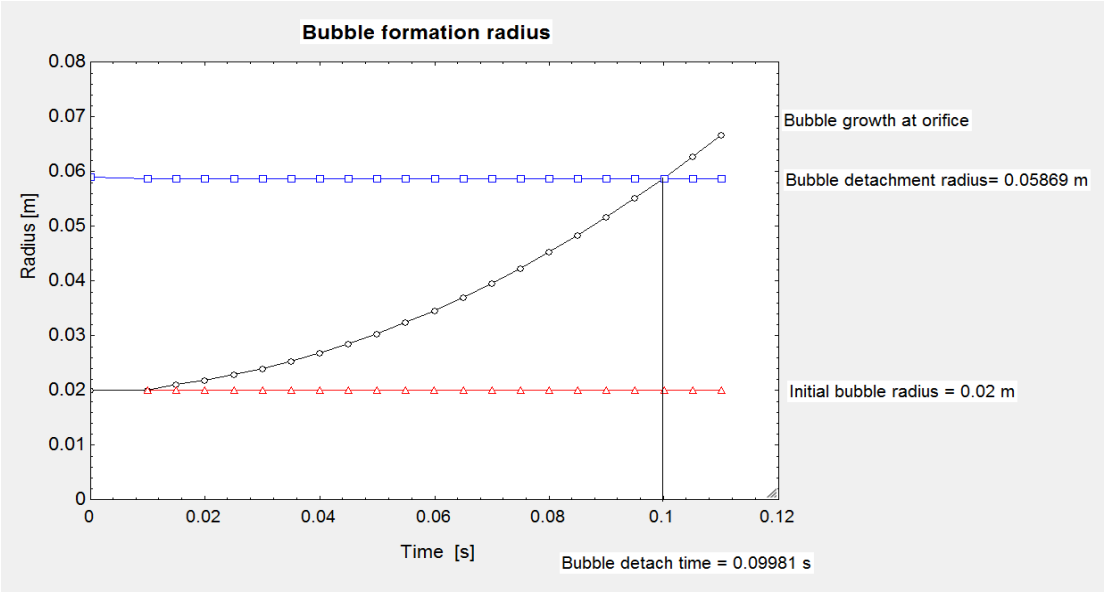

Figure 18: Formation and growth of a bubble in the open feed water heater.

The bubble formation radius also converges as predicted and the bubble formation time is so short that it can be assumed to be instantaneous, which is similar to the experimental test of Davidson and Shüler which is discussed in Section 4.2.2.

Table 3: Comparison between equilibrium and non-equilibrium transient state simulation results for Sub-model A.

		Lemasson	Integrated simulation results	Integrated simulation results	
		Equilibrium steady state	**Equilibrium steady state**	**Non-equilibrium transient state**	
		Value	**Value**	**Value**	**Error**
Sub-model B	**Input: Chamber 3**				
	Pressure [kPa]	551.3			
	Mass flow [kg/s]	1159.1			
	Temperature [K]	-	419.79		
	Input : IPT3				
	Temperature [K]	505.85			
	Pressure [kPa]	751.3			
	Mass flow [kg/s]	19.74			
	Output: Bubble Formation				
	Bubble formation time [s]	-	-	0.1	-
	Bubble formation diameter [m]	-	-	0.059	-

5.1.2.2 Bubble ascension simulation model results

Once the steam bubble has formed and detaches, the bubble moves into the ascension stage. The bubble has an initial ascension velocity as it ascends through the bulk liquid and loses mass and heat as it condenses. As the steam bubble condenses the velocity of the bubble will also decrease. The results gained from the bubble ascension simulation are tabulated in Table 4.

Table 4: Comparison between equilibrium and non-equilibrium transient state simulation results for the bubble ascension simulation.

		Lemasson	Integrated simulation results	Integrated simulation results	
		Equilibrium steady state	**Equilibrium steady state**	**Non-equilibrium transient state**	
		Value	**Value**	**Value**	**Error**
Sub-model B	**Input: Chamber 3**				
	Pressure [kPa]	551.3			
	Mass flow [kg/s]	1159.1			
	Temperature [K]	-	419.79		
	Input : IPT3				
	Temperature [K]	505.85			
	Pressure [kPa]	751.3			
	Mass flow [kg/s]	19.74			
	Output: Bubble Ascension				
	Ascension velocity [m/s]	-	-	1.055	-
	Depletion time [s]	-	-	1.194	-
	# bubbles in bubble column[-]	-	-	11.96	-
	Output: Energy and mass transfer				
	Rate of energy transferred single column [J/s]	-	-	4287	-
	Rate of energy transferred multiple bubble column[J/s]	-	4.45E+07	4.00E+07	10.11%

It was determined that the initial ascension velocity of the bubble is 1.055 m/s. After detachment, the bubble starts to condense, illustrated in Figure 19, and forms a saturation water layer around the bubble.

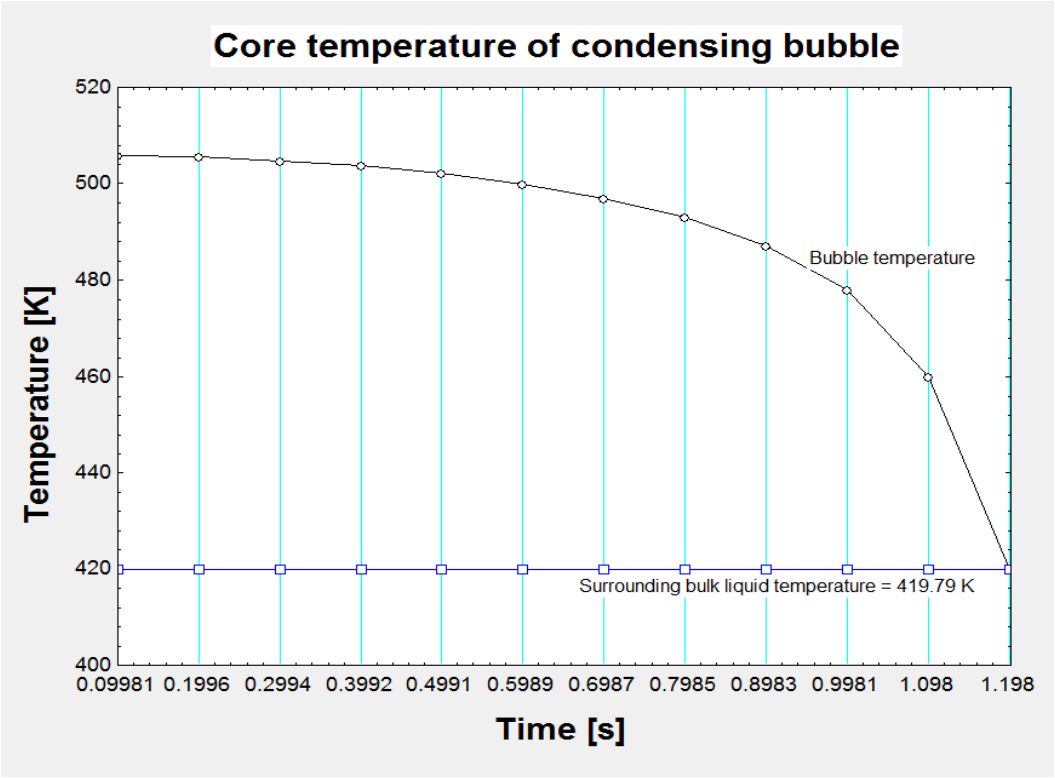

Figure 19: Core temperature of a steam bubble as it depletes.

The saturation film layer is at the saturation temperature of the steam pressure. With the increase in saturation film layer, the steam bubble reduces in radius. As the bubble radius decreases more mass and heat are transferred to the surrounding film layer.

In Figure 20 the decrease in radius of a single steam bubble is illustrated. Once the bubble has depleted at 1.194 seconds there are no more mass or heat to be transferred. According to Moalem and Sideman, a single component system should have a dimensionless depletion time of 1.182 seconds, the non-equilibrium transient simulation has a dimensionless depletion time of 1.18 when the dimensionless radius is 0.005. Therefore the results gained from the simulation are similar to that of Moalem and Sideman with the difference, average error of 1.988%, being attributed to the variation in flow conditions. The dimensionless time and radius results are illustrated in Figure 16 and documented in Appendix C.3.

It is important to note that steam is continuously injected into the open feed water heater through the sparger tube and therefore a continuous formation and ascension of steam bubbles occur. This is noted with i=1,2,3….n. At, i, a new bubble have formed and detaches from the orifice. In a depletion time of the initial steam bubble, 11 other steam bubbles have formed, detached and ascended.

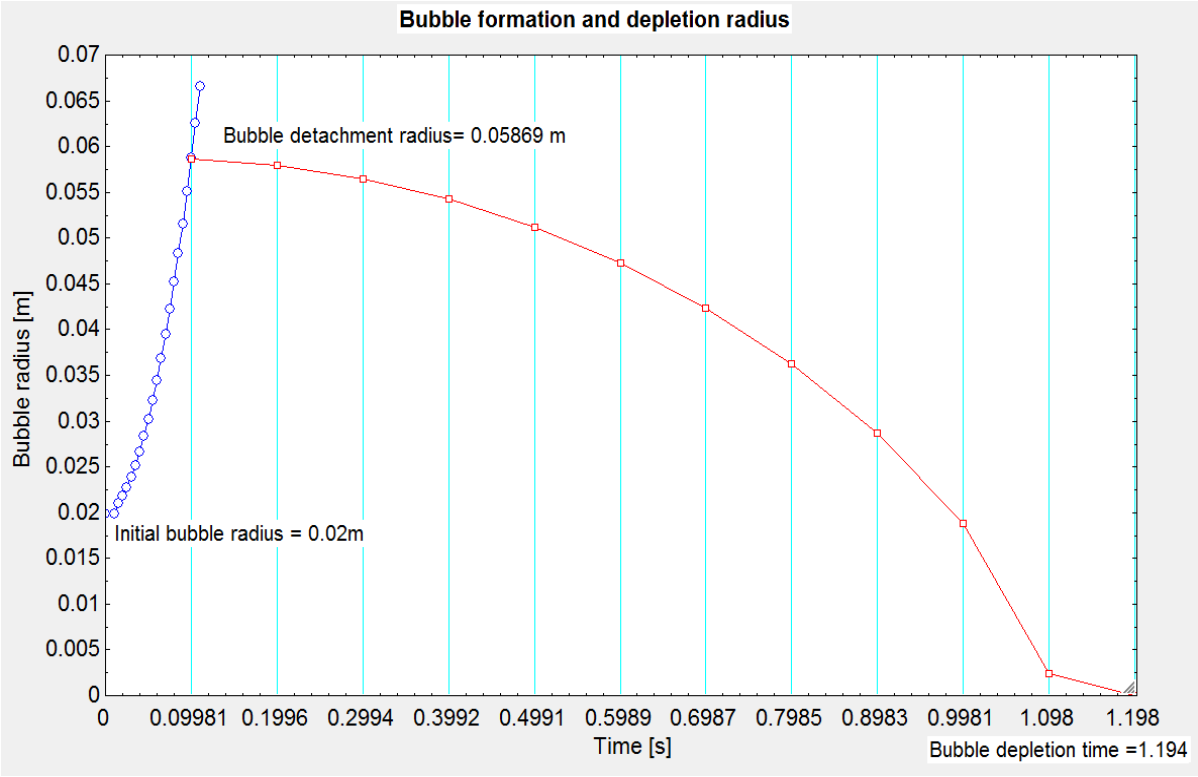

Figure 20: Formation and depletion of a bubble in the open feed water heater.

The energy that is transferred for a single condensing steam bubble to the surrounding film layer is illustrated in Figure 21. It can be seen in the early stages of depletion, more energy is transferred to the surrounding film layer compared to the steam bubble nearing depletion.

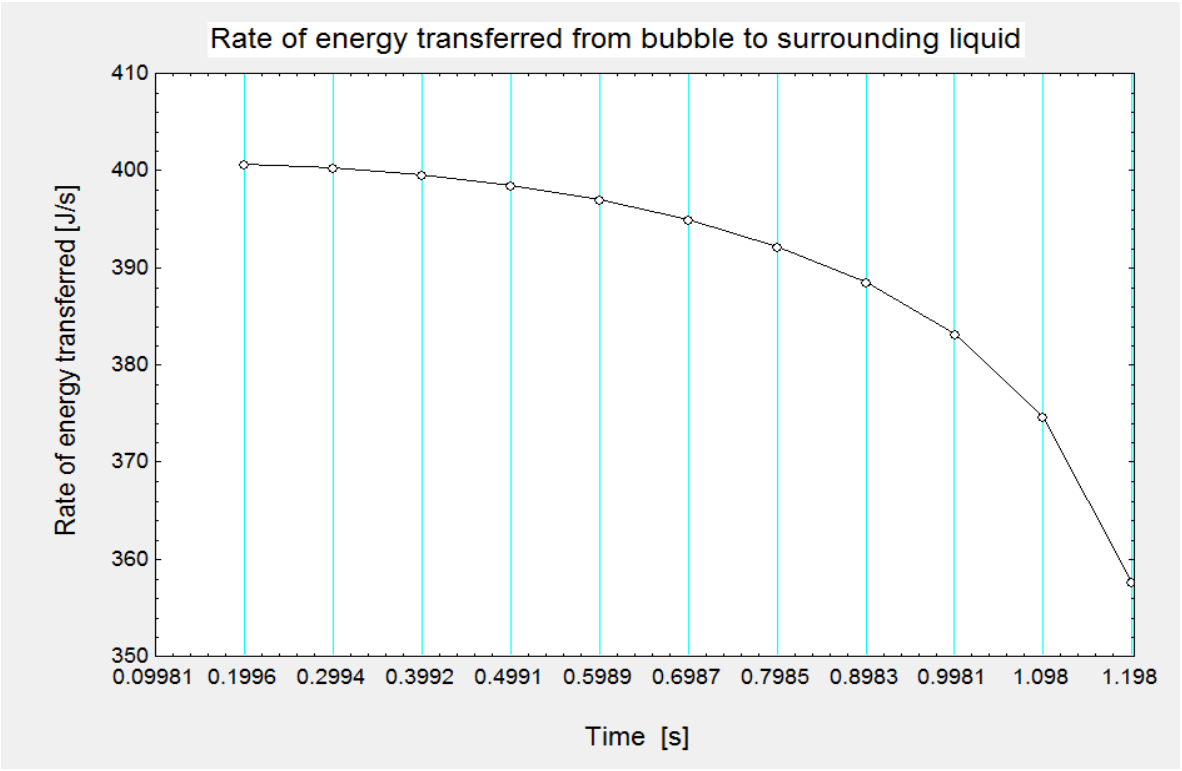

Figure 21: Heat transfer of a steam bubble as it depletes.

It was calculated that for a single bubble column 4287 J/s energy is transferred to the surrounding liquid. The sparger tube does not only consist of a pipe and a single orifice but multiple orifices. In the case study there are 932 orifices in the sparger tube and through each of them, steam is injected into the feed water. This is also known as multiple bubble columns. The total energy rate by the multiple bubble columns to the surrounding feed water was calculated to be 4.00E+07J/s. The equilibrium steady state approach estimates that 4.45E+070 J/s energy is transferred, as calculated by Equation B-2.4 in Appendix B.2. Therefore there is a difference of 10.11% between the two approaches.

5.1.3 Results obtained from Sub-model C

The energy transferred rate from the multiple bubble columns to the surrounding bulk liquid increases the temperature, tabulated in Table 5.The transfer ensures a temperature rise of 8.01 K, resulting in the temperature of the feed water that exits the OFWH is 427.8K.

Table 5: Comparison between equilibrium and non-equilibrium transient state simulation results for Sub-model C.

		Lemasson	Integrated simulation results	Integrated simulation results	
		Equilibrium steady state	**Equilibrium steady state**	**Non-equilibrium transient state**	
		Value	**Value**	**Value**	**Error**
Sub-model C	**Input: Chamber 3**				
	Pressure [kPa]	551.3			
	Mass flow [kg/s]	1159.1			
	Temperature [K]	419.79			
	Input : IPT3				
	Temperature [K]	505.85			
	Pressure [kPa]	751.3			
	Mass flow [kg/s]	19.74			
	Output: Chamber 3				
	Pressure [kPa]	553			
	Mass flow [kg /s]	1178.84			
	Temperature [K]	428.72	428.7	427.8	0.21% (0.92 K)

When the results of the non-equilibrium transient approach are compared to that of the equilibrium steady state approach it is noted that the non-equilibrium transient state approach delivers a feed water temperature which is slightly lower than that of the equilibrium steady state. The difference between the approaches is 0.92 K.

5.2 Non-equilibrium operational incidents on an OFWH

The main factors that typically influence a system are that of temperature and mass flow. When considering the open feed water heater, there are three fluid streams entering the open feed water tank. The properties associated with these fluid streams influence the feed water which exits the open feed water heater. As soon as the incoming

fluid stream properties changes, due to changes within the power plant, the properties of the stream exiting the open feed water heater will also change. The incidents that will be assessed is i) a failure of Pre-Heaters 5-7 and ii) a pipe rupture from Intermediate Pressure Turbine 3.

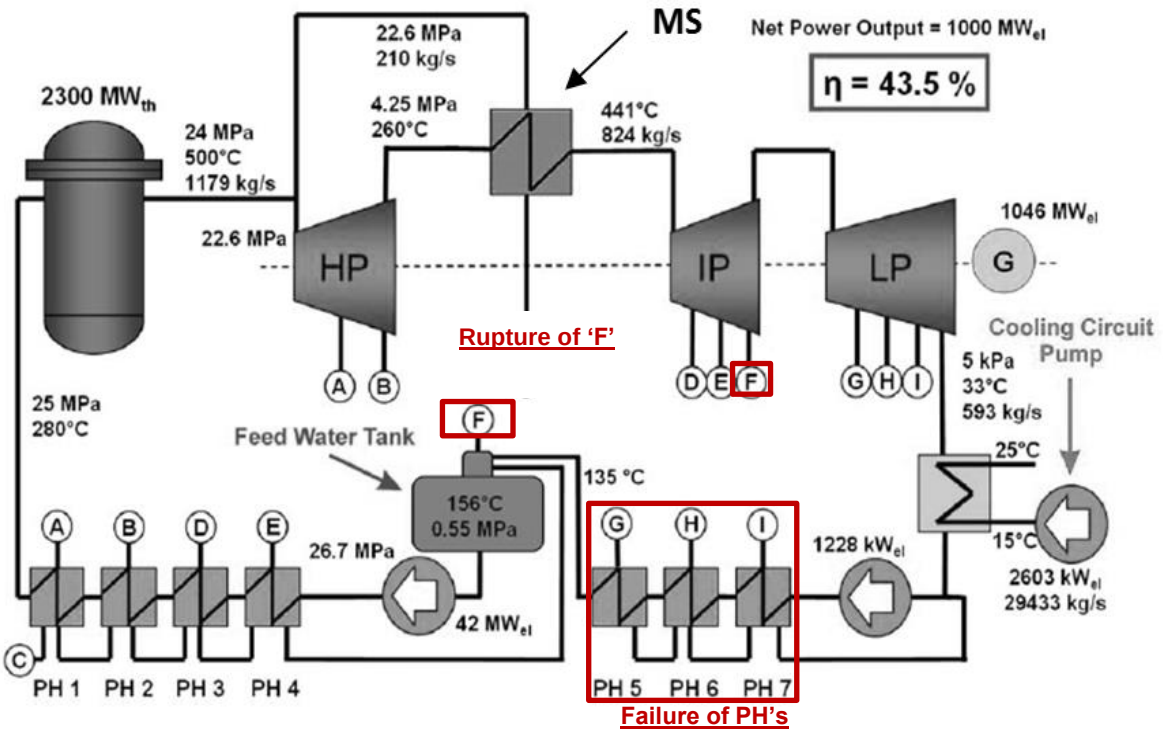

Figure 22: Operational incidents induced on the OFWH.

The first scenario that will be assessed is that of the failure of PH 5 to 7 as indicated in Figure 22. The design parameters state that preheater 5 to 7 increases the feed water temperature from 33°C to 135°C. If the pre-heating does not occur, the feed water entering the open feed water heater will be cooler than initially designed for.

The second operational incident that will be assessed is a pipe rupture in the line that transports steam from the intermediate turbine to the open feed water heater, also illustrated in Figure 22. The design parameters state that steam with a mass flow of 19.74 kg/s should be injected into the open feed water heater. If a smaller mass flow is supplied, insufficient heat is transferred to the feed water in the open feed water heater.

This will result in cooler feed water leaving the OFWH which will enter the second set of pre-heater (PH 1 to 4), as well as cooler feed water entering the reactor core.

Figure 23 illustrates how a sudden decrease in the temperature of the feed water entering the open feed water heater affects the temperature of the feed water leaving the OFWH. The temperature of the feed water exiting the open feed water heater is approximately 64°C lower that the design temperature.

Once the connecting steam pipe between IPT3 and the OFWH ruptures and there is a loss of 90% of the steam flow. The system adapts to the new boundary conditions and thus tries to establish a new state of operation which is not the designed operational point. Figure 24 illustrates how a sudden reduction in the mass flow of steam supply affects the temperature of the feed water leaving the OFWH. The temperature of the feed water exiting the open feed water heater is 8°C lower that the design temperature.

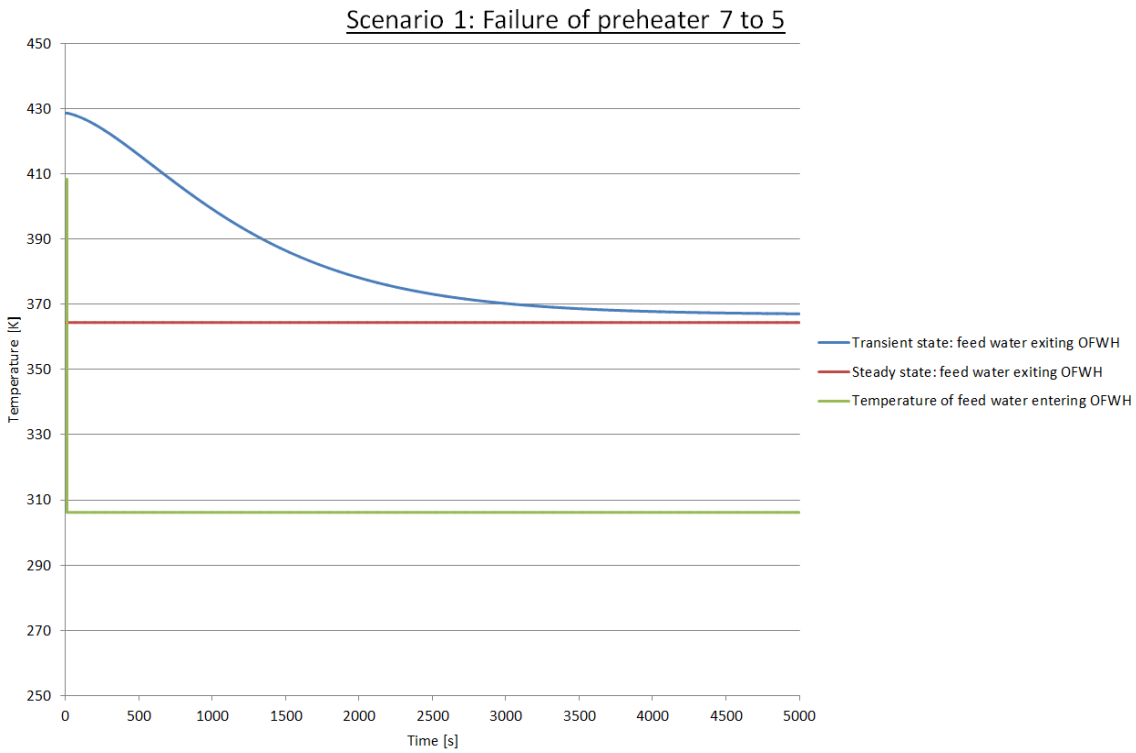

Figure 23: Graphical representation of operational incident 1 on the open feed water tank.

If the feed water that enters the reactor is cooler than anticipated, the instrumentation that monitors the reactor may become unreliable. The effect of inaccurate design and operating conditions in feed water heating is discussed in Section 2.1.3.

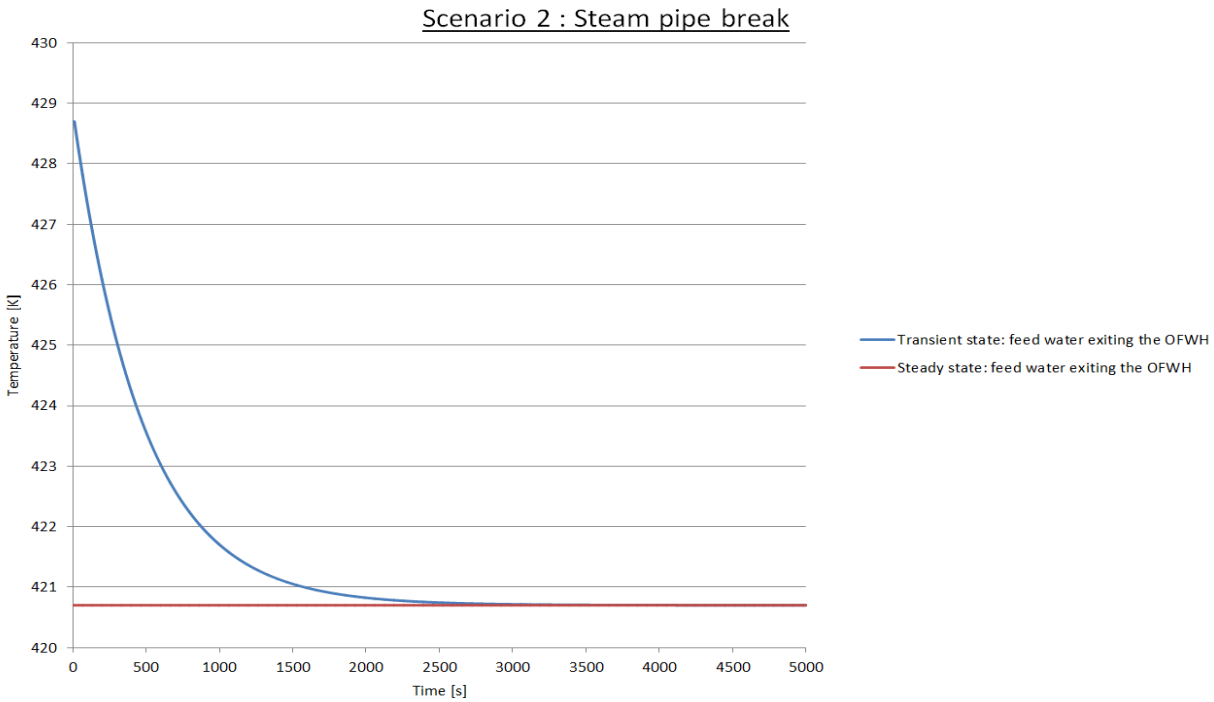

Figure 24: Graphical representation of operational incident 2 on the open feed water tank.

Figure 25 illustrates the bubble formation for the operational incidents. The bubble detachment radius for the first operational incident is 59 mm at 0.1 seconds. Regarding the second operational incident, as soon as the steam mass flow is reduced the bubble formation radius is 27.3 mm at a detachment time of 0.03453 s.

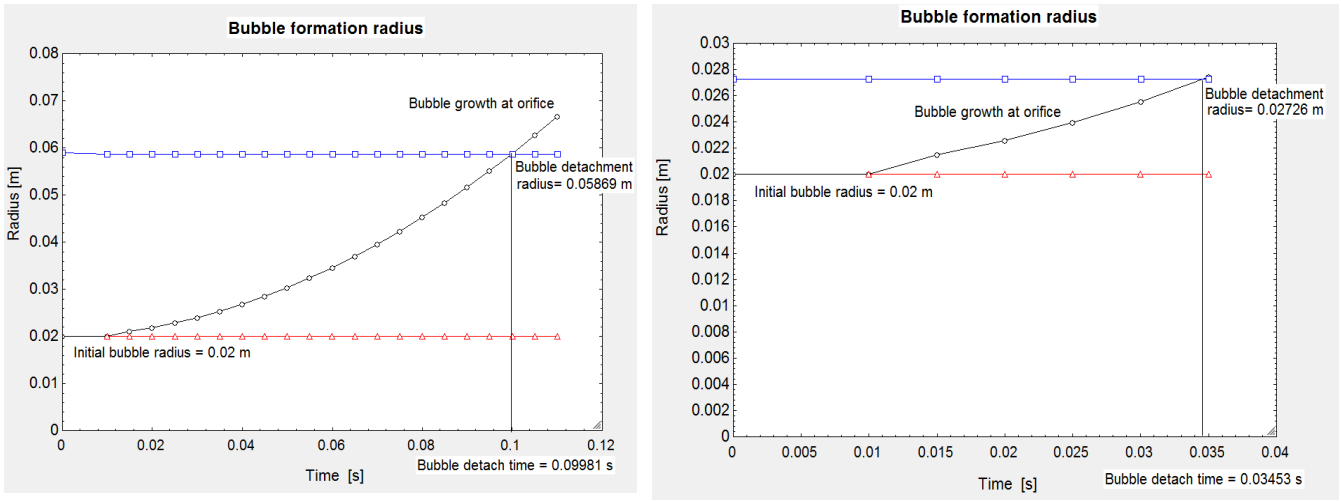

a) **b)**

Figure 25: Formation and growth of a bubble in the open feed water heater when a) operational incident 1 and b) operational incident 2 are applied.

The temperature difference between the bulk liquid and the steam bubble ensure that heat is transferred from the steam bubble to the surrounding liquid; the core temperature of the condensing bubble is illustrated in Figure 26.

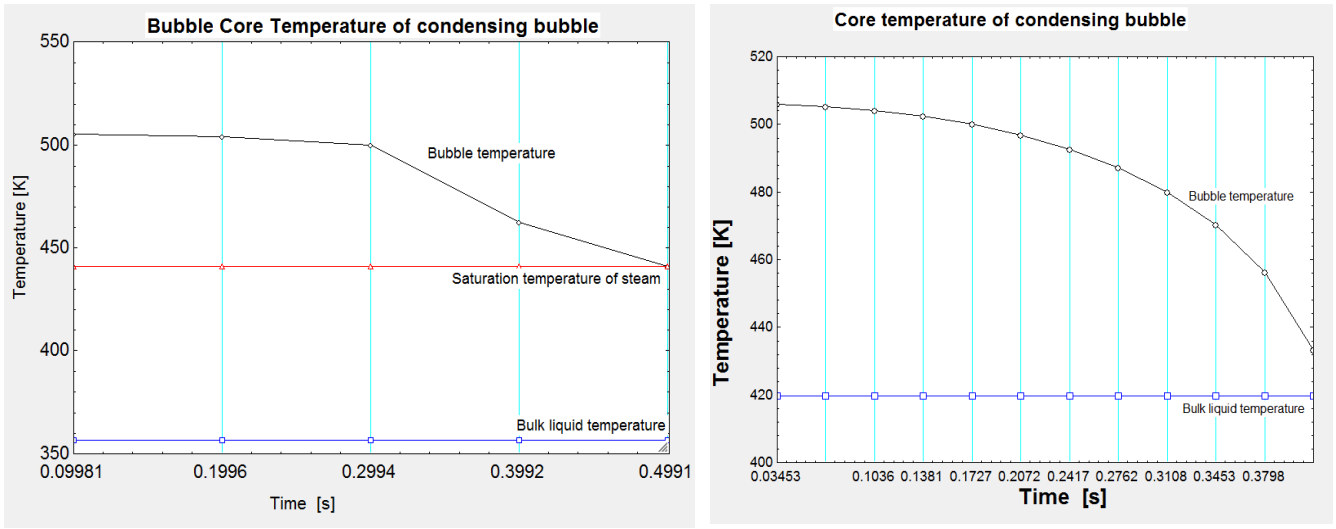

a) **b)**

Figure 26: Core temperature of a bubble in the OFWH when a) operational incident 1 and b) operational incident 2 are applied.

Figure 27 illustrates the formation and depletion of a single bubble for the operational incidents. The bubble depletion time when incident one is induced is 0.4954 s and 0.4139 s for the second operational incident.

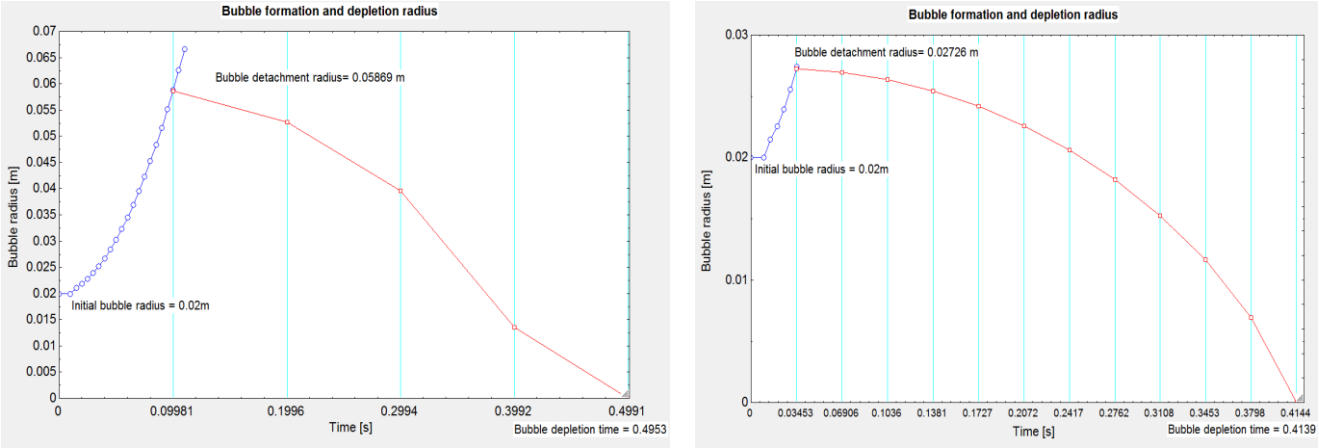

a) **b)**

Figure 27: Formation and depletion of a bubble in the OFWH when a) operational incident 1 and b) operational incident 2 are applied.

The operational incidents simulated are extreme but it shows the effect of a change operating conditions. If the design temperature and mass flow are not carefully calculated, the predicted hydraulic conditions of the thermodynamic cycle will be incorrect. The working conditions of the HPLWR will be affected and the desired output conditions may not be met.

6 Conclusion

6.1 Comparison between a non-equilibrium and equilibrium approach

The focus of this study was to evaluate the accuracy when predicting the operating conditions of an OFWH in the HPLWR generation cycle when applying a non-equilibrium approach compared to an equilibrium approach.

Simulating the OFWH by means of a non-equilibrium transient approach is more time consuming, than the approach of equilibrium steady state. The results gained from the non-equilibrium are similar to that of the equilibrium approach; the energy transferred from the steam to the feed water is predicted within 90% accuracy and the outlet temperature of the feed water differs 0.21% (0.92 K).

The advantage of the non-equilibrium transient approach is that the approach illustrates how energy is gradually transferred and not instantaneously. The non-equilibrium approach also illustrates that the energy from the steam is not completely transferred to the liquid; therefore the temperature of the feed water may differ from design operating conditions. When using a transient approach, operational incidents can be induced and the behaviour of the system can be predicted.

6.2 Recommendation for further studies

After completion of the study of the non-equilibrium two-phase flow of an open feed water heater in the HPLWR power plant, the following recommendations are made for future investigations.

Detailed data should be obtained from the operation of an OFWH in a nuclear power generation plant. The operating conditions should be evaluated according to the non-equilibrium transient simulation model designed in this study.

The mathematical models in the literature, used to describe the bubble formation, ascension and depletion, are based on limited experimental data. Research on superheated vapour bubbles in sub-cooled liquids done in modern experimental facilities equipped with high-speed cameras can be used to verify the accuracy of the existing models.

The mathematical models for bubble formation, ascension and depletion were developed for low steam mass flows. Follow-up research should focus on superheated vapour bubbles in sub-cooled liquids for steam flow rates that are typical of OFWH operating conditions.

7 References

1. AG, Gestra. 2015. Flowserve. Date of access: 124 Feb 2015. <http://www.gestra.com/products/vessels.php>
2. ARCA. Date of access: 11 Nov 2014. <http://www.arca.de/index/lang/en/artikel/2249>
3. Bitterman, D. Starflinger, J. Schulenberg, T. 2004. Turbine Technologies for High Performance Light Water Reactors, Proceedings of ICAPP '04, Paper 4195. Pittsburgh, PA, USA.
4. Borgnakke, C. & Sonntag, R, E. 2009. Fundamentals of thermodynamics, 7th Ed, International student version.
5. Brandauer, M. Schlagenhaufer, M. Schulenberg, T. 2009. Steam cycle optimization for HPLWR. (In 4th International Symposium on Supercritical Water-Cooled Reactors. Paper No. 36. Heidelberg, Germany.)
6. Campos, F. B. Lage, P. L. 2000 a. Heat and mass transfer modelling during the formation and ascension of superheated bubbles. International Journal of heat and mass Transfer, 43:2883-2894. 15 October.
7. Campos, F B & Lage, P L. 2000. Simultaneous heat and mass transfer during ascension of superheated bubbles. International Journal of Heat and Mass Transfer, 43:179-189.
8. Campos, F. B & Lage, P.L. C. 2001. Modelling and simulation of direct contact evaporators. Brazilian Journal of Chemical Engineering, 18(3):277-286. Sept.
9. Davidson, J. F & Shüler, B. O.G. 1960. Bubble formation at an orifice in an inviscid liquid. TRANS. INSTN CHEM. ENGRS, 38
10. Dobashi, K, Oka, Y & Koshizuka, S. 1998. Conceptual design of a high temperature power reactor cooled and moderated by supercritical water. Ann. Nuclear. Energy 25:487-505.
11. El-wakil, M.M. 1984. Power plant Technology. Singapore: McGraw-Hill.
12. F-CHART SOFTWARE. Date of access: 01 Nov 2014. <http://www.fchart.com>
13. FLOWNEX Simulation environment. Date of access: 16 Nov 2014. <http:/www.flownex.com>
14. GIF. 2002. Technology Roadmap for Generation 4 Nuclear Energy Systems.
15. Green, Don W & Perry, Robert H. 2008. Perr's Chemical Engineers' Handbook, 8th Ed. Mc Graw-Hill.
16. Grimes, B. K. 1996. United States Nuclear Regulatory Commission. Date of access: 7 April 2016. <http://www.nrc.gov/reading-rm/doc-collections/gen-comm/info-notices/1996/in96041.html>
17. Herbell, H, Weschung, M & SChulenberg, T. 2009. A turbine design concept for the High Performance Light Water Reactor. (In 4th International Symposium on SCWR, Paper 76. Heidelberg, Germany.)
18. Hochreiter, L. E. Robinson, G. E. 2004. Nuclear Engineering 430: Elements of Nuclear Reactor Design.PA: The Pennsylvania State University, Department of Mechanical and Nuclear Engineering.
19. Hofmeister, J, Waata, C, Starflinger, J, Schulenberg, T & Laurien, E. 2007. Fuel assembly design study for a reactor with supercritical water. Nuclear Engineering Design, 237:1513-15121.
20. Hurst Boiler and welding company, Inc. Date of access: 11 Nov 2014. <http://s3.amazonaws.com/hurstboiler/documents/oxy-miser.pdf>
21. INCROPERA, F. P, Dewitt, D, P, Bergman, T. L & Lavine, A. S. 2007. Fundamentals of heat and mass transfer. USA: John Wiley & Sons, Inc.
22. Isenberg, J. & Sideman, S. 1970. Direct contact heat transfer with change of phase: Bubble condensation in immiscible liquids. International Journal of Heat and Mass transfer, 13:997-1011.
23. Jinbo, Yoshinori, Ogasawara, Toshiyuki & Takahira, Hiroyuki. 2015. Influence of the non-equilibrium phase transition on the collapse of inertia non-spherical bubbles in a compressible liquid. Experimental Thermal and Fluid Science, 60:374-384.

24. Kalman, H & Mori, Y H. 2002. Experimental analysis of a single vapour bubble condensing in subcooled liquid. Chemical Engineering Journal, 85:197-206.

25. Karamanev, D G. 1994. Rise of gas bubbles in quiescent liquids. AIChE Journal, 40(8) August.

26. Kolev, N. I. 2011. Multiphase flow dynamics. Heidelberg, Berlin: Springer-Verslag.

27. Koretsky, M. D. 2004. Engineering and Chemical Thermodynamics. Oregon, United States of America: John Wiley and Sons,Inc.

28. Lamarsh, J. R. Baratta, A. J. 2001. Introduction to Nuclear Engineering. 3rd Edition. Upper Saddle River, NJ. Pearson Prentice Hall.

29. Lemasson, D. 2009. Design of a feedwater tank for the High Performance Light Water Reactor, Internship report. Germany.

30. Lewis, E, E. 2008. Fundamentals of Nuclear Reactor Physics.

31. Meng, M, Peng, X. F, YE, P & Duan, Y. Y. 2009. Bubble dynamical behaviour and thermal non equilibrium during flow boiling in U-turn bends of hairpin tubes. Chemical Engineering and Processing: Process Intensification, 48:1177-1186.

32. Moalem, D. & Sideman, S. 1973. The effect of motion on bubble collapse. International Journal of Heat and Mass Transfer, 16:2321-2329.

33. OECD/IEA. 2008. Australian Energy Consumption and Production, historical trends and projections,

34. ABARE Research Report 1999.http://www.world-nuclear.org/info/Current-and-Future-Generation/World-Energy-Needs-and-Nuclear-Power/#.UefFRFegZOI: 28/06/2013.

35. Rastogi, R. P. 2008. Introduction to Non-equilibrium Physical Chemistry.

36. Ribeiro, C. P. Lage, P L. 2004. Population balance modelling of a bubble size distributions in a direct-contact evaporator using a sparger model. Chemical Engineering Science, 59: 2636-2377. Chemical Engineering Science, 59:2363-2377.

37. Ribeiro, C. P. & Lage, P.L. C. 2004. Direct-contact evaporation in the homogeneous and heterogeneous bubbling regimes. Part I: experimental analysis. International Journal of Heat and Mass Transfer, 47:3825-3840. 6 May.

38. Schlagenhaufer, M. Starflinger, J. Schulenberg, T. 2008. Steam Cycle Analysis for HPLWR, International Students Workshop on High Performance Light Water Reactors. Germany, Karlsruhe.

39. Schulenberg, T. Starflinger, J. Marsault, P. Bitterman, D. Maraczy, C. Laurien, E. Lycklama a Nijeholt, J. A. Anglart, H. Andreani, M. Ruzickova, M. Toivonen, A. 2011. European supercritical water cooled reactor. Nuclear Engineering and Design, 241: 3505-3513.

40. Schulenberg, T & Starflinger, J. 2012. High Performance Light Water Reactor: Design and Analysis.Kalsruher Institute for Technology.

41. Spirax-Sarco. Date of access: 11 Nov 2014. <http://www.spiraxsarco.com/Documents/Boiler_feedtank_systems-Sales_Brochure.pdf>

42. Squarer, D, Schulenberg, T, Struwe, D, Oka, Y, Bitterman, D, Aksan, N, Maraczy, C, Kyrki-rajamäki, R, Souyri, A & Dumaz, P. 2003. High Performance Light Water Reactor. Nuclear Engineering and Design, 221:167-180.

43. Starflinger, J & Schulenberg, T. 2010. High Performance Light Water Reactor Phase 2. Public final report.

44. Tordeas, N E & Kazimi, M S. 1990. Nuclear System 1: Thermal Hydraulic Fundamentals. United States of America.

45. Tsikluari, G. Talbert, R. Schmitt, B. Filippov, G. Bogoyavlensky, R. Grishanin. 2004. Supercritical steam cycle for nuclear power plants. Nuclear Engineering and Design, 235: 1651-1664.

46. Wilson, P. D. 1996. The nuclear fuel cycle,OUP.http://world-nuclear.org/info/Nuclear-Fuel-Cycle/Power-Reactors/Nuclear-Power-Reactors:28/06/2013.

47. WNA. 2013. Economics of Nuclear Power. http://www.world-nuclear.org/info/Economic Aspects/Economics-of-Nuclear-Power/#.UefO_1egZOI: 28/06/2013.

48. WNA. 2013. Generation 4 Nuclear Reactors http://world-nuclear.org/info/Nuclear-Fuel-Cycle/Power Reactors/Generation-IV-Nuclear-Reactors/#.Uc2JRVegZOI (28/06/2013).

49. Yoo, J, Ishiwatari, Y, Oka, Y & Liu, J. 2006. Conceptual design of a compact supercritical water-cooled fast reactor with thermal hydraulic coupling. Annals of Nuclear Energy, 33:945-956.

50. Yoon, H. J, Ishii, M & Revankar, S. T. 2006. Chocking flow modelling with mechanical and thermal non-equilibrium. International Journal of Heat and Mass Transfer, 49:171-186.

Appendix A Literature Study

A.1 Supercritical Light Water Reactor

Initial studies on the Supercritical Light Water Reactor (SCWR) were conducted since the 1950's. The SCWR was a futuristic concept of a Light Water Reactor (LWR) which operates with superheated steam at supercritical pressures (Schulenberg & Starflinger, 2012). In recent years the concept of the SCWR was improved with Oka et al. documenting all the design concepts in 2010 (Schulenberg & Starflinger, 2012).

The SCWR system is regarded as one of the most promising and innovative concepts of Generation IV reactor design (Yoo et al., 2006). Due to this fact, various nations including Canada, Germany, Japan, Korea, Russia and the USA have taken the concept and adapted it to their specific needs and technology availability.

From the SCWR plant layout, illustrated in Figure 1, it is important to note that the SCWR feed water preheating system included an open feed tank (Squarer et al., 2003).

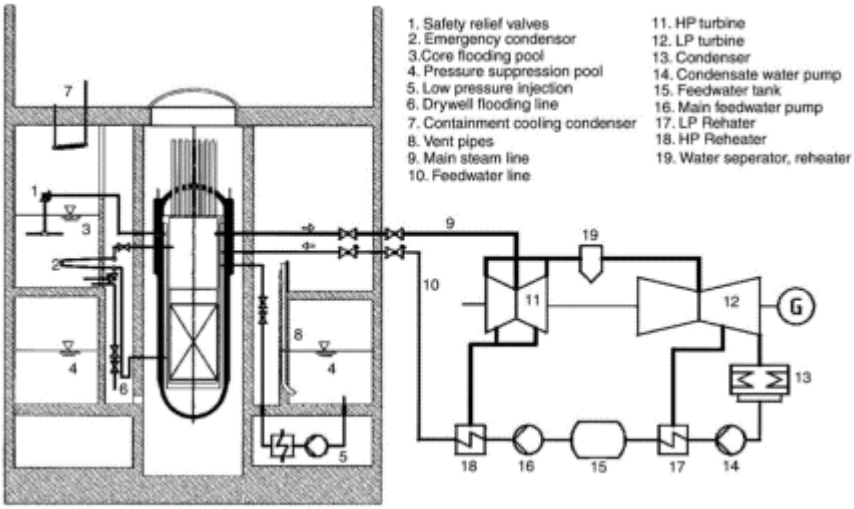

SCWR overall plant layout concept (Squarer et al., 2003).

In 2000 a consortium of European research institutes and industrial partners decided to investigate the feasibility, plant characteristics and development challenges of the Japanese SCWR concept (Schulenberg & Starflinger, 2012). The European Supercritical Water Cooled Reactor that evolved from this research is called the High-Performance Light Water Reactor (HPLWR) (Schulenberg, 2011).

The main advantage of the system is that the reactor is cooled and moderated by supercritical water with a critical pressure above 22.1 MPa. Supercritical water does not exhibit a phase change and therefore a boiling crisis is eliminated along with hot spots in the core (Schulenberg & Starflinger, 2012). The advantage to eliminate the boiling crisis is that no vapour blanket forms around the fuel when the water temperature rises, thus minimising the possibility of fuel meltdown (Lewis, 2008). Heat can be effectively removed above or at the pseudo-critical temperature of 385°C and sub-critical pressure of 25 MPa.

The efficiency of the core is determined by the outlet steam temperature. Dobashi et al (1998) illustrated this in a graph which can be seen in Figure 2. Due to material restrictions at extremely high temperatures the optimal exit temperature was designed to be 508°C at 25 MPa, which resulted in a primary efficiency of 44% (Dobashi et al., 1998).

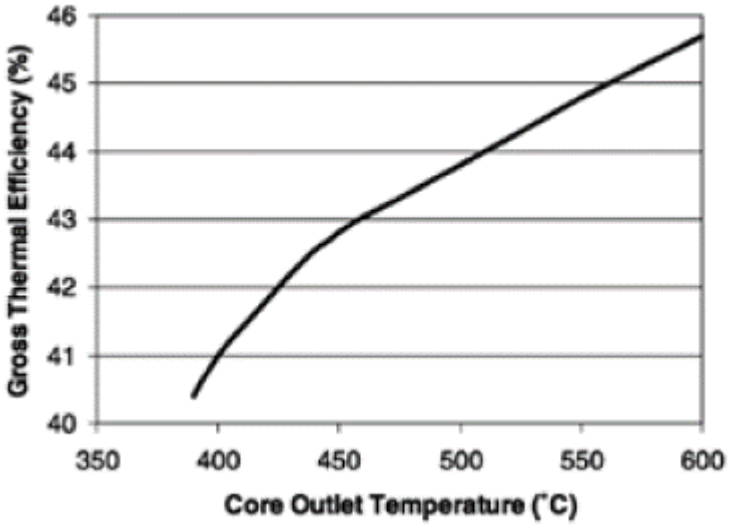

Thermal efficiency according to the SCWR core outlet temperature (Squarer et al., 2003).

From this primary selected operational point, the reactor's name was derived. The reactor operates at high temperature, high pressure, high efficiency and high power density and thus the name was selected as a High-Performance Light Water Reactor (Squarer et al., 2003).

A.2 High-Performance Light Water Reactor: Primary Circuit

The primary loop consists of the reactor pressure vessel (RPV) and its internals as well as the support systems. In this section, the primary circuit will only be analysed in terms of the feed water which serves as a cooling and moderating medium.

Bitterman et al introduced the RPV for the European HPLWR concept in 2003 (Schulenberg & Starflinger, 2012) as illustrated in below.

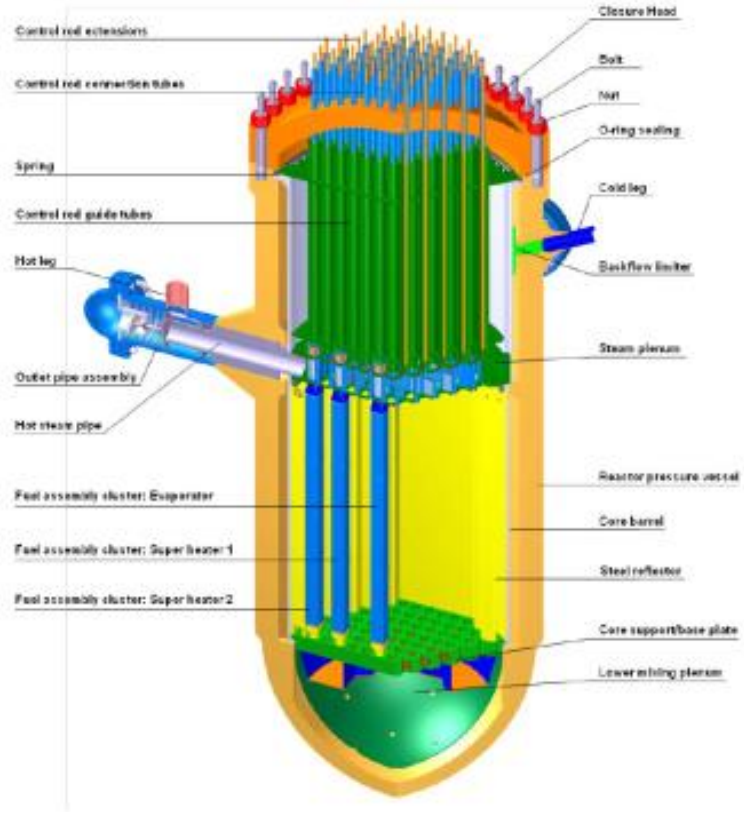

RPV for the European HPLWR concept Design (Schulenberg & Starflinger, 2012)

The reactor pressure vessel concept is based on a PWR design and includes the core, along with the core barrel, a mixing plenum located above and underneath the core and the control rod drive (Starflinger & Schulenberg, 2010).

In 2008 Fisher et al. analysed the thermal stresses and deformations of the RPV with the focus on the steam plenum, which can occur due to the exposure of colder feed water to the wall of the RPV and the exposure of other components to the superheated steam. It was concluded that the stresses are sufficiently low and the design was confirmed to be acceptable. It was also suggested that a transient analysis to be done so that fatigue and fracture formation possibilities could be determined (Schulenberg, 2011).

Core cooling

The thermal power of the core is estimated to be 2300 MW if the electrical power output of the power plant is 1000 MW with an efficiency of 44%.Earlier studies by Dobashi et al. (Dobashi et al., 1998) stated that the optimum thermal efficiency is reached when the feed water enters the core at 280°C and an outlet water temperature of 500°C at a system pressure of 25 MPa. The outlet temperature is low in comparison to other once through steam cycles but still challenging in regards to available fuel cladding materials. A mass flow rate of 1179 kg/s for the coolant is required when the target temperatures and power are taken into consideration.

The core of the HPLWR is a three stage heat-up configuration based on the assembly design of Hofmeister et al (Hofmeister et al., 2007) as shown below.

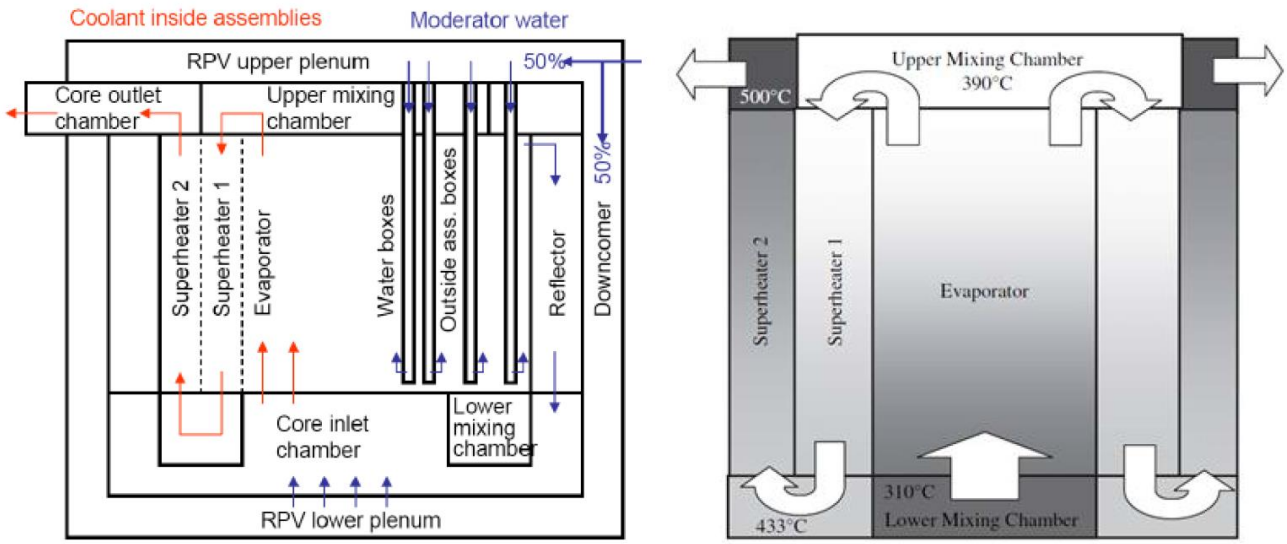

Three pass core design of the HPLWR (Starflinger & Schulenberg, 2010).

In the first heat-up stage the coolant serves as moderator with 25% of the total feed water flowing downwards through the gaps between the assembly boxes. The moderator also flows through the moderator boxes. The flow in this stage is a downward flow which results in heating the moderator to 360°C and is similar to economisers in coal-fired boilers. The moderator is then mixed with fresh coolant supplied through the downcomer. The mixing occurs in the lower core plenum with a resulting core inlet temperature of 310°C.

The second stage of heating, as illustrated in Figure 3, occurs in the evaporator assemblies, consisting of 52 clusters located in the centre of the core. The flow is upward in the core centre and the coolant is then conditioned with feed water, which is supplied through jets of feed water nozzles, in the plenum located above the core. In this phase, which is known as the evaporator, water is heated to 390°C. The coolant is then directed into the 52 clusters of the first super heater, located around the evaporator. Moving in a downward flow the coolant is heated to 433°C. This is followed by a tertiary mixing stage in the outer part of the chamber located below the core. It should be noted that no additional coolant is added to this mixing stage.

The third and final heating are enabled by the upward flow through the assemblies of the second super heater stage, with the final stage ensuring a 500°C outlet water temperature. The second super heater also consists of 52 clusters which surround the first super heater (Schulenberg, 2011).

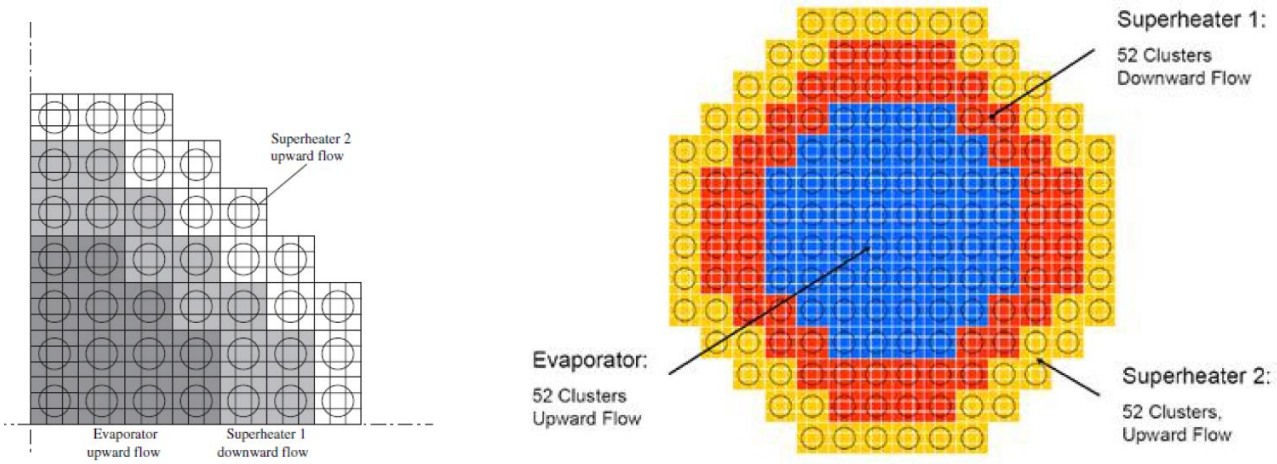

Core layout of the HPLWR (Starflinger & Schulenberg, 2010).

A.3 Layout of Niederaussem Power Plant

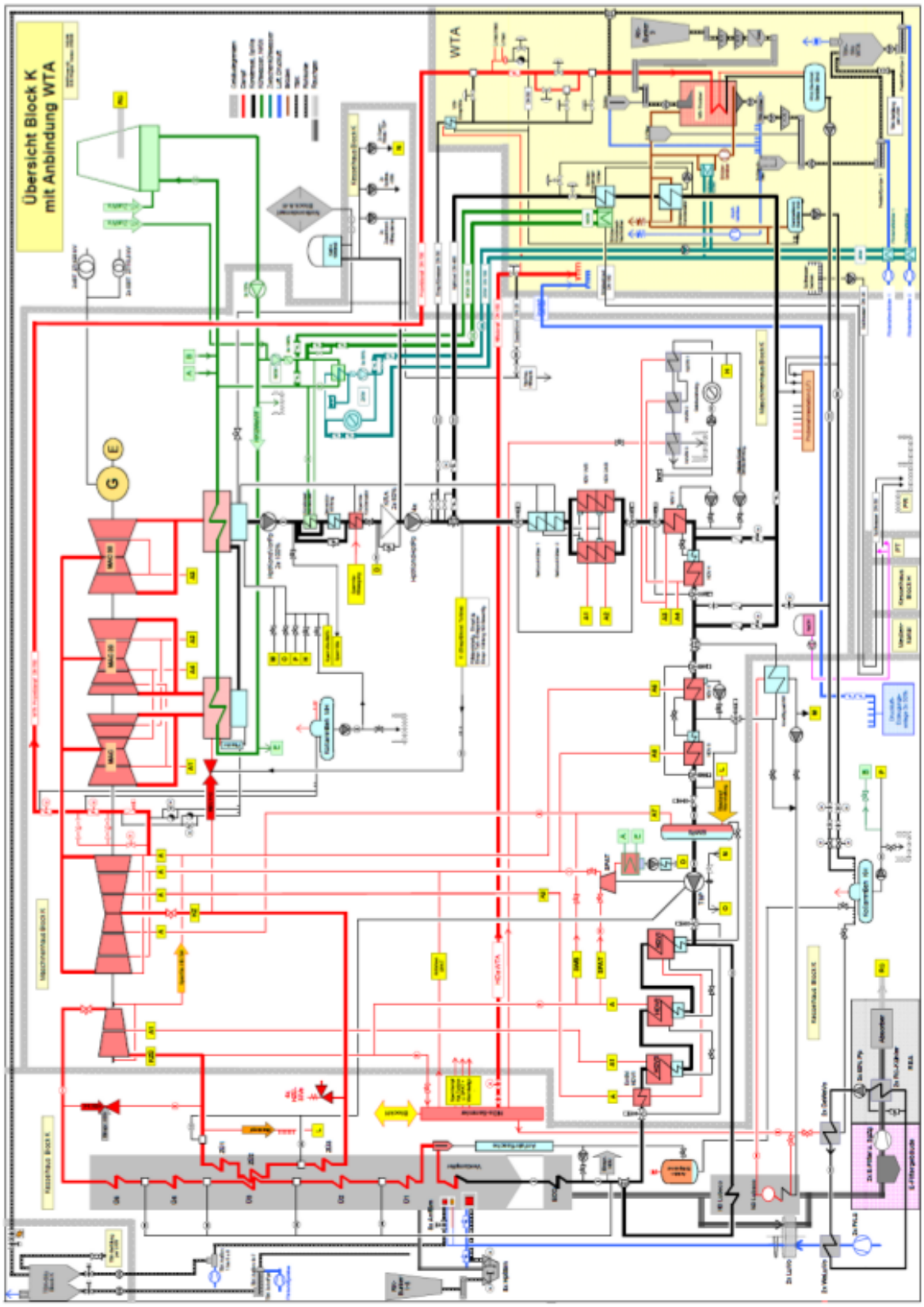

Schematic of the NIEDERAUSSEM UNIT K power generation plant.

A.4 Modern Open Feed Water Heaters

Due to technology improvements, the concept of the open feed water has also improved in design and material selection. In this section, some of the more modern concepts will be discussed.

The first concept is that of Flowserve (AG, 2006). The feedwater deaerating plant supplied by Flowserve Gestra, consist of a conventional deaerating dome and a feed water tank. The purpose of the deaerator dome is to remove dissolved gases such as carbon dioxide, oxygen and incondensable gases from the feed water which can cause corrosion to the metal parts of the boiler. The feed water flows directly into the tank after being deaerated, the tank is flanged to the deaerator dome. The feed water tank is then heated by injected steam via, injectors. Most feed water tanks are similar to that of the Flowserve design and is based on the same processes. The following figure illustrates the process and components that are part of the feed water plant (AG, 2015).

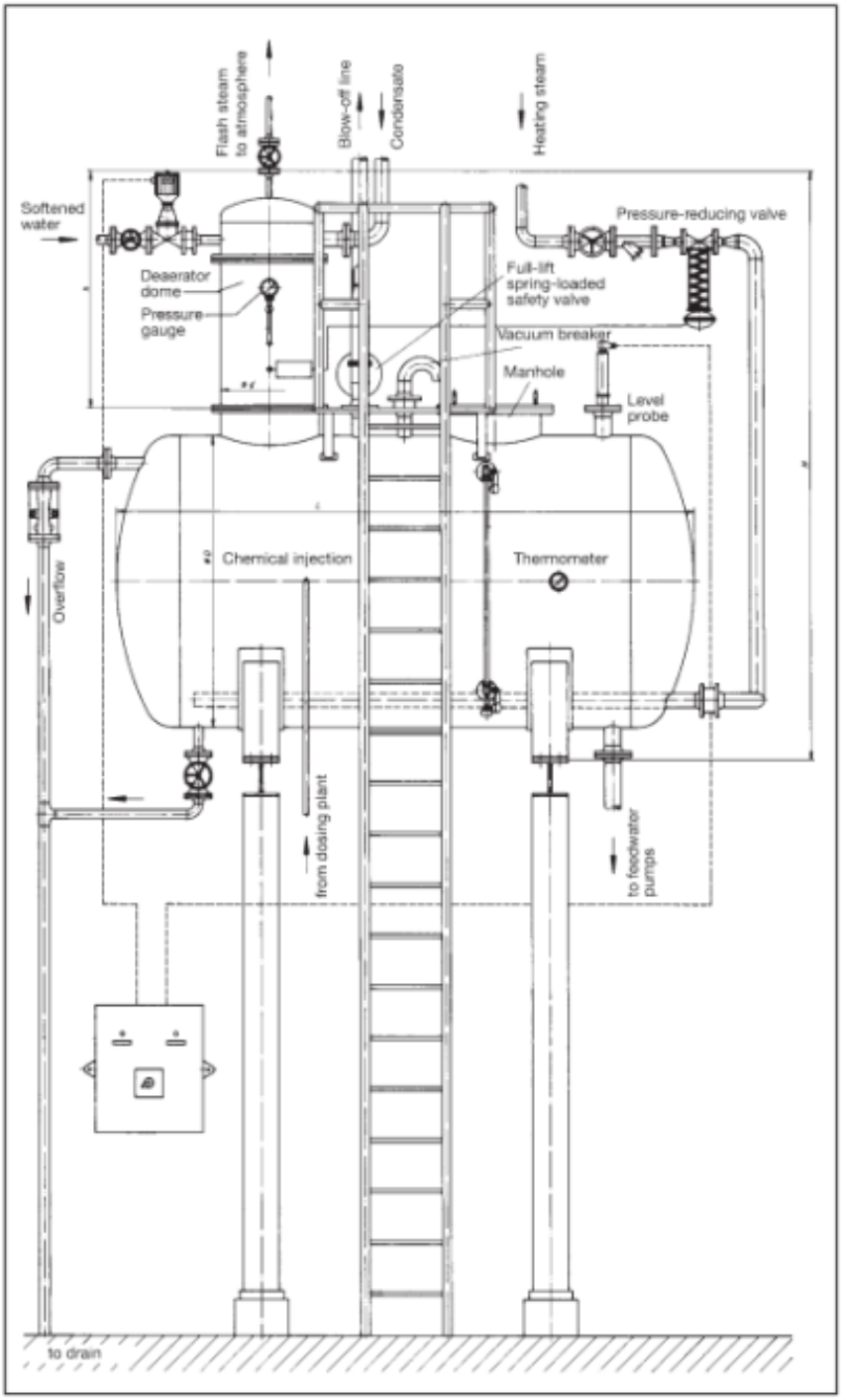

Feed water heater plant (ARCA, 2014).

The second design is that of the Hurst Boiler and Welding company, Inc. (Hurst Boiler and welding company, Inc., 2014) shown in the next figure. The fresh make-up water is fed through an inlet water connection into the deaerator, thus passing through the steam-filled and venting sections. As the temperature of the water is raised many of the incondensable gases are released. The water then flows into a scrubber which establishes the final deaerating. The steam is then introduced to break the water down into a fine mist. The water from the deaerator is then passed on to the feed tank and the gas is vented to the atmosphere. The water temperature is also raised to eliminate thermal shock in the boiler or reactor (Hurst Boiler and welding company, Inc., 2014).

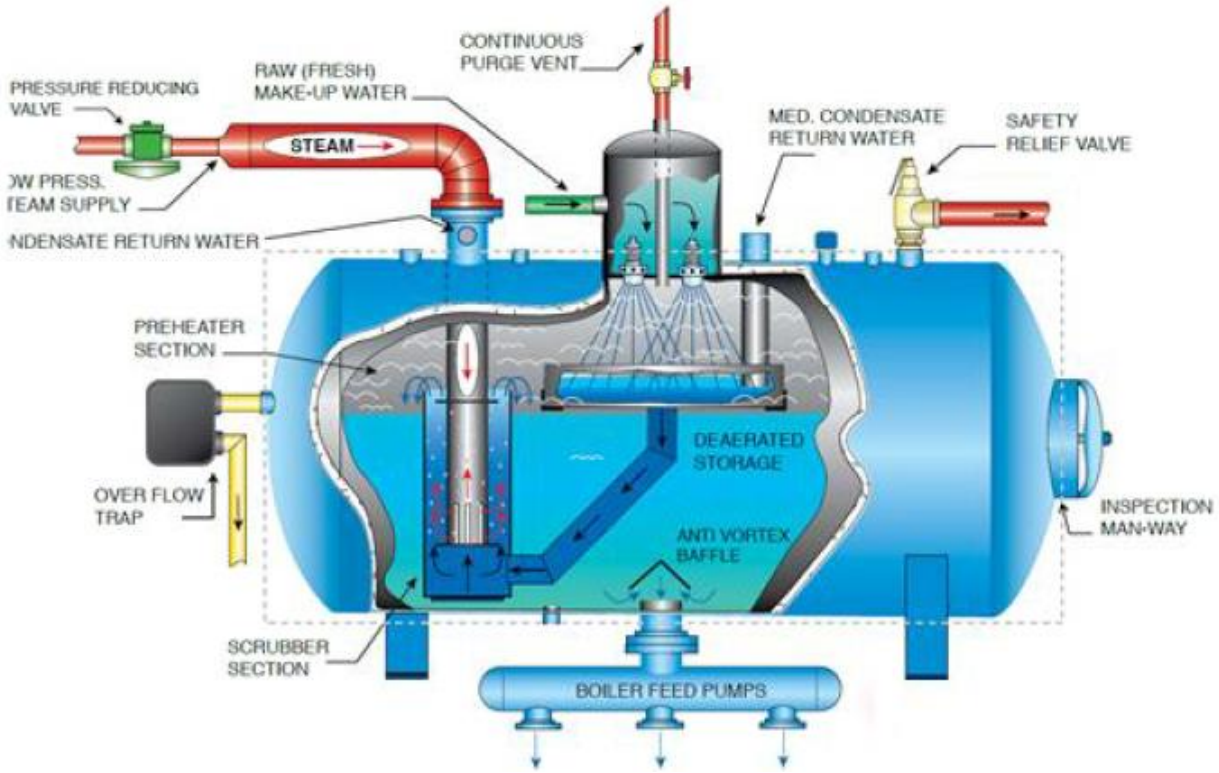

Illustration of the oximiser feed water deaerators form the Hurst Boiler And Welding Company, Inc (HURST BOILER AND WELDING COMPANY, INC., 2014)

The feed water tank designed by Sprax Sarco (Spirax-Sarco, 2015), may seem different but operates in the same manner as that of Flowserve (AG, 2015). The unit consists of a flash condensing head, a makeup tank and a steam injector system. The design makes use of two feed water heating technologies. The first is flashing steam and the second is that of steam injection. Steam flashing is when make-up water and flashing condensate are fed into the feed water tank above the surface. The energy of the flash steam is lost to the atmosphere and thus leaving the condensate at a lowered temperature than which is required. On the other hand, the preferred way of heating the feed water is by distributing the streams through sparging pipes below the water surface. These processes are illustrated in the next figure.

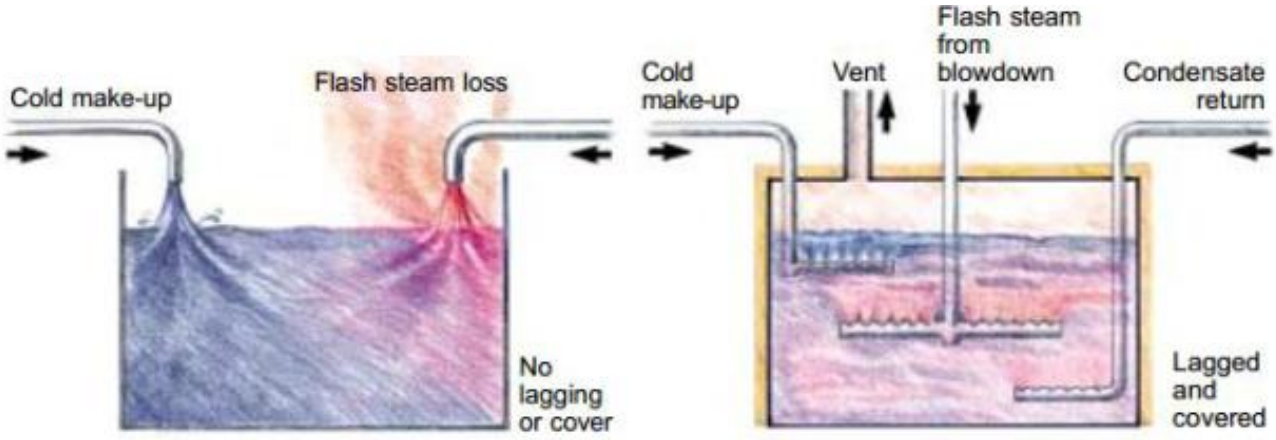

Illustration of the oximiser feed water deaerators form the Hurst Boiler And Welding Company, Inc. (Hurst Boiler And Welding Company, Inc., 2014).

The processes are implemented in the condensing head that is placed into the square feed water vessel .Cold make-up water, which is rich in oxygen, is mixed with condensate and flash steam, from the blowdown heat recovery, to remove the oxygen and other gases. The condensate then flows into the feed water vessel by means of a sparge tube. The header serves as a mixing unit which brings all the incoming flows together. Spirax (Spirax-Sarco, 2015) believes that the head eliminates the cost and possible problems of a sparge system and the usual three separate tank connections. The steam injection system ensures the silent but vigorous mixing of steam into the feed water; the feed water temperature is maintained at a high yet steady level to ensure smooth boiler operations (Spirax-Sarco, 2015).

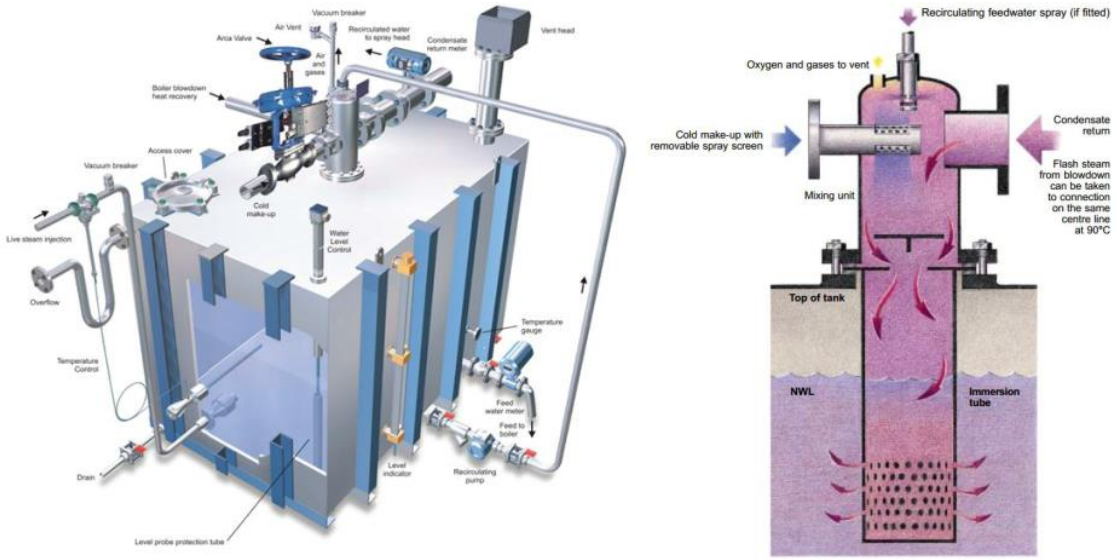

Illustration of the SPIRAX-SARCO deaerating head and feed water vessel (SPIRAX-SARCO, 2015).

Appendix B Theoretical Background

B.1 Equilibrium Approach

There are two steady state models to be developed, with the first consisting of single stage mixing and the second will consist of multi-stage mixing. For the simulation models, it is assumed that equilibrium conditions exist thus there is no tendency to spontaneously change with time. (Koretsky, 2004)

The basis of the steady-state single stage mixing model is to assume that the open feed water heater designed by Lemasson (2009) is a single mixing chamber. All fluid streams that enter the open feed water heater will mix instantaneously and therefore the thermodynamic processes of heat and mass transfer also occur simultaneously. The single stage mixing model serves as a basis on which the non-equilibrium model will be developed.

In the practical setup, as illustrated in the next figure, the open feed water heater actually consists of three mixing chambers. It is assumed for the multi-stage mixing model that steady state mixing occurs within each chamber; however mixing does not occur simultaneously in these chambers together but rather in sequence. The purpose of this multi-stage mixing model is to determine the properties of the feed water that are mixed prior to steam injection, along with the properties of the feed water that exit the open feed water heater when energy and mass are transferred to the bulk liquid. The energy and mass that are transferred to the bulk liquid are determined by the bubble formation- and ascension models.

SINGLE STAGE MIXING MODEL

The first equilibrium steady state simulation consists of single stage mixing. This model will replicate the analysis that was initially done by Lemasson (Lemasson, 2009) and implies that all of the fluid streams are combined in a single stage, as illustrated in the following figure.

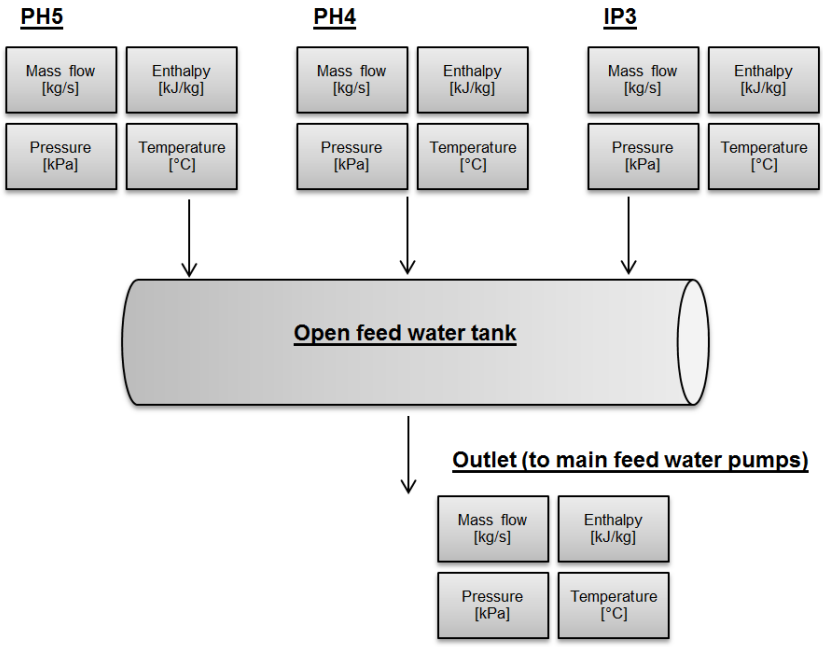

Diagrammatic layout of the single stage mixing mathematical model.

To determine the outlet properties of the OFWH the conservation laws of mass, energy and momentum are used as follows:

Conservation of mass

For the selected control volume, OFWH, the continuity equation will be applied. The control volume is defined as a collection of unchanging contents. The continuity equation is described as follows:

$$\frac{\partial}{\partial t}\int \rho d\forall + \sum \rho_{out} A_{out} v_{out} - \sum \rho_{in} A_{in} v_{in} = 0 \quad \text{(B-1.1)}$$

In the continuity equation, the rate of change in mass within the control volume is included, it is assumed that the mass is unchanged therefore $\frac{\partial}{\partial t}\int \rho d\forall = 0$ thus reducing the continuity equation to:

$$\sum \rho_{out} A_{out} v_{out} - \sum \rho_{in} A_{in} v_{in} = 0 \quad \text{(B-1.2)}$$

The conservation of mass is then as follows for a fixed control volume:

$$\dot{m}_{out} - \dot{m}_{in} = 0 \quad \text{(B-1.3)}$$

Once Equation B-1.3 is applied to the OFWH, the conservation of mass is defined as follows:

$$\dot{m}_{Outlet} = \dot{m}_{PH5} + \dot{m}_{PH4} + \dot{m}_{IP3} \quad \text{(B-1.4)}$$

Conservation of energy

The conservation of energy, also known as the first law of thermodynamics or the energy equation, is described by the time rate of increase of the total energy stored in the control volume which is equal to the sum of the net time rate of energy addition by heat transfer into the control volume and the net time rate of energy addition by work transfer into the control volume. The energy equation is as follows:

$$\frac{D}{Dt}\int e\rho d\forall = \left(\sum \dot{Q}_{in} - \sum \dot{Q}_{out}\right) + \left(\sum \dot{W}_{in} - \sum \dot{W}_{out}\right) \quad \text{(B-1.5)}$$

The time rate of increase of the total energy stored in the control volume, $\frac{D}{Dt}\int e\rho d\forall$ is zero for steady state conditions. Due to no work being done in the control volume, the net time rate of energy addition by work transfer into the system is also zero. Thus reducing the conservation of energy equation to the following:

$$\sum \dot{Q}_{in} = \sum \dot{Q}_{out} \quad \text{(B-1.6)}$$

Given Equation B-1.6 is applied to the OFWH, the conservation of energy is as follows:

$$\dot{m}_{Outlet} h_{Outlet} = \dot{m}_{PH5} h_{PH5} + \dot{m}_{PH4} h_{PH4} + \dot{m}_{IP3} h_{IP3} \quad \text{(B-1.7)}$$

MULTI-STAGE MIXING MODEL

Once the feed water vessel is viewed in more detail as shown in the following figure, the streams aren't mixed in a single stage. Condensate from preheater 4 (PH4) and feed water from preheater 5 (PH5) are mixed in the first chamber. After the first chamber is filled, the feed water flows over into the secondary chamber where it is mixed again with feed water from PH5. The two streams mix and flow to the third chamber where steam from the intermediate steam turbine is injected into the water mass which causes the temperature of the mixture to increase.

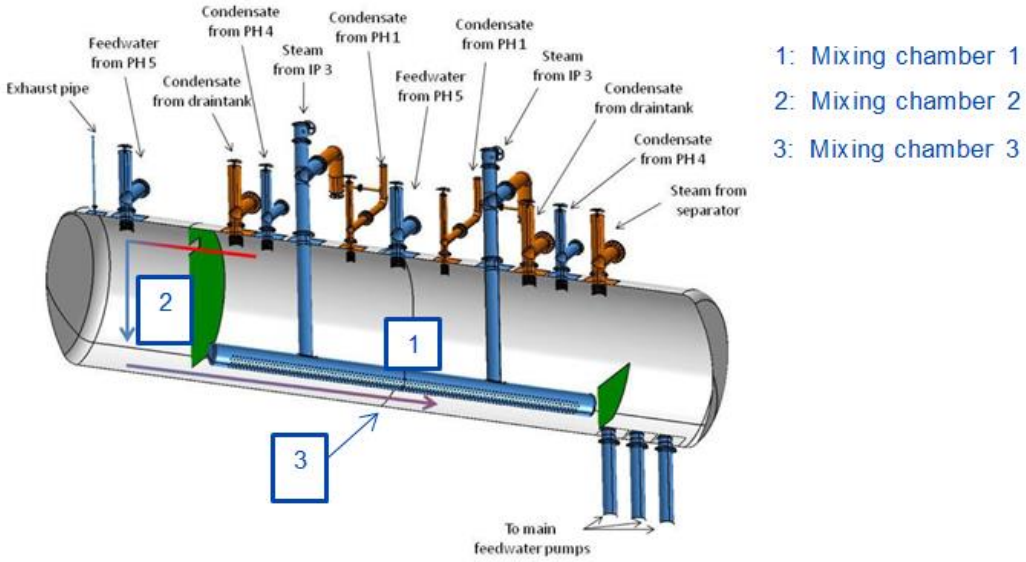

Open feed water tank with indicated mixing chambers (Lemasson, 2009).

As illustrated in the next figure, inside the first chamber a fraction of the feed water from preheater 5 (PH5) is sprayed into the feed water heater and is heated with the stream from preheater 4 (PH4) which is partially condensed (Lemasson, 2009).

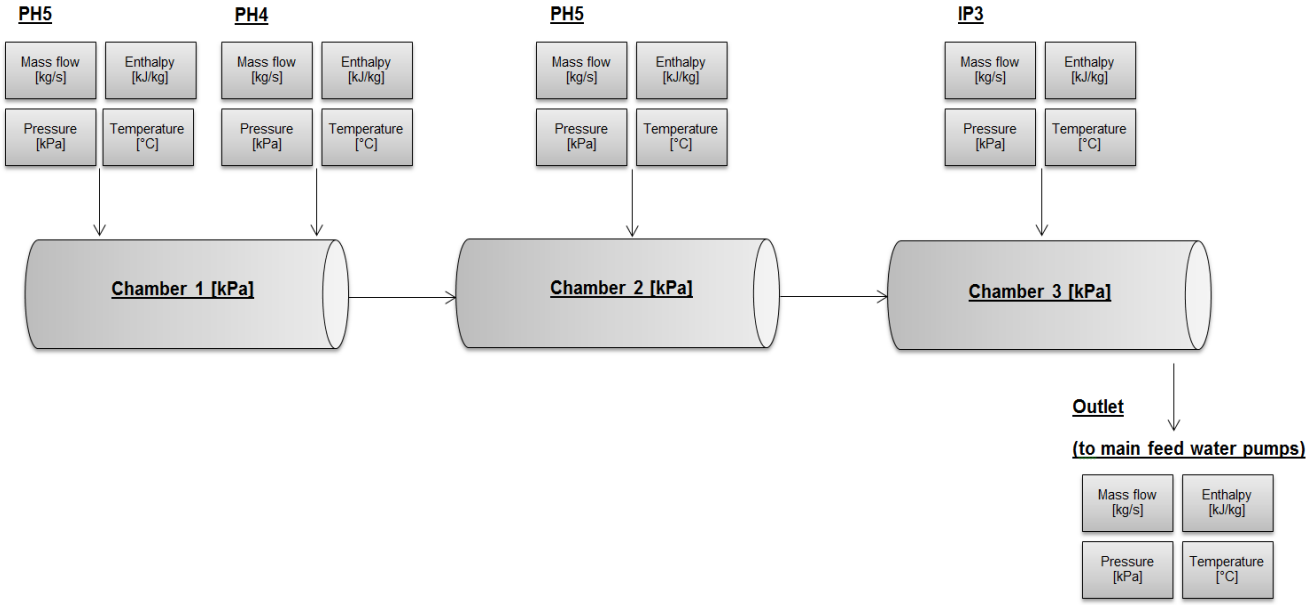

Diagram of the multistage mixing process.

The conservation laws for the mixing of the streams in the first chamber are as follow:

Conservation of mass

Once Equation B-1.3 is applied to the OFWH, the conservation of mass is as follows:

$$\dot{m}_{C1} = y_m \dot{m}_{PH5} + \dot{m}_{PH4} \quad \text{(B-1.8)}$$

Whereas y_m is the mass fraction of the mass flow from PH5 that is mixed with fluid from PH4 in the first chamber.

Conservation of energy

As soon as Equation B-1.6 is applied to the OFWH, the conservation of energy is as follows:

$$\dot{m}_{C1}h_{C1} = y_m\dot{m}_{PH5}h_{PH5} + \dot{m}_{PH4}h_{PH4} \quad \text{(B-1.9)}$$

The remaining fraction of feed water from PH5 is sprayed into the second chamber. The conservation laws for the mixing of streams in the second chamber are as follows:

Conservation of mass

Once Equation B-1.3 is applied to the OFWH, the conservation of mass is as follows:

$$\dot{m_{C2}} = (1 - y_m)\dot{m}_{PH5} + \dot{m_{C1}} \quad \text{(B-1.10)}$$

Conservation of energy

Equation B-1.6 is applied to the OFWH, the conservation of energy is as follows:

$$\dot{m}_{C2}h_{C2} = \dot{m}_{C1}h_{C1} + (1 - y_m)\dot{m}_{PH5}h_{PH5} \quad \text{(B-1.11)}$$

The level of water in the second chamber increases due to the addition of the remainder of the stream from PH5. The water from the second chamber flows into the third chamber, where it is heated with steam from the intermediate pressure turbine. The purpose of the steam is to heat the feed water to 155.6°C as per the calculation of Lemasson (Lemasson, 2009).

Conservation of mass

Once Equation B-1.3 is applied to the OFWH, the conservation of mass is as follows:

$$\dot{m}_{Outlet} = \dot{m}_{IP3} + \dot{m}_{C2} \quad \text{(B-1.12)}$$

Conservation of energy

Equation B-1.6 is applied to the OFWH, the conservation of energy is as follows:

$$\dot{m}_{Outlet}h_{Outlet} = \dot{m}_{C2}h_{C2} + \dot{m}_{IP3}h_{IP3} \quad \text{(B-1.13)}$$

B.2 Non-equilibrium approach: Multiple bubble columns

MULTIPLE BUBBLE COLUMNS: HEAT AND MASS TRANSFER

From the Campos and Lage (2001) model and simulation of direct contact evaporators, the total energy and mass transferred within the depletion time can be determined.

The liquid phase of the model balances the liquid mass, solute mass and energy as follows:

Conservation of mass

Once Equation B-1.3 is applied to the OFWH, the conservation of mass is as follows:

$$\dot{m}_{liquid} = \dot{m}_{inlet\ liquid\ in\ evaporator} + \dot{m}_{evaporated} - \dot{m}_{outlet\ flow\ of\ liquid}. \quad \text{(B-2.1)}$$

$$Y\dot{m}_{liquid} = Y\dot{m}_{inlet\ liquid\ in\ evaporator} - Y\dot{m}_{outlet\ flow\ of\ liquid}. \quad \text{(B-2.2)}$$

Conservation of energy

As soon as Equation B-1.6 is applied to the OFWH, the conservation of energy is as follows:

$$\dot{m}_{liquid} C_{p_{liquid}} \left(T_{liquid,new} - T_{liquid}\right) = Q_{steam\ to\ fluid,system} + Q_{distrubution} - Q_{thermal\ loss}. \quad \text{(B-2.3)}$$

For this study, the thermal losses and the energy added by the distribution system will be neglected. The previous equation can be simplified to the following:

$$\dot{m}_{liquid} C_{p_{liquid}} \left(T_{liquid,new} - T_{liquid}\right) = Q_{steam\ to\ fluid,system}. \quad \text{(B-2.4)}$$

To determine the total mass and energy transfer in the depletion time the formation frequency, f, and the total amount of orifices are incorporated. The formation frequency as well as the total mass and energy transferred are as follows:

Conservation of mass

Once Equation B-1.3 is applied to the OFWH the conservation of mass is as follows:

$$\dot{m}_{evaporated} = \dot{m}_{transferred} * \#_{orifice} * f \quad \text{(B-2.5)}$$

Where $f = \frac{total\ number\ of\ bubbles\ in\ bubble\ column}{depletion\ time}$. (B-2.6)

Conservation of energy

As soon as Equation B-1.6 is applied to the OFWH the conservation of energy is as follows:

$$Q_{steam\ to\ fluid,system} = Q_{steam\ to\ fluid} * \#_{orifice} * f. \quad \text{(B-2.7)}$$

INTEGRATED OFWH MODEL

The integrated model consists of the equilibrium model as well as the transient non-equilibrium state model. The equilibrium model is required to obtain the feed water conditions after the feed water from the various preheaters has been mixed. These conditions will serve as the initial conditions before the steam is injected into the bulk liquid. The steam injection phase is represented by the transient state non-equilibrium model. The resulting open feed water temperature is determined from the heat that is transferred to the liquid by the superheated steam bubble.

Appendix C Simulation models and verification

C.1 Simulation and verification of Equilibrium steady state: Single stage model

SIMULATION AND VERIFICATION OF SINGLE STAGE MIXING MODEL

EES Model and Results

```
"Equilibrium steady state simulation"
"Single stage mixing model"

"Boundary conditions"

"IP3"
m_dot_IP3=19.74
P_IP3=751.3
T_IP3=232.7+273.15
h_IP3=Enthalpy(Steam,T=T_IP3,P=P_IP3)

"PH5"
m_dot_PH5=721.5
P_PH5=751.3
T_PH5=135.24+273.15
h_PH5=Enthalpy(Water,T=T_PH5,P=P_PH5)

"PH4"
m_dot_PH4=437.6
P_PH4=1245
T_PH4=165.13+273.15
h_PH4=Enthalpy(Water,T=T_PH4,P=P_PH4)

"Conservation of mass"
m_dot_outlet=m_dot_PH5+m_dot_PH4+m_dot_IP3

"Conservation of energy"
m_dot_outlet*h_outlet=m_dot_PH5*h_PH5+m_dot_PH4*h_PH4+m_dot_IP3*h_IP3

P_outlet=551.3
T_outlet=Temperature(Water,P=P_outlet,h=h_outlet)
```

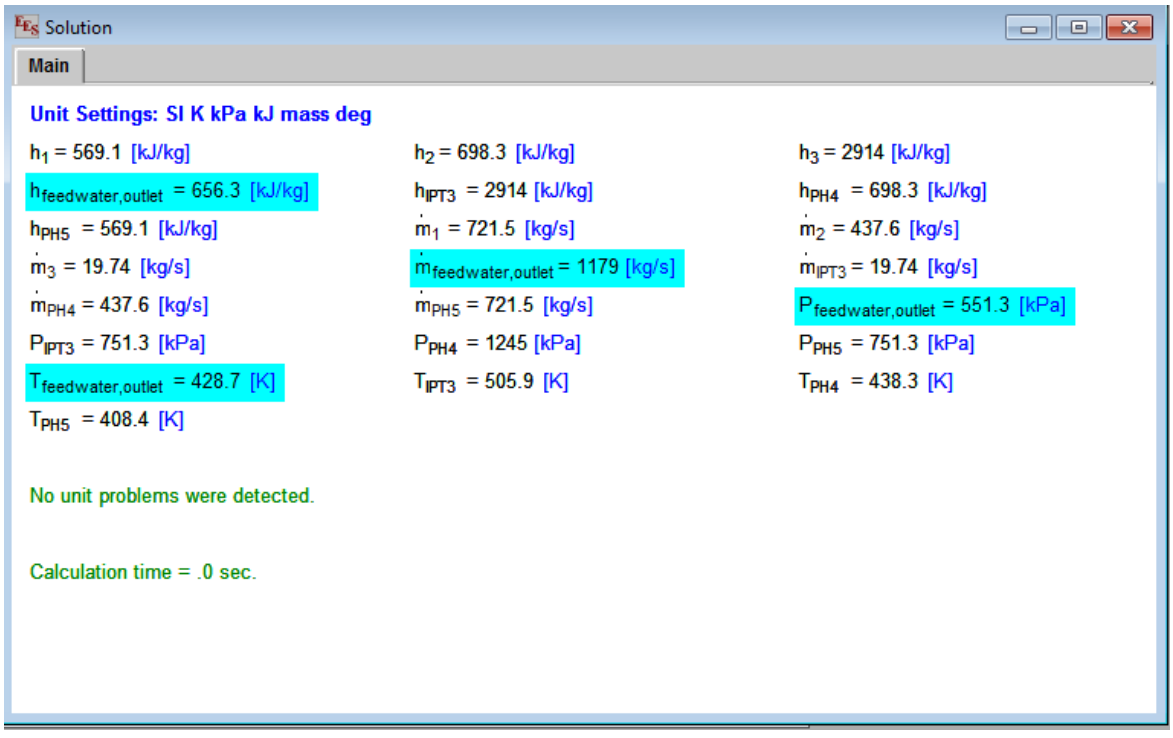

Flownex Model and Results

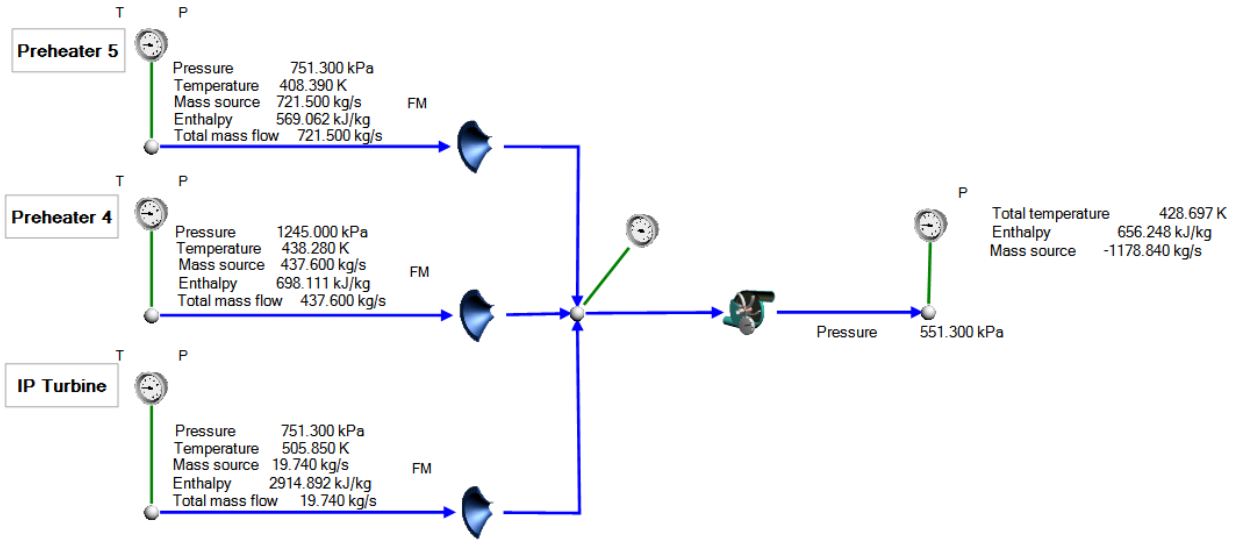

Comparison and verification of single stage mixing simulation in EES and FLOWNEX

	Lemasson	EES		FLOWNEX	
	Pre-determined value	Simulated value	Error [%]	Simulated value	Error [%]
IP3					
Fixed: Temperature [K]	505.85	505.85	0	505.85	0
Fixed: Pressure [kPa]	751.3	751.3	0	751.3	0
Enthalpy [kJ/kg]	2915	2914	0.0343	2914.892	0.0037
Fixed: Mass flow [kg/s]	19.74	19.74	0	19.74	0
PH5					
Fixed: Temperature [K]	408.39	408.39	0	408.39	0
Fixed: Pressure [kPa]	751.3	751.3	0	751.3	0
Enthalpy [kJ/kg]	569	569.1	0.0176	569.062	0.0109
Fixed: Mass flow [kg/s]	721.5	721.5	0	721.5	0
PH4					
Fixed: Temperature [K]	438.28	438.28	0	438.28	0
Fixed: Pressure [kPa]	1245	1245	0	1245	0
Enthalpy [kJ/kg]	698.22	698.3	0.0115	698.111	0.0156
Fixed: Mass flow [kg/s]	437.6	437.6	0	437.6	0
Outlet					
Temperature [K]	428.72	428.7	0.0047	428.697	0.0054
Pressure [kPa]	551.3	551.3	0	551.3	0
Enthalpy [kJ/kg]	656.26	656.3	0.0061	656.248	0.0018
Mass flow [kg/s]	1179	1179	0	1178.84	0.0136

C.2 Simulation and verification of Equilibrium steady state: Multi stage model

SUB-MODEL A: FEED WATER PREPARATION

Flownex Model and Results

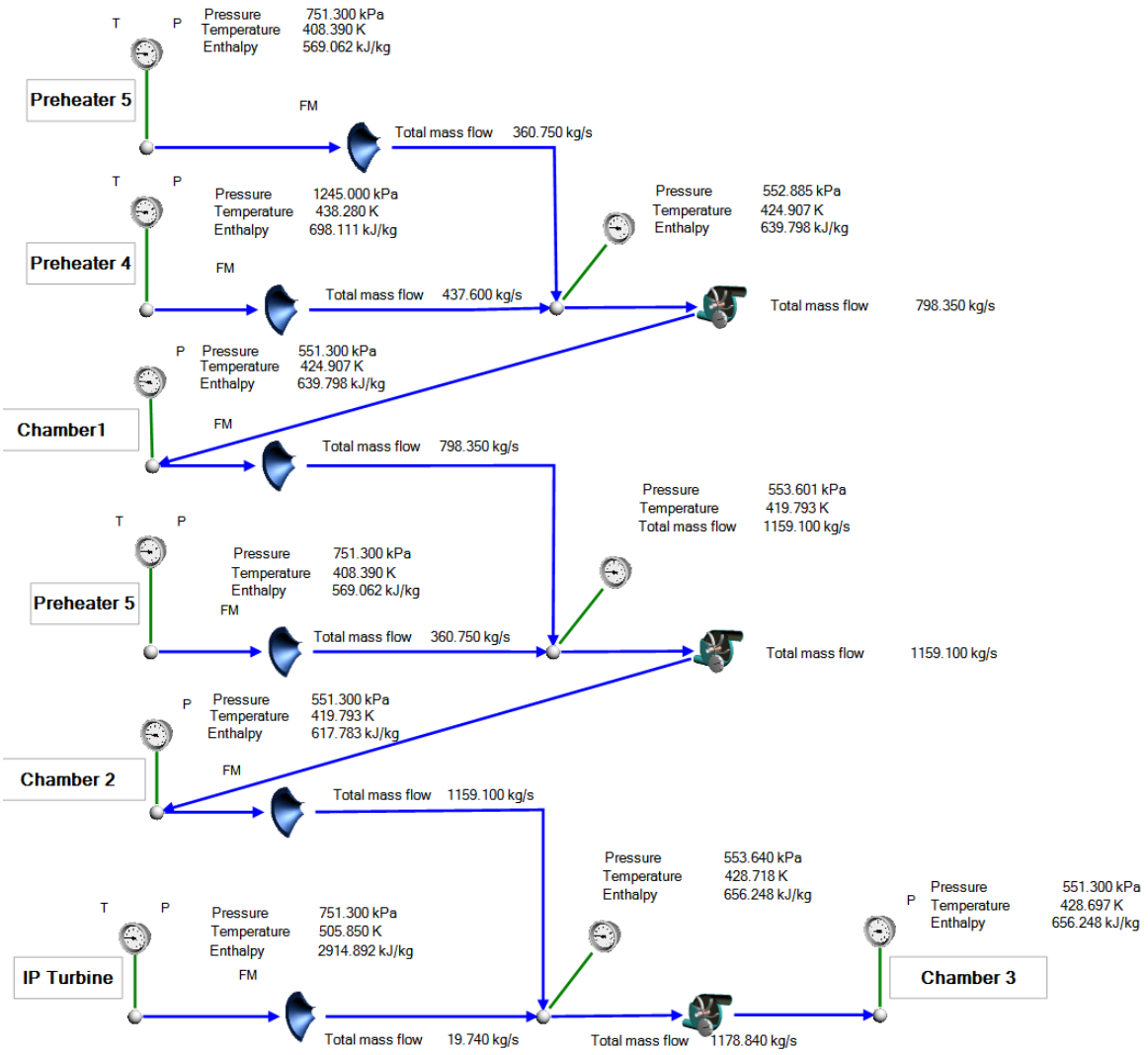

		Lemasson	FLOWNEX	
		Pre-determined value	Simulated value	Error [%]
Inlet conditions	IP3			
	Fixed: Temperature [K]	505.85	505.85	0
	Fixed:Pressure [kPa]	751.3	751.3	0
	Enthalpy [kJ/kg]	2915	2914.892	0.0037
	Fixed:Mass flow [kg/s]	19.74	19.74	0
	PH5			
	Fixed: Temperature [K]	408.39	408.39	0
	Fixed:Pressure [kPa]	751.3	751.3	0
	Enthalpy [kJ/kg]	569	569.062	0.0109
	Fixed:Mass flow [kg/s]	721.5	721.5	0
	PH4			
	Fixed: Temperature [K]	438.28	438.28	0
	Fixed:Pressure [kPa]	1245	1245	0
	Enthalpy [kJ/kg]	698.22	698.111	0.0156
	Fixed:Mass flow [kg/s]	437.6	437.6	0
Outlet properties	Chamber 1			
	Temperature [K]		424.907	-
	Pressure [kPa]		551.3	-
	Enthalpy [kJ/kg]		639.798	-
	Mass flow [kg/s]		798.350	-
	Chamber 2			
	Temperature [K]		419.793	-
	Pressure [kPa]		551.3	-
	Enthalpy [kJ/kg]		617.783	-
	Mass flow [kg/s]		1159.1	-
	Chamber 3			
	Temperature [K]	428.72	428.697	0.0054
	Pressure [kPa]	551.3	551.3	0
	Enthalpy [kJ/kg]	656.26	656.248	0.0018
	Mass flow [kg/s]	1179	1178.84	0.0136

C.3 Simulation and verification of Non-equilibrium transient state

SUB-MODEL B: BUBBLE FORMATION, BUBBLE ASCENSION AND HEAT AND MASS TRANSFER

Experimental bubble formation volumes and simulation results for an orifice size of 0.15cm

Medium	Density		Velocity		Surface tension		Initial radius		Gas flow rate		Bubble volume	
	g/ml	kg/m^3	cm/s	m/s	dyn/cm	N/m	cm	m	ml/s	m^3/s	ml	m^3
Water	1	1000	1	0.01	72.7	7.27	0.15	0.0015	13.53	1.35E-05	0.624	6.24E-07
									20	2.00E-05	0.871	8.71E-07
									21.76	2.18E-05	0.929	9.29E-07
									25.29	2.53E-05	1.059	1.06E-06
									26.47	2.65E-05	1.094	1.09E-06
									30	3.00E-05	1.292	1.29E-06
									36.47	3.65E-05	1.494	1.49E-06

Simulation bubble formation volumes and simulation results for an orifice size of 0.15cm

Medium	Experimental Bubble volume		Simulated bubble volume (0.016s)			Simulated bubble volume (0.0175s)			Simulated bubble volume (0.018s)			Simulated bubble volume (0.02s)		
	ml	m^3	ml	m^3	%error	ml	m^3	%error	ml	m^3	%error	ml	m^3	%error
Water	0.624	6.24E-07	0.625	6.25E-07	0.16%	0.664	6.64E-07	6.41%	0.677	6.77E-07	8.49%	0.728	7.28E-07	16.67%
	0.871	8.71E-07	0.819	8.19E-07	5.97%	0.873	8.73E-07	0.23%	0.891	8.91E-07	2.30%	0.962	9.62E-07	10.45%
	0.929	9.29E-07	0.870	8.70E-07	6.35%	0.928	9.28E-07	0.11%	0.947	9.47E-07	1.94%	1.020	1.02E-06	10.12%
	1.059	1.06E-06	0.970	9.70E-07	8.40%	1.040	1.04E-06	1.79%	1.060	1.06E-06	0.09%	1.140	1.14E-06	7.65%
	1.094	1.09E-06	1.030	1.03E-06	5.85%	1.070	1.07E-06	2.19%	1.090	1.09E-06	0.37%	1.180	1.18E-06	7.86%
	1.292	1.29E-06	1.100	1.10E-06	14.86%	1.180	1.18E-06	8.67%	1.200	1.20E-06	7.12%	1.300	1.30E-06	0.62%
	1.494	1.49E-06	1.270	1.27E-06	14.99%	1.360	1.36E-06	8.97%	1.390	1.39E-06	6.96%	1.510	1.51E-06	1.07%
Average error					8.08%			4.05%			3.90%			7.78%

Comparison between experimental and simulation results for an orifice size of 0.15cm

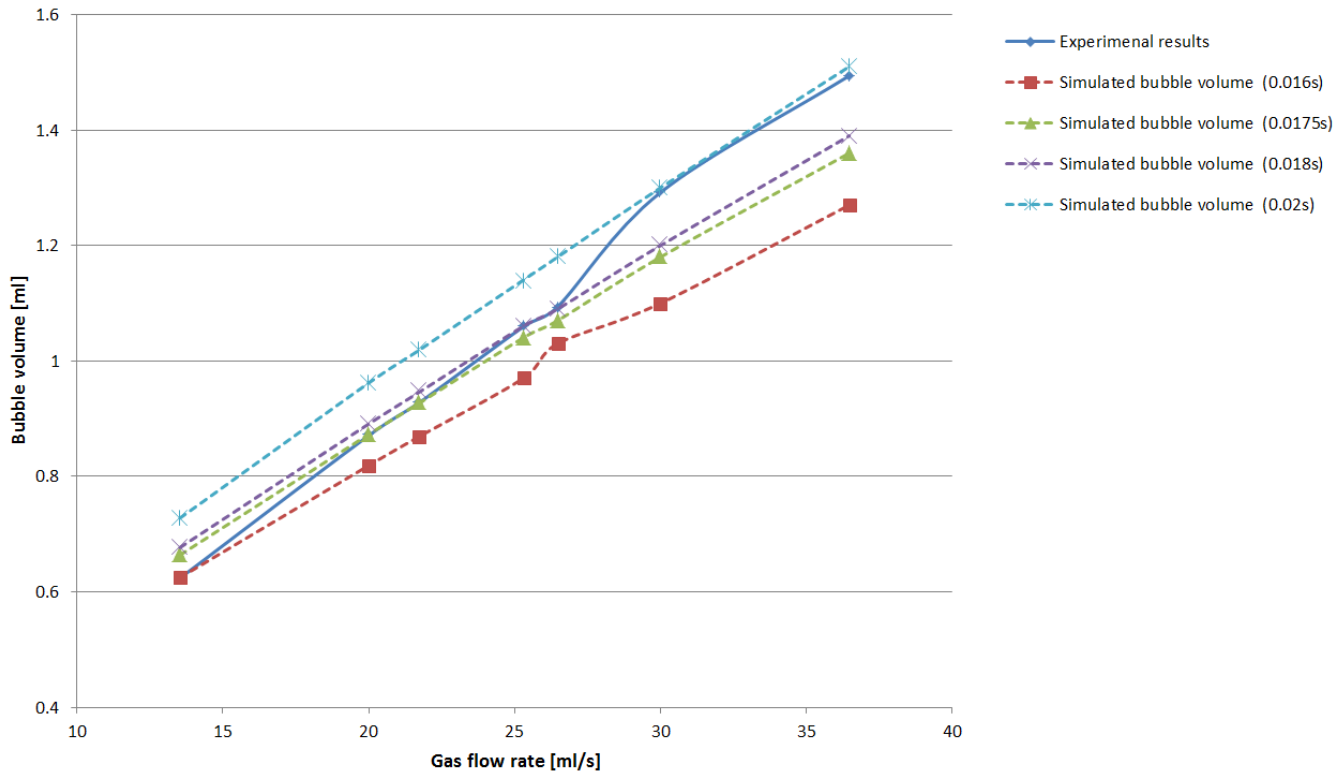

Experimental bubble formation volumes and simulation results for an orifice size of 0.2cm

Medium	Density		Velocity		Surface tension		Initial radius		Gas flow rate		Bubble volume	
	g/ml	kg/m^3	cm/s	m/s	dyn/cm	N/m	cm	m	ml/s	m^3/s	ml	m^3
Water	1	1000	1	0.01	72.7	7.27	0.2	0.002	14.7	1.47E-05	0.635	6.35E-07
									17.353	1.74E-05	0.753	7.53E-07
									21.17	2.12E-05	0.882	8.82E-07
									22.94	2.29E-05	0.988	9.88E-06
									30	3.00E-05	1.247	1.25E-06
									31.74	3.17E-05	1.341	1.34E-06
									35.294	3.53E-05	1.482	1.48E-06

Simulation bubble formation volumes and simulation results for an orifice size of 0.2cm

Medium	Gas flow rate		Experimental Bubble volume		Simulated bubble volume (0.0107s)			Simulated bubble volume (0.0118s)			Simulated bubble volume (0.012s)			Simulated bubble volume (0.014s)		
	ml/s	m^3/s	ml	m^3	ml	m^3	%error	ml	m^3	%error	ml	m^3	%error	ml	m^3	%error
Water	14.7	1.47E-05	0.635	6.35E-07	0.724	7.24E-07	14.08%	0.763	7.63E-07	20.20%	0.805	8.05E-07	26.79%	0.839	8.39E-07	32.13%
	17.353	1.74E-05	0.753	7.53E-07	0.792	7.92E-07	5.22%	0.837	8.37E-07	11.13%	0.885	8.85E-07	17.46%	0.924	9.24E-07	22.71%
	21.17	2.12E-05	0.882	8.82E-07	0.886	8.86E-07	0.45%	0.939	9.39E-07	6.44%	0.995	9.95E-07	12.79%	1.040	1.04E-06	17.91%
	22.94	2.29E-05	0.988	9.88E-07	0.929	9.29E-07	5.97%	0.985	9.85E-07	0.31%	1.050	1.05E-06	5.77%	1.090	1.09E-06	10.32%
	30	3.00E-05	1.247	1.25E-06	1.090	1.09E-06	12.35%	1.160	1.16E-06	6.82%	1.240	1.24E-06	0.80%	1.300	1.30E-06	4.25%
	31.74	3.17E-05	1.341	1.34E-06	1.130	1.13E-06	15.59%	1.210	1.21E-06	10.14%	1.280	1.28E-06	4.33%	1.350	1.35E-06	0.67%
	35.294	3.53E-05	1.482	1.48E-06	1.210	1.21E-06	18.29%	1.290	1.29E-06	12.96%	1.380	1.38E-06	7.22%	1.450	1.45E-06	2.16%
Average error							10.28%			9.71%			10.74%			12.88%

Comparison between experimental and simulation results for an orifice size of 0.2cm

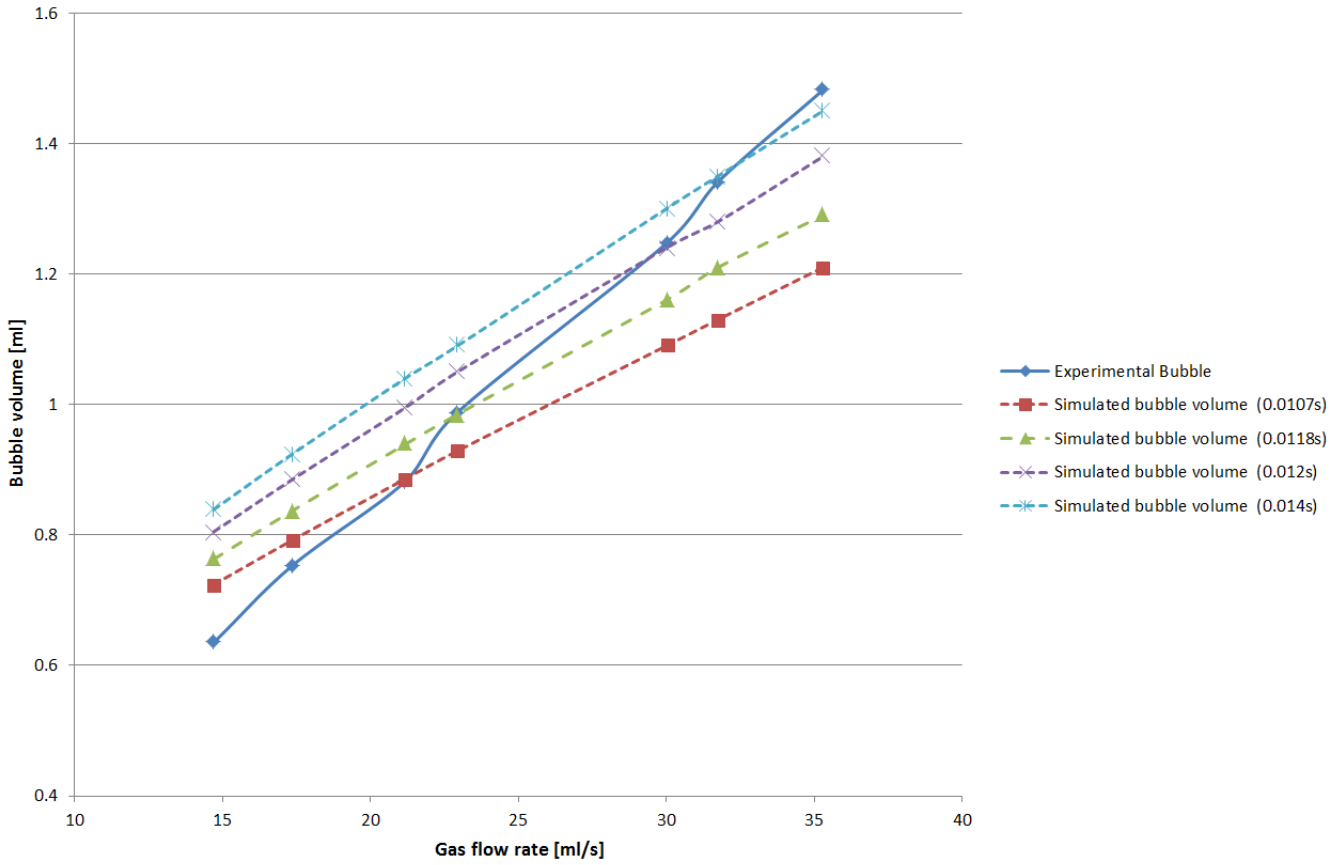

Experimental bubble formation volumes and simulation results for an orifice size of 0.25cm

Medium	Density		Velocity		Surface tension		Initial radius		Gas flow rate		Bubble volume	
	g/ml	kg/m^3	cm/s	m/s	dyn/cm	N/m	cm	m	ml/s	m^3/s	ml	m^3
Water	1	1000	1	0.01	72.7	7.27	0.25	0.0025	19.11	1.91E-05	0.8	8.00E-07
									20	2.00E-05	0.84	8.40E-07
									22.9	2.29E-05	0.95	9.50E-07
									27.05	2.71E-05	1.12	1.12E-06
									28.83	2.88E-05	1.2	1.20E-06
									33.23	3.32E-05	1.38	1.38E-06

Simulation bubble formation volumes and simulation results for an orifice size of 0.25cm

Medium	Gas flow rate		Experimental Bubble volume		Simulated bubble volume (0.01s)			Simulated bubble volume (0.0103s)			Simulated bubble volume (0.011s)			Simulated bubble volume (0.0135s)		
	ml/s	m^3/s	ml	m^3	ml	m^3	%error	ml	m^3	%error	ml	m^3	%error	ml	m^3	%error
Water	19.11	1.91E-05	0.8	8.00E-07	0.805	8.05E-07	0.62%	0.818	8.18E-07	2.25%	0.849	8.49E-07	6.13%	0.957	9.57E-07	19.63%
	20	2.00E-05	0.84	8.40E-07	0.826	8.26E-07	1.67%	0.840	8.40E-07	0.00%	0.872	8.72E-07	3.81%	0.983	9.83E-07	17.02%
	22.9	2.29E-05	0.95	9.50E-07	0.892	8.92E-07	6.11%	0.908	9.08E-07	4.42%	0.944	9.44E-07	0.63%	1.070	1.07E-06	12.63%
	27.05	2.71E-05	1.12	1.12E-06	0.985	9.85E-07	12.05%	1.000	1.00E-06	10.71%	1.040	1.04E-06	7.14%	1.190	1.19E-06	6.25%
	28.83	2.88E-05	1.2	1.20E-06	1.020	1.02E-06	15.00%	1.040	1.04E-06	13.33%	1.090	1.09E-06	9.17%	1.240	1.24E-06	3.33%
	33.23	3.32E-05	1.38	1.38E-06	1.120	1.12E-06	18.84%	1.140	1.14E-06	17.39%	1.190	1.19E-06	13.77%	1.360	1.36E-06	1.45%
Average error							9.05%			8.02%			6.78%			10.05%

Comparison between experimental and simulation results for an orifice size of 0.25cm

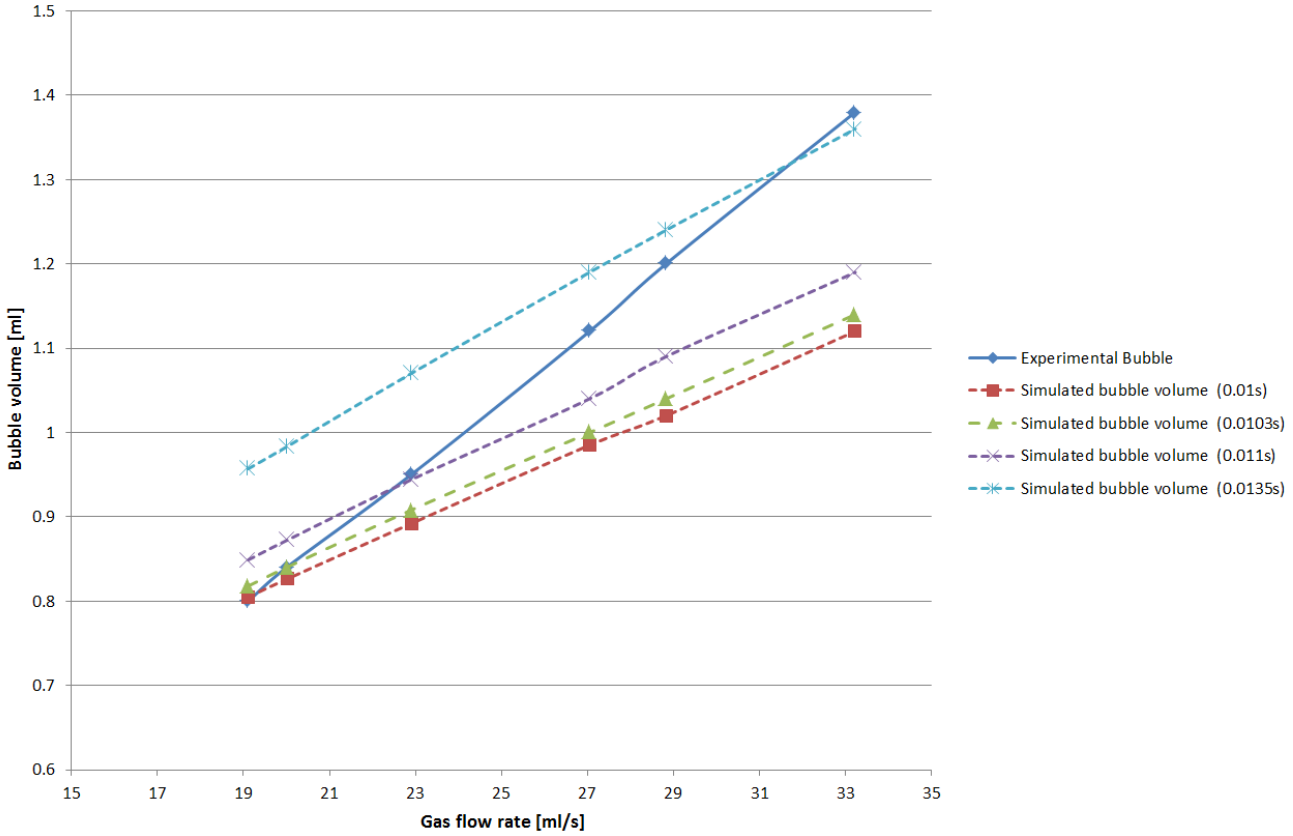

Bubble Ascension: Bubble Heat and mass transfer simulation and verification

Experimental results by Moalem and Sideman (1973)

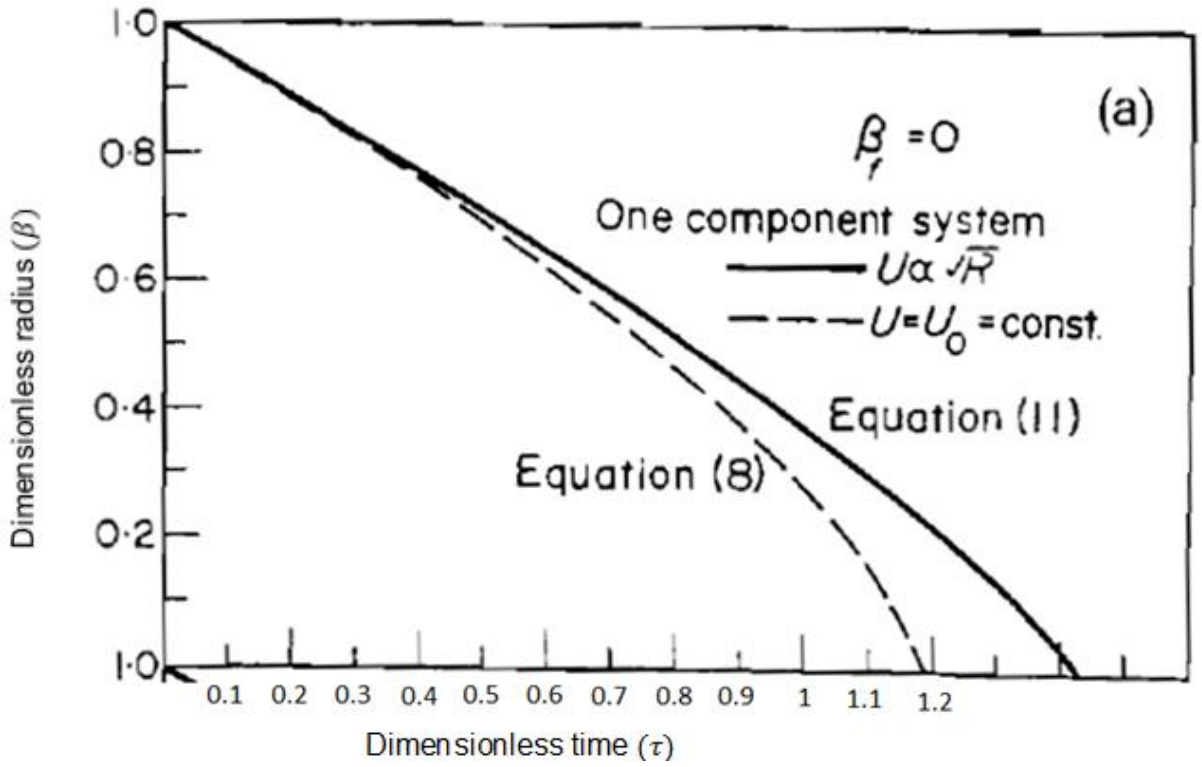

Comparison between the constant and radius dependent rise velocity (Moalem & Sideman, 1973).

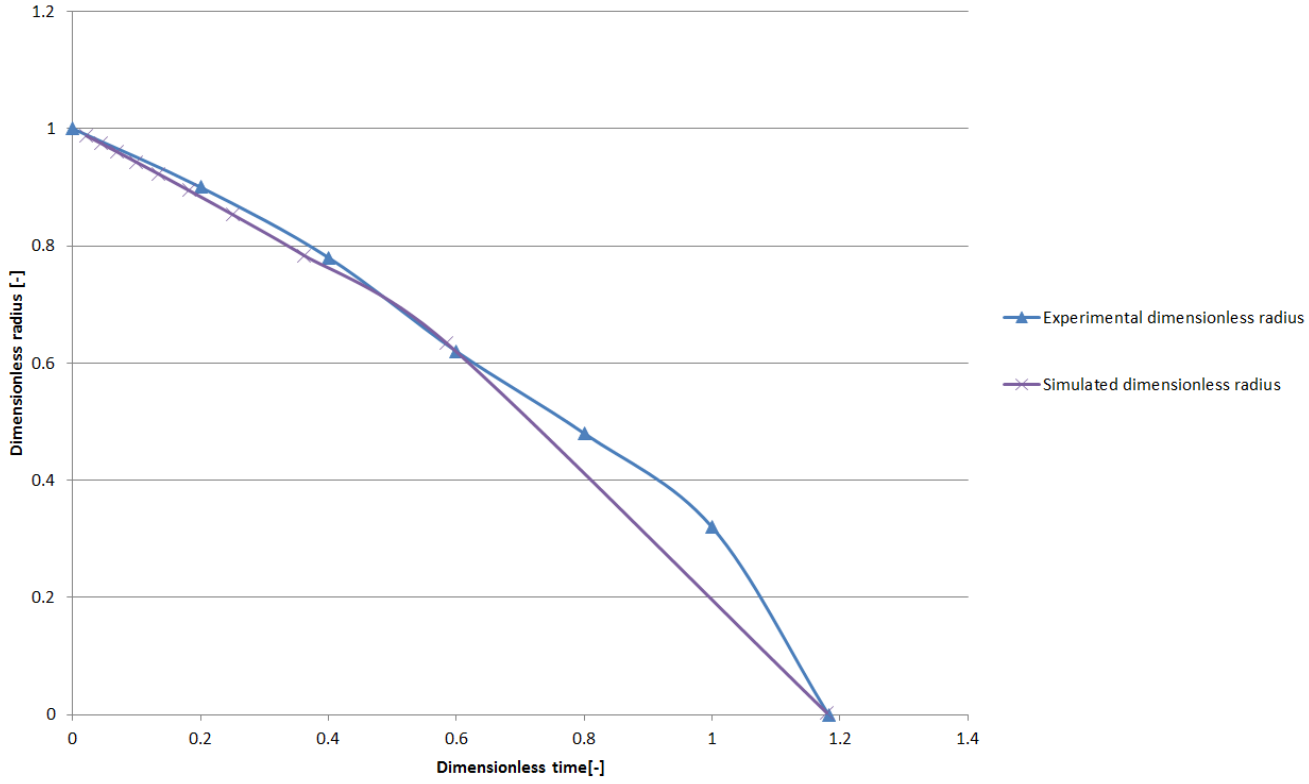

Dimensionless time	Experimental dimensionless radius	Simulated dimensionless radius	Error [%]
0.022	0.983	0.988	0.498
0.045	0.968	0.975	0.706
0.070	0.954	0.960	0.622
0.099	0.941	0.943	0.256
0.135	0.926	0.923	0.425
0.182	0.908	0.895	1.443
0.251	0.876	0.853	2.628
0.362	0.808	0.784	3.006
0.584	0.633	0.635	0.356
1.179	0.009	0.004	58.312
		Average error	6.825

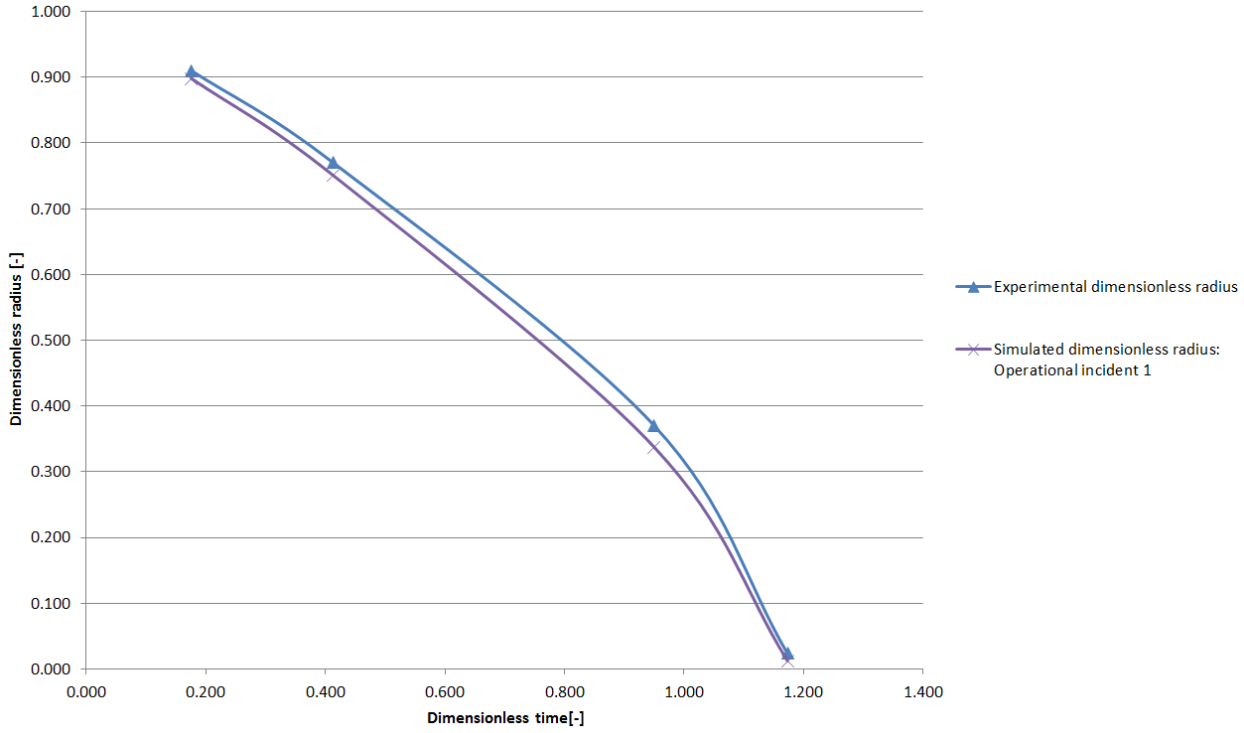

Dimensionless time	Experimental dimensionless radius	Simulated dimensionless radius: Operational incident 1	Error [%]
0.176	0.910	0.898	1.318
0.413	0.770	0.751	2.501
0.950	0.370	0.338	8.850
1.173	0.024	0.013	46.655
		Average error	14.831

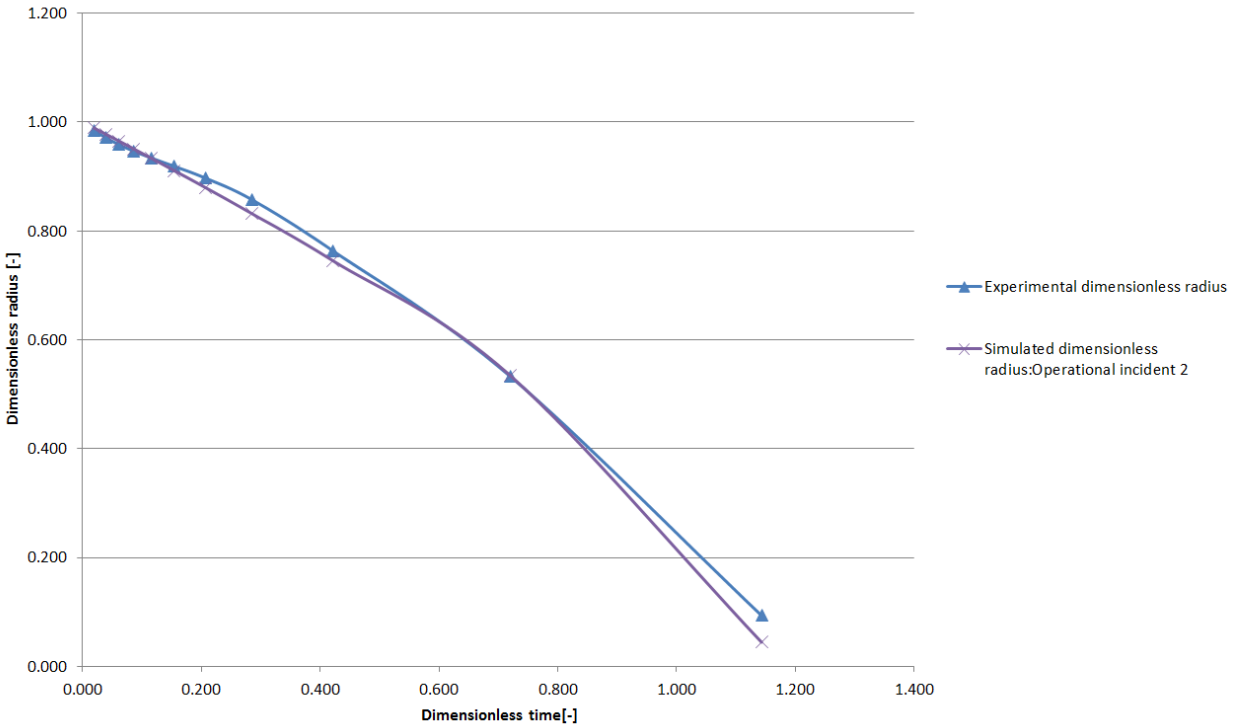

Dimensionless time	Experimental dimensionless radius	Simulated dimensionless radius: Operational incident 2	Error [%]
0.020	0.984	0.989	0.467
0.040	0.971	0.978	0.682
0.062	0.958	0.965	0.679
0.086	0.946	0.951	0.439
0.116	0.934	0.933	0.567
0.155	0.919	0.911	0.592
0.207	0.897	0.880	0.569
0.285	0.857	0.832	0.542
0.421	0.764	0.746	0.567
0.720	0.533	0.534	0.568
1.143	0.094	0.045	0.561
		Average error	0.567

Appendix D Results

D.1 Integrated non-equilibrium simulation model and results

INTEGRATED SIMULATION MODEL

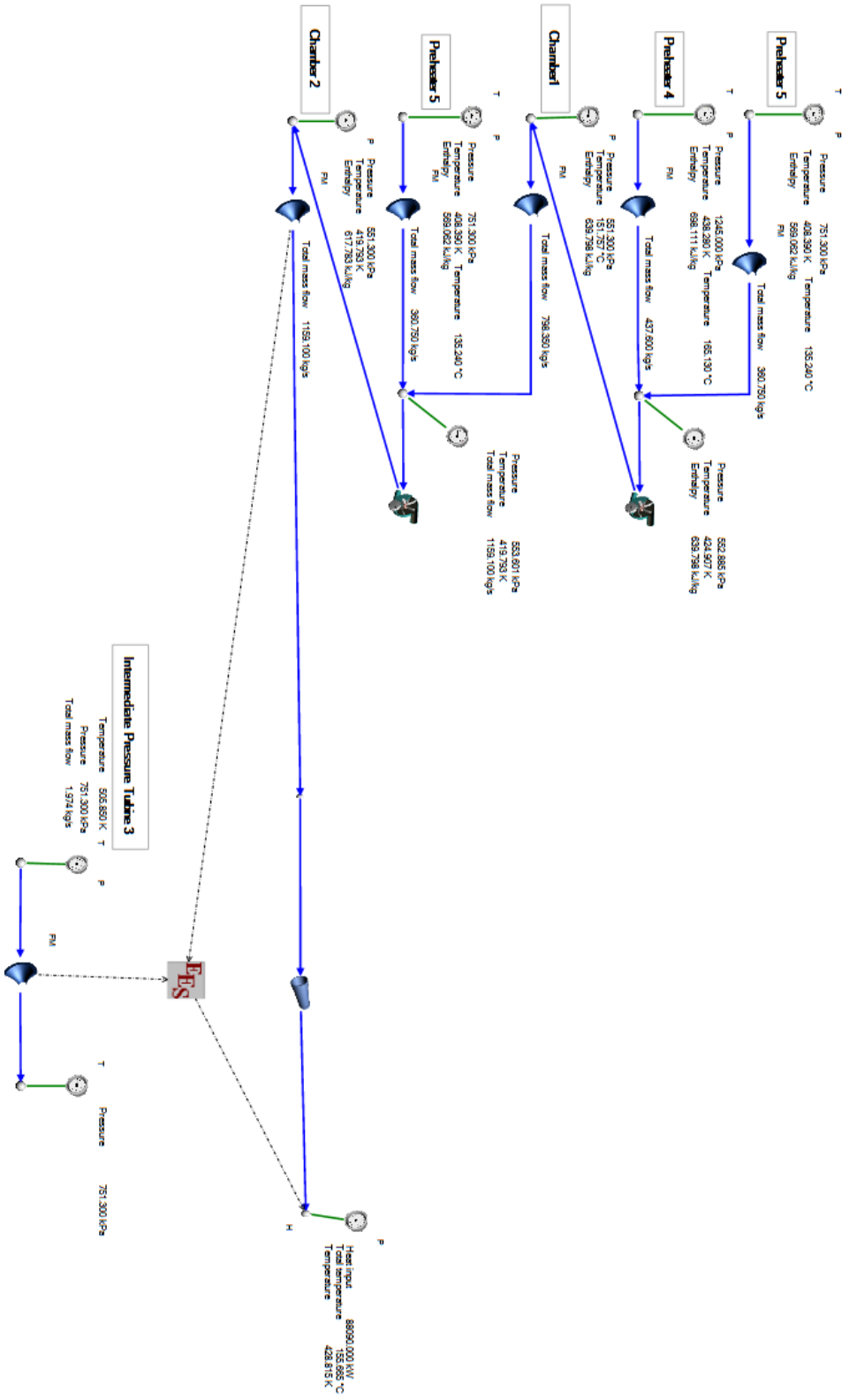

SUB MODEL A AND RESULTS

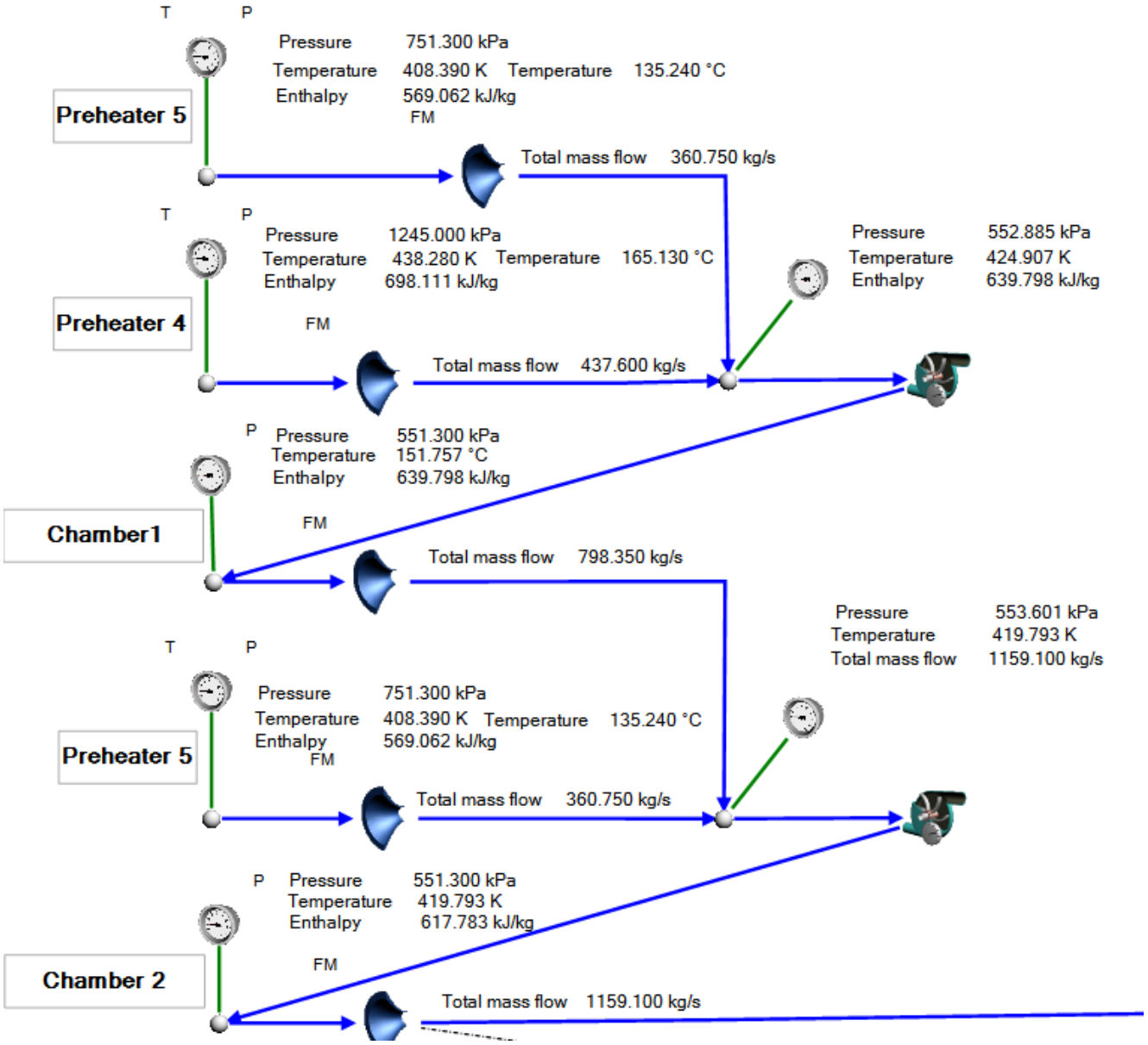

Sub Model B and Results

Initial steam boundary conditions: Flownex

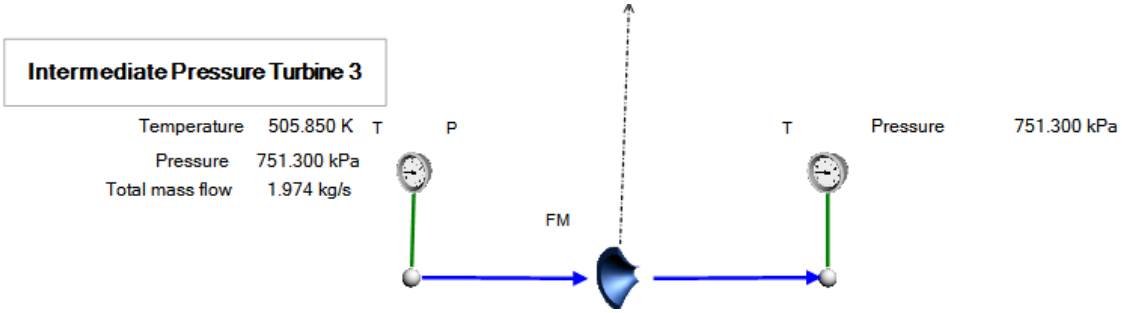

Heat and mass transfer model of a multiple bubble column in an OFWH

$Import 'EESInput.txt',T_IP,P_IP,M_IP,T_liquid,P_liquid,M_liquid

Q= Q_system[1]

$Export 'EESOutput.txt',T_IP,P_IP,M_IP,T_liquid,P_liquid,M_liquid,Q

"Bubble formation volume and time"

"Boundary conditions"

"IPT3"

m_dot_IPT3=M_IP

P_IPT3=P_IP

T_IPT3=T_IP

h_IPT3=enthalpy(Steam,T=T_IPT3,P=P_IPT3)

rho_IPT3=density(Steam,T=T_IPT3,P=P_IPT3)

T_sat_IP3=temperature(Steam,x=1,P=P_IPT3)

"Steam velocity per orifice"

Quantity_orifice=932 "932 orifice in sparger tube"

d_orifice=40/1000 "40 mm"

r_orifice=d_orifice/2 "20 mm"

A_orifice=pi*(r_orifice^2) "0.001257 m^2"

g=9.81 "gravity"

"Constant steam flow rate through an orifice"

Quantity_orifice=((4*m_dot_IPT3)/(rho_IPT3*nu_steam*pi*(d_orifice^2))+1)

V_dot_Steam=nu_steam*A_orifice

V_bubble=1.378*((V_dot_Steam^(6/5))/(g^(3/5)))

V_bubble_initial=(4/3)*pi*(r_orifice^3)

V_bubble_detachment=V_bubble+V_bubble_initial

V_bubble_detachment=(4/3)*pi*(r_detachment^3)

"Bubble formation volume"
increment=0.005
N=20
t_step[0]=0.01
r_orifice[0]=r_orifice
s[0]=r_orifice

Duplicate i=1,N
t_step[i]=t_step[i-1]+increment
r_orifice[i]=r_orifice
A_orifice[i]=A_orifice
V_bubble_initial[i]=V_bubble_initial
V_dot_Steam[i]=V_dot_Steam
V_bubble_detachment[i]=V_bubble_detachment

a[i]=(t_step[i]^2)/4
b[i]=(V_bubble_initial[i]*t_step[i])/(2*V_dot_Steam[i])
c[i]=(V_bubble_initial[i]^2)/(2*(V_dot_Steam[i]^2))
d[i]=ln(((V_dot_Steam[i]*t_step[i])+V_bubble_initial[i])/(V_bubble_initial[i]))
s[i]=s[0]+((16*g)/11)*(a[i]+b[i]-c[i]*d[i])
V_bubble_detachment[i]=(4/3)*pi*(r_detachment[i]^3)
End

S_row=lookuprow('Formation',2,r_detachment)
S_value=lookup('Formation',S_row,2)
Time_formation=lookup('Formation',S_row,1)

"Bubble ascension velocity"
"Surrounding fluid properties"
P_liquid[1]=P_liquid
T_liquid[1]=T_liquid
V_liquid[1]=350
m_dot_liquid[1]=M_liquid
cp_liquid[1]=cp(Water,T=T_liquid[1],P=P_liquid[1])
mu_liquid[1]=viscosity(Water,T=T_liquid[1],P=P_liquid[1])
k_liquid[1]=conductivity(Water,T=T_liquid[1],P=P_liquid[1])
Pr_liquid[1]=prandtl(Water,T=T_liquid[1],P=P_liquid[1])
rho_liquid[1]=density(Water,T=T_liquid[1],P=P_liquid[1])

"Steam bubble properties"
r_bubble[1]=r_detachment
d_bubble[1]=r_bubble[1]*2

T_bubble[1]=T_IPT3

P_bubble[1]=P_IPT3

V_bubble[1]=V_bubble_detachment

rho_bubble[1]=density(Steam,T=T_bubble[1],P=P_bubble[1])

k_bubble[1]=conductivity(Steam,T=T_bubble[1],P=P_bubble[1])

cp_bubble[1]=cp(Steam,T=T_bubble[1],P=P_bubble[1])

h_bubble[1]=enthalpy(Steam,T=T_bubble[1],P=P_bubble[1])

mu_bubble[1]=viscosity(Steam,T=T_bubble[1],P=P_bubble[1])

M=15

Duplicate j=1,M

Time[j]=Time_formation

Time[j+1]=Time[j]+Time_formation

Re[j]=(rho_liquid[j]*nu_steam*d_bubble[j])/mu_liquid[j]

C_d[j]=((24*(1+0.173*(Re[j]^0.657)))/(Re[j]))+(0.413)/(1+16300*(Re[j]^(-1.09)))

U[j]=(((2*g*((pi*(d_bubble[1]^3))/6)*(rho_liquid[j]-
rho_bubble[j]))/(C_d[j]*pi*rho_liquid[j]*((pi*(d_bubble[1]^2))/4)))^0.5)

"Bubble mass transfer"

gamma_liquid[j]=k_liquid[j]/(rho_liquid[j]*cp_liquid[j])

Fo[j]=(gamma_liquid[j]*(Time[j]))/(r_bubble[j]^2)

T_sat_liquid[j]=temperature(Water,x=0,P=P_liquid[j])

rho_sat_v_bubble[j]=density(Water,x=1,P=P_bubble[j])

rho_sat_v_liquid[j]=density(Water,x=1,P=P_liquid[j])

h_sat_v_liquid[j]=enthalpy(Water,x=1,P=P_liquid[j])

h_sat_l_liquid[j]=enthalpy(Water,x=0,P=P_liquid[j])

h_sat_v_bubble[j]=enthalpy(Water,x=1,P=P_bubble[j])

h_sat_l_bubble[j]=enthalpy(Water,x=0,P=P_bubble[j])

Re_rise[j]=(rho_liquid[j]*U[j]*d_bubble[j])/mu_liquid[j]

Ja[j]=(rho_liquid[j]/rho_sat_v_bubble[j])*((cp_liquid[j]*(T_sat_liquid[j]-T_liquid[j]))/(h_sat_v_bubble[j]-
h_sat_l_bubble[j]))

Pe[j]=(2*r_bubble[1]*U[j])/gamma_liquid[j]

r_bubble[j+1]/r_bubble[j]=((1-0.846*((Re_rise[j]^0.5)*(Pr_liquid[j]^(0.5))*Ja[j]*Fo[j]))^(2/3))

d_bubble[j+1]=2*r_bubble[j+1]

Beta_Moalem_and_Sideman[j]=r_bubble[j+1]/r_bubble[j]

Beta_Moalem_and_Sideman_m[j]=((1-((3/2)*(0.25*(Pr_liquid[1])^(-2/3))/(pi^0.5)*(Ja[j]*((Pe[j])^0.5)*Fo[j])))^(2/3))

Tau_m[j]=(Ja[j]*((Pe[j])^0.5)*Fo[j])

Tau[j]=(2/3)*(pi^0.5)*(1-((Beta_Moalem_and_Sideman[j]^(3/2))))

"Bubble heat transfer"

Pe_liquid[j]=(d_bubble[j]*U[j])/gamma_liquid[j]

NU_bubble[j]=2+(0.65*(Pe_liquid[j]^1.7))/(((1+((0.84*Pe_liquid[j]^1.6)^3))^(1/3))*(1+Pe_liquid[j]^1.2))

eta_liquid[j]=1/V_bubble[j]

alpha[j]=V_bubble[j]/V_liquid[j]

Delta_R[j]=-(gamma_liquid[j]*NU_bubble[j]*Ja[j])/(2*r_bubble[j])

Mu_transfer[j]=4.84*rho_sat_v_bubble[j]*(eta_liquid[j]^(1/3))*(alpha[j]^(2/3))*(Delta_R[j])

Q_heat_to_liquid[j]=Mu_transfer[j]*(h_sat_v_liquid[j]-h_sat_l_liquid[j]) "Eq: 3.46"

h_c[j]=(k_liquid[j]/d_bubble[j])*NU_bubble[j]

((T_bubble[j+1]-T_liquid[j])/(T_bubble[j]-T_liquid[j]))=exp(-Time[j]*(h_c[j]*4*pi*(r_bubble[j]^2))/(rho_bubble[j]*V_bubble[j]*cp_liquid[j]))

A_bubble[j]=(4)*pi*(r_bubble[j]^2)

Q_heat_to_liquid[j]*V_liquid[j]=m_dot_liquid[1]*cp_liquid[1]*(T_liquid[j]-T_liquid[j+1])

(Q_heat_transfer[j])=(Q_heat_to_liquid[j])*V_liquid[j]

"Continuation of variables"

"Liquid"

P_liquid[j+1]=P_liquid[j]

Pr_liquid[j+1]=prandtl(Water,T=T_liquid[j+1],P=P_liquid[j+1])

cp_liquid[j+1]=cp(Water,T=T_liquid[j+1],P=P_liquid[j+1])

V_liquid[j+1]=V_liquid[j]

k_liquid[j+1]=conductivity(Water,T=T_liquid[j+1],P=P_liquid[j+1])

mu_liquid[j+1]=viscosity(Water,T=T_liquid[j+1],P=P_liquid[j+1])

rho_liquid[j+1]=density(Water,T=T_liquid[j+1],P=P_liquid[j+1])

"Steam"

P_bubble[j+1]=P_bubble[j]

V_bubble[j+1]=(4/3)*pi*(r_bubble[j+1]^3)

A_bubble[j+1]=(4)*pi*(r_bubble[j+1]^2)

cp_bubble[j+1]=cp(Steam,T=T_bubble[j+1],P=P_bubble[j+1])

h_bubble[j+1]=enthalpy(Steam,T=T_bubble[j+1],P=P_bubble[j+1])

k_bubble[j+1]=conductivity(Steam,T=T_bubble[j+1],P=P_bubble[j+1])

rho_bubble[j+1]=density(Steam,T=T_bubble[j+1],P=P_bubble[j+1])

mu_bubble[j+1]=viscosity(Steam,T=T_bubble[j+1],P=P_bubble[j+1])

Re[j+1]=(rho_liquid[j+1]*nu_steam*d_bubble[j+1])/mu_liquid[j+1]

alpha[j+1]=V_bubble[j+1]/V_liquid[j+1]

eta_liquid[j+1]=1/V_bubble[j+1]

"Multiple bubble columns: Heat and mass transfer"

"Formation frequency"

Bubbles_formed[1]=lookuprow('Ascension',2,0.0005)

time_depeletion[1]=lookup('Ascension',Bubbles_formed[1],1)

formation_frequency[1]=Bubbles_formed[1]/time_depeletion[1]

Deplete[1]=lookuprow('Ascension',1,time_depeletion[1])

Beta_f[1]=lookup('Ascension',Deplete[1],6)

Tau_f[1]=lookup('Ascension',Deplete[1],7)

Q_bubble_col[1]=sum(Q_heat_transfer[I],I=1,11)

Q_system[1]=formation_frequency[1]*(-Q_bubble_col[1])*Quantity_orifice

Q_system[1]=m_dot_liquid[1]*cp_liquid[1]*(T_system[1]-T_liquid[1])

Q_system_Lemmason[1]=m_dot_liquid[1]*cp_liquid[1]*(T_system_t[1]-T_liquid[1])

End

Results: Heat and mass transfer model of a multiple bubble column in an OFWH

- Bubble formation

Sort	$t_{step,i}$ [s]	a_i [s^2]	b_i [s^2]	c_i [s^2]	d_i [-]	s_i [m]	$A_{orifice,i}$ [m^2]	$r_{orifice,i}$ [m]	$V_{bubble,initial,i}$ [m^3]	$V_{Steam,i}$ [m^3/s]	$V_{bubble,detachment,i}$ [m^3]	$r_{detachment,i}$ [m]
[0]	0.01					0.02		0.02				
[1]	0.015	0.00005625	0.0003937	0.0013778	0.2513	0.02148	0.001257	0.02	0.00003351	0.0006383	0.00008483	0.02726
[2]	0.02	0.0001	0.000525	0.0013778	0.3228	0.02257	0.001257	0.02	0.00003351	0.0006383	0.00008483	0.02726
[3]	0.025	0.0001563	0.0006562	0.0013778	0.3895	0.02393	0.001257	0.02	0.00003351	0.0006383	0.00008483	0.02726
[4]	0.03	0.000225	0.0007874	0.0013778	0.452	0.02566	0.001257	0.02	0.00003351	0.0006383	0.00008483	0.02726
[5]	0.035	0.0003063	0.0009187	0.0013778	0.5109	0.02743	0.001257	0.02	0.00003351	0.0006383	0.00008483	0.02726
[6]												
[7]												
[8]												
[9]												
[10]												
[11]												
[12]												
[13]												
[14]												
[15]												
[16]												

- Bubble ascension

Main

Sort	13 Time$_i$ [s]	14 U$_i$ [m/s]	15 r$_{bubble,i}$ [m]	16 T$_{bubble,i}$ [K]	17 P$_{liquid,i}$ [kPa]	18 Re$_i$ [-]	19 T$_{liquid,i}$ [K]	20 d$_{bubble,i}$ [m]	21 μ$_{liquid,i}$ [kg/m-s]	22 ρ$_{liquid,i}$ [kg/m^3]	23 C$_{d,i}$ [mixed]	24 V$_{bubble,i}$ [m^3]	25 P$_{bubble,i}$ [kPa]	26 ρ$_{bubble,i}$ [kg/m^3]	27 cp$_{liquid,i}$ [J/kg-K]	28 γ$_{liquid,i}$ [m2/s]	29 k$_{liquid,i}$ [W/m-K]	30 Fo$_i$ [-]	31 Ja$_i$ [-]	32 T$_{sat,liquid,i}$ [K]
[0]																				
[1]	0.03453	0.6946	0.02726	505.9	553	136233	419.8	0.05452	0.0001871	920.2	0.4688	0.00008483	751.3	3.322	4303	1.689E-07	0.6688	0.00007849	5.251	428.9
[2]	0.06906	0.6945	0.02696	505.7	553	134729	419.8	0.05391	0.0001871	920.2	0.4689	0.00008205	751.3	3.323	4303	1.689E-07	0.6688	0.00001605	5.25	428.9
[3]	0.1036	0.6944	0.02635	505.4	553	131698	419.8	0.0527	0.0001871	920.2	0.469	0.00007664	751.3	3.325	4303	1.689E-07	0.6688	0.0000252	5.246	428.9
[4]	0.1381	0.6942	0.02543	505	553	127087	419.8	0.05086	0.0001871	920.2	0.4693	0.00006887	751.3	3.328	4303	1.689E-07	0.6688	0.00003608	5.241	428.9
[5]	0.1726	0.6939	0.02417	504.3	553	120813	419.8	0.04834	0.0001871	920.2	0.4696	0.00005916	751.3	3.333	4303	1.689E-07	0.6688	0.0000499	5.233	428.9
[6]	0.2072	0.6936	0.02256	503.5	553	112747	419.8	0.04512	0.0001871	920.2	0.4701	0.00004809	751.3	3.339	4303	1.689E-07	0.6688	0.00006876	5.223	428.9
[7]	0.2417	0.6932	0.02055	502.3	553	102690	419.8	0.04109	0.0001871	920.2	0.4706	0.00003633	751.3	3.348	4303	1.689E-07	0.6688	0.0000967	5.208	428.9
[8]	0.2762	0.6929	0.01807	500.7	553	90330	419.8	0.03615	0.0001871	920.2	0.4711	0.00002473	751.3	3.361	4303	1.689E-07	0.6688	0.0001428	5.189	428.9
[9]	0.3108	0.6926	0.01503	498.3	553	75132	419.8	0.03006	0.0001871	920.2	0.4714	0.00001423	751.3	3.379	4303	1.689E-07	0.6688	0.0002323	5.161	428.9
[10]	0.3453	0.6932	0.01121	494.7	553	56023	419.8	0.02242	0.0001871	920.2	0.4705	0.000005899	751.3	3.408	4303	1.689E-07	0.6688	0.0004641	5.118	428.9
[11]	0.3798	0.6999	0.005988	488	553	29926	419.8	0.01198	0.0001871	920.2	0.4617	8.992E-07	751.3	3.462	4303	1.689E-07	0.6688	0.001789	5.037	428.9
[12]	0.4143	-9999	1	467.5	553	-9999	419.8	-9999	0.0001871	920.2	-9999	-9999	751.3	3.643	4303	1.689E-07	0.6688	-9999	4.787	428.9
[13]	0.4489	-9999	-9999	-9999	553	-9999	-9999	-9999	-9999	-9999	-9999	-9999	751.3	-9999	-9999	-9999	-9999	-9999	-9999	428.9
[14]	0.4834	-9999	-9999	-9999	553	-9999	-9999	-9999	-9999	-9999	-9999	-9999	751.3	-9999	-9999	-9999	-9999	-9999	-9999	428.9
[15]	0.5179	-9999	-9999	-9999	553	-9999	-9999	-9999	-9999	-9999	-9999	-9999	751.3	-9999	-9999	-9999	-9999	-9999	-9999	428.9
[16]	0.5525		-9999	-9999	553	-9999	-9999	-9999	-9999	-9999		-9999	751.3	-9999	-9999		-9999			

Sort	33 h$_{sat,bubble,i}$ [J/kg]	34 h$_{sat,l,liquid,i}$ [J/kg]	35 h$_{sat,liquid,i}$ [J/kg]	36 h$_{sat,v,liquid,i}$ [J/kg]	37 ρ$_{sat,liquid,i}$ [kg/m^3]	38 ρ$_{sat,v,liquid,i}$ [kg/m^3]	39 ρ$_{sat,vapour,i}$ [kg/m^3]	40 Pr$_{liquid,i}$ [-]	41 β$_{Moalem,and,Side}$ [-]	42 Pe$_{liquid,i}$ [-]	43 ν$_{bubble,i}$ [-]	44 η$_{liquid,i}$ [m-3]	45 V$_{liquid,i}$ [m^3]	46 α$_i$ [-]	47 δ$_{R,i}$ [m/s]	48 H$_{transfer,i}$ [kg/m3-s]	49 h$_{bubble,i}$ [J/kg]	50 Q$_{heat,to,liquid,i}$ [W/m^3]	51 h$_{c,i}$ [W/m2-K]	52 A$_{bubble,i}$ [m^2]
[0]																				
[1]	2.766E+06	656986	709903	2.753E+06	911.7	2.933	3.92	1.204	0.989	224198	2	11788	350	2.424E-07	-0.00003254	-4.087E-07	2.914E+06	-0.8568	24.54	0.009337
[2]	2.766E+06	656986	709903	2.753E+06	911.7	2.933	3.92	1.204	0.9775	221703	2	12187	350	2.344E-07	-0.00003289	-4.086E-07	2.913E+06	-0.8565	24.81	0.009132
[3]	2.766E+06	656986	709903	2.753E+06	911.7	2.933	3.92	1.204	0.965	216674	2	13048	350	2.190E-07	-0.00003362	-4.083E-07	2.913E+06	-0.8559	25.38	0.008725
[4]	2.766E+06	656986	709903	2.753E+06	911.7	2.933	3.92	1.204	0.9506	209030	2	14521	350	1.968E-07	-0.00003481	-4.079E-07	2.912E+06	-0.855	26.3	0.008125
[5]	2.766E+06	656986	709903	2.753E+06	911.7	2.933	3.92	1.204	0.9332	198636	2	16902	350	1.690E-07	-0.00003656	-4.073E-07	2.911E+06	-0.8537	27.67	0.007343
[6]	2.766E+06	656986	709903	2.753E+06	911.7	2.933	3.92	1.204	0.9108	185288	2	20796	350	1.374E-07	-0.0000391	-4.065E-07	2.909E+06	-0.852	29.65	0.006395
[7]	2.766E+06	656986	709903	2.753E+06	911.7	2.933	3.92	1.204	0.8796	168670	2	27524	350	1.038E-07	-0.00004281	-4.054E-07	2.906E+06	-0.8497	32.55	0.005305
[8]	2.766E+06	656986	709903	2.753E+06	911.7	2.933	3.92	1.204	0.8317	148289	2	40439	350	7.065E-08	-0.00004849	-4.039E-07	2.902E+06	-0.8466	37.01	0.004105
[9]	2.766E+06	656986	709903	2.753E+06	911.7	2.933	3.92	1.204	0.7457	123299	2	70279	350	4.065E-08	-0.00005799	-4.017E-07	2.897E+06	-0.842	44.49	0.00284
[10]	2.766E+06	656986	709903	2.753E+06	911.7	2.933	3.92	1.204	0.5342	92018	2	169510	350	1.686E-08	-0.00007711	-3.983E-07	2.889E+06	-0.8349	59.67	0.001579
[11]	2.766E+06	656986	709903	2.753E+06	911.7	2.933	3.92	1.204	-9999	49623	2	1.112E+06	350	2.569E-09	-0.0001421	-3.920E-07	2.875E+06	-0.8218	111.7	0.0004505
[12]	2.766E+06	656986	709903	2.753E+06	911.7	2.933	3.92	1.204	-9999	-9999	-9999	-9999	350	-9999	-9999	-9999	2.829E+06	-9999	-9999	-9999
[13]	2.766E+06	656986	709903	2.753E+06	911.7	2.933	3.92	-9999	-9999	-9999	-9999	-9999	350	-9999	-9999	-9999	-9999	-9999	-9999	-9999
[14]	2.766E+06	656986	709903	2.753E+06	911.7	2.933	3.92	-9999	-9999	-9999	-9999	-9999	350	-9999	-9999	-9999	-9999	-9999	-9999	-9999
[15]	2.766E+06	656986	709903	2.753E+06	911.7	2.933	3.92	-9999	-9999	-9999	-9999	-9999	350	-9999	-9999	-9999	-9999	-9999	-9999	-9999
[16]								-9999				-9999	350	-9999			-9999			-9999

53 cp$_{bubble,i}$ [J/kg-K]	54 k$_{bubble,i}$ [W/m-K]	55 μ$_{bubble,i}$ [kg/m-s]	56 Q$_{heat,transfer,i}$ [W]	57 Bubbles$_{formed,i}$ [-]	58 formation$_{freque}$ [s-1]	59 time$_{depeletion,i}$ [s]	60 Q$_{bubble,col,i}$ [W]	61 Q$_{system,i}$ [W/s]	62 ṁ$_{liquid,i}$ [kg/s]	63 Re$_{rise,i}$ [-]	64 β$_{Moalem,and,Side}$ [-]	65 τ$_i$	66 Pe$_i$ [-]	67 h$_{sat,l,bubble,i}$ [J/kg]	68 h$_{sat,v,bubble,i}$ [J/kg]
2171	0.03834	0.00001736	-299.9	11.92	28.96	0.4115	-3264	8.809E+07	1159	186279	0.9976	0.01952	224198	709903	2.766E+06
2171	0.03833	0.00001735	-299.8							184207	0.995	0.03989	224177	709903	2.766E+06
2172	0.03831	0.00001734	-299.6							180029	0.9922	0.06258	224136	709903	2.766E+06
2173	0.03827	0.00001732	-299.2							173678	0.9888	0.0895	224074	709903	2.766E+06
2174	0.03822	0.00001729	-298.8							165043	0.9845	0.1236	223990	709903	2.766E+06
2176	0.03815	0.00001726	-298.2							153952	0.9787	0.1699	223887	709903	2.766E+06
2178	0.03806	0.00001721	-297.4							140145	0.9701	0.2383	223767	709903	2.766E+06
2181	0.03793	0.00001714	-296.3							123210	0.9558	0.3505	223646	709903	2.766E+06
2186	0.03775	0.00001704	-294.7							102447	0.928	0.5668	223575	709903	2.766E+06
2195	0.03748	0.00001689	-292.2							76456	0.8545	1.124	223766	709903	2.766E+06
2212	0.03698	0.0000166	-287.6							41231	0.3408	4.284	225904	709903	2.766E+06
2283	0.03563	0.00001573	-9999							-9999	-9999	-9999	-9999	709903	2.766E+06
-9999	-9999	-9999	-9999							-9999	-9999	-9999	-9999	709903	2.766E+06
-9999	-9999	-9999	-9999							-9999	-9999	-9999	-9999	709903	2.766E+06
-9999	-9999	-9999	-9999							-9999	-9999	-9999	-9999	709903	2.766E+06
-9999	-9999	-9999													

Sub model C